UNIVERSITÀ DEGLI STUDI DI SASSARI

SCUOLA DI DOTTORATO DI RICERCA
Scienze e Biotecnologie
dei Sistemi Agrari e Forestali
e delle Produzioni Alimentari

Indirizzo
AGROMETEOROLOGIA ED ECOFISIOLOGIA
DEI SISTEMI AGRARI E FORESTALI

Ciclo XXVII

EMPIRICAL ESTIMATIONS OF CO$_2$ FLUX COMPONENTS OVER DIFFERENT ECOSYSTEMS

Dr. Veronica Bellucco

Direttore della Scuola   Prof. Alba Pusino
Referente di Indirizzo   Prof. Donatella Spano
Docente Guida   Prof. Donatella Spano
Tutor   Dr. Serena Marras

Anno accademico 2013 - 2014

UNIVERSITÀ DEGLI STUDI DI SASSARI

SCUOLA DI DOTTORATO DI RICERCA
Scienze e Biotecnologie
dei Sistemi Agrari e Forestali
e delle Produzioni Alimentari

Indirizzo
AGROMETEOROLOGIA ED ECOFISIOLOGIA
DEI SISTEMI AGRARI E FORESTALI

Ciclo XXVII

To Gavino and my family

Contents

Abstract

Vertical CO_2 fluxes are the result of the net exchange between an ecosystem and the overlying atmosphere. The complex balance among biogenic and anthropogenic components varies from site to site and can be observed by using the micrometeorological Eddy Covariance (EC) technique. Different approaches can be used then to partition the EC flux measurements in order to understand the influence of each contribution to the flux.

The general aim of this PhD thesis is to relate carbon balance of different ecosystems to the main controlling factors and to look for general and empirical relations that allow to estimate CO_2 flux components by using environmental variables and the percentage of vegetation cover.

The work is organized into three main parts: the first is about CO_2 flux partitioning over three Mediterranean sites by using literature-based empirical relations and a new combined approach. The second part is about estimating anthropogenic components of the CO_2 flux. A review of empirical methods is presented, as well as the recent improvements of the process-based model ACASA and its evaluation over a suburban site. Finally, the third part combines the results of previous chapters to present a new developed empirical simple model, based on land cover fraction and environmental variables. It can simulates the daily mean trend of CO_2 flux over different ecosystems, and a first validation of the biogenic module, both over a natural

and a suburban site, is presented.

Chapter 1

Introduction

Alterations to the global climatic system have been measured since the last mid century. It has been observed that greenhouse gases (GHG) and mean surface temperature have increased ($+0.85$°C based on $1880 - 2012$ linear trend) (Stocker et al., 2013). At the same time, there is evidence of increased ocean temperature ($+0.11$°C/decade from 1971 to 2010 in the first $75\,m$), sea level, precipitation, extreme meteorological and climatic events, together with a reduction of ice cover. For the Northern Hemisphere, the thirty-year period $1983 - 2012$ is likely to have been the warmest of the last 1400 years (Stocker et al., 2013).

The most important GHG and radiative forcing to climate change is carbon dioxide (CO_2) (Stocker et al., 2013). Carbon cycle is closely linked to the climate system as the rate of change of atmospheric CO_2 reflects the balance between carbon emissions from human activities (fossil-fuel combustion and land use change) and the dynamics of a number of terrestrial and ocean processes that remove or emit CO_2. In the Pre-Industrial Era (1750), global atmospheric CO_2 concentration values, inferred from ice core records, were ~ 278 parts per million (ppm) (Stocker et al., 2013) but they have
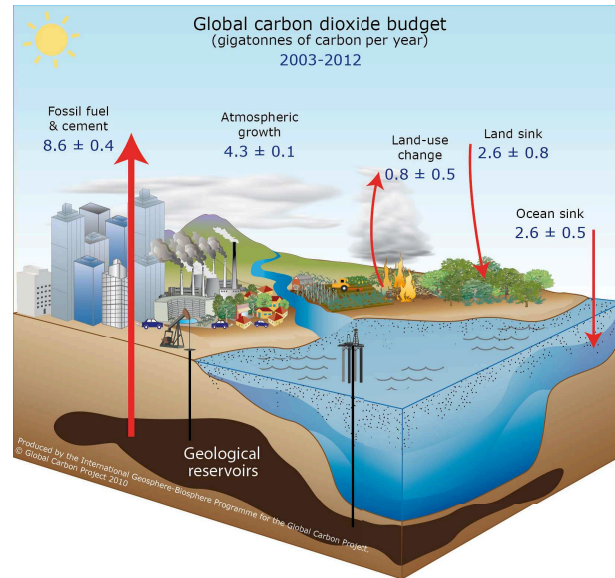
Figure 1.1: *Representation of global carbon cycle and estimated values of each component for the last decade (2003 − 2012) (from Le Quéré et al., 2014)*

increased reaching an annual average of 396.48 ppm in 2013 and a monthly mean value of 401.75 ppm in May 2014 (Tans and Keeling, 2014) in Mauna Loa, Hawaii. At this site, continuous measurements of atmospheric CO_2 concentration started in 1958 and for the first time in 2013 (May 9) daily mean peak exceeded the value of 400 ppm (Dlugokencky and Tans, 2013). Atmospheric CO_2 concentration is estimated to have increased for more than 20% since 1958 and about 40% since the Pre-Industrial Era (Stocker et al., 2013). Fossil-fuel combustion and cement production are the main responsible for this positive trend. It is estimated that in the last decade, 2003 − 2012, they contributed for the 90% to total carbon dioxide emissions, whereas changes in land use and land cover accounted for 10% (Le Quéré et al., 2014). The atmosphere stores almost half of these CO_2 emissions (45%) and the rest is partitioned between land (29%) and ocean (26%) (Figure 1.1).

Because climate change effects have an impact on ecosystems, it is ne-

cessary to monitor GHG atmospheric concentration and in particular that of carbon dioxide. It is important to understand changes in global carbon budget to manage the adaptation of natural sinks and find out strategies to mitigate this global warming in action.

There are several methods with which atmospheric carbon dioxide can be monitored at local scale. One of these is the Eddy Covariance (EC) method, a widely used micrometeorological technique based on the postulates of Reynolds (Reynolds, 1895, see section A.2). This method provides a direct measure of the net exchange of a gas between the surface and the lowest part of the atmosphere as well as sensible and latent heat, and momentum fluxes. Ideally, the surface has to be flat and horizontally homogeneous so that the flux is proportional to the covariance between the fluctuations of vertical wind velocity and the scalar quantity of interest. Another condition to met when applying this method is the vertical constancy of turbulence and fluxes. It is assumed to be reached, depending on atmospheric stability and roughness of the underlying ground, at about 10-50 m, depending on the surface (i.e. trees, grass, buildings) (Aubinet et al., 2012). EC measurements are representative of the upwind area (*flux footprint*) which increases with measurements height, reduced surface roughness and thermal stability (Burba, 2013). A typical Eddy Covariance tower is equipped with a 3D sonic anemometer, a gas analyser (open or closed-path) and a fine-wire thermo-couple.

In addition, an accurate knowledge of the atmospheric vertical profile is necessary to understand transport mechanisms acting in different parts of the lower atmosphere (*troposphere*) as well as monitor land-atmosphere exchanges and pollutants diffusing there. An overview about tropospheric vertical structure and parameters, as well as the theory behind the Eddy

Covariance technique are described in the Appendix.

1.1   Objectives

Carbon emissions are released from different sources, such as human activities (fossil-fuel combustion and land use change) and natural processes of terrestrial and ocean ecosystems, that can both remove or emit atmospheric CO_2. Ecosystems are, in fact, both carbon sinks and carbon sources and, in order to study the main factors affecting the global carbon cycle (and future climate scenarios), it is necessary to understand the mechanisms controlling carbon exchanges between the surface and the atmosphere.

The micrometeorological Eddy Covariance method is acknowledged by the scientific community to be a reliable technique through which ecosystems can be observed and, both for short and long periods, the ability of natural, agricultural and urban ecosystems to act as carbon sources or sinks can be monitored.

So far, a lot of studies used EC measurements to investigate the role of different ecosystems in the global carbon budget and it is of primary importance to understand how anthropogenic emissions could be mitigated by vegetation, especially in complex systems such as cities. Inside cities, vegetation can play a crucial role, especially during the growing season, offsetting the extra carbon emissions due to traffic and buildings heating systems and, recently, studies on eddy covariance measurements have shown that the more the vegetation cover fraction is, the more the carbon emissions reduce. However, it is not so simple (also due to highly cost demand) to directly monitor carbon exchanges over cities and different kind of models can be used to estimate CO_2 emissions sources and the sequestration ability of such ecosystems.

Models are generally used to estimate energy and mass fluxes whenever measurements are not available or for an upscale from local to greater scales. They can be based on physical processes or on empirical relations for the description of the ecosystems response to environmental conditions and their mechanisms.

The general aim of this PhD thesis is to relate carbon balance of different ecosystems to the main controlling factors and to look for general and empirical relations that allow to estimate CO_2 flux components by using environmental variables and the percentage of vegetation cover. Experimental and literature data are used to develop such a model, through which it is possible to assess the carbon balance of both vegetated and urban systems whenever direct measurements of carbon exchanges are not available.

Depending on the environment, drought conditions and high temperature can greatly affect carbon balance, so the first objective of this work is to investigate this aspect in an area where prolonged drought occurs annually in relatively predictable manners. In this contest, Mediterranean area is ideal to investigate the dynamic of CO_2 exchanges in response to soil water availability and temperature. Three Mediterranean sites (two vineyards and one Maquis ecosystem), characterized by different cover fraction and management, were used to relate CO_2 fluxes to environmental conditions and to test different models in order to partition the biogenic components of the CO_2 flux (Net Ecosystem Exchange, NEE) into the two eco-physiological processes: the Gross Primary Production (GPP) and the ecosystem respiration (R_{eco}). The relations between NEE and the environment in natural and agricultural ecosystems are, then, the object of the analysis carried out in the Chapter 2, and the final result of this work is a model used to partition the CO_2 flux into photosynthetic uptake and ecosystem respiration (by using

site specific coefficients) in non-anthropic ecosystems.

The second objective of this study is to understand the differences between natural and urban ecosystems in terms of carbon exchanges. Chapter 3 is, then, dedicated to describe in details the non-biogenic (i.e. anthropogenic) components of NEE in urban areas. The used approach is a review based on literature, which analyzes the most used models and methods to estimate the different CO_2 emissions sources in urban environments. In addition, this chapter describes the new urban implementations of the process-based ACASA model and an evaluation of half-hourly and composite CO_2 model simulations over the suburban site of Helsinki are shown and discussed.

Finally, Chapter 4 tries to combine and generalize the results and information obtained and discussed in the previous chapters in a simple model able to simulate CO_2 fluxes both over natural and urban ecosystems. This model, is mainly composed by two modules, one accounting for biogenic and one for anthropogenic components, and based on commonly measured input variables. So far, the biogenic module, which takes into account the site-specific characteristics and reproduces the different NEE components (photosynthesis and respiration processes due to soil and vegetation) over different ecosystems, was developed and validated. The application and evaluation of this module is reported over two different ecosystems: the suburban site of Helsinki during the summer growing season and the Mediterranean Maquis ecosystem in non water-stress conditions. The anthropogenic CO_2 emissions module is still under development, however, a brief description of the proposed approach is reported.

References

Aubinet, M., Vesala, T., and Papale, D. (2012). *Eddy covariance: a practical guide to measurement and data analysis*. Springer.

Burba, G. (2013). *Eddy Covariance Method for Scientific, Industrial, Agricultural and Regulatory Applications*. LI-COR Biosciences.

Dlugokencky, E. and Tans, P. (2013). http://www.esrl.noaa.gov/news/2013/CO2400.html.

Le Quéré, C., Peters, G. P., Andres, R. J., Andrew, R. M., Boden, T. A., Ciais, P., Friedlingstein, P., Houghton, R. A., Marland, G., Moriarty, R., et al. (2014). Global carbon budget 2013. *Earth System Science Data*, 6(1):235–263.

Reynolds, O. (1895). On the dynamical theory of incompressible viscous fluids and the determination of the criterion. *Philosophical Transactions of the Royal Society of London. A*, pages 123–164.

Stocker, T. F., Qin, D., Plattner, G.-K., Tignor, M., Allen, S. K., Boschung, J., Nauels, A., Xia, Y., Bex, V., Midgley, P. M., et al. (2013). Climate Change 2013. The Physical Science Basis. Working Group I Contribution to the Fifth Assessment Report of the Intergovernmental Panel on Climate Change - Summary for Policymakers. Technical report, Intergovernmental Panel on Climate Change-IPCC, C/O World Meteorological Organization, 7bis Avenue de la Paix, CP 2300 CH-1211 Geneva 2 (Switzerland).

Tans, P. and Keeling, R. (2014). Dr Pieter Tans, NOAA/ESRL (www.esrl.noaa.gov/ gmd/ccgg/trends) and Ralph Keeling, Scripps Institution of Oceanography (scrippsco2.ucsd.edu/).

Chapter 2

NEE biogenic flux partitioning

2.1 Introduction

Far from anthropogenic pollutant sources, natural ecosystems together with oceans remove about 55% of anthropogenic emissions (Le Quéré et al., 2014). They contribute to the carbon budget with their natural processes. Carbon released into the atmosphere and stored by natural environments contribute to the Net Ecosystem Exchange (NEE), that is the budget between the total amount of carbon and energy required for all ecosystem processes (gross primary production, -GPP) and the CO_2 flux released by ecosystem respiration (R_{eco}) (Gilmanov et al., 2003). By micrometeorological convention, positive fluxes indicate carbon emissions and negative fluxes carbon sequestration, so that R_{eco} is always positive whereas GPP is negative during the day and zero at night. The carbon budget is therefore summarized as follows:

$$NEE = R_{eco} + GPP \qquad (2.1)$$

R_{eco} is in turn obtained by summing the soil efflux (R_S), that is the CO_2 flux released from the soil, also called heterotrophic respiration, and plant

respiration (R_V), also called autotrophic respiration:

$$R_{eco} = R_S + R_V \tag{2.2}$$

Different methods are used to directly quantify or estimate NEE. By using the Eddy Covariance (EC) technique, it is possible to monitor NEE of a specific ecosystem and validated models can help in simulating CO_2 fluxes whenever measurements are not available. There are two main approaches for modeling NEE: one based on physical and ecophysiological processes and one based on empirical relations derived from experimental data. Depending on the scope of a study, physical or empirical based approach can be preferred. A detailed description of the physical and physiological processes to reproduce ecosystem behaviour is, usually, more accurate than an empirical approach, but it is also more difficult and requires a lot of information and parameters to correctly reproduce the ecosystem complexity. Empirical models are, on the contrary, easier to build since they reproduce the ecosystem processes based on the analysis of the ecosystem response to environmental conditions through experimental data. In the empirical approach, the system complexity is simplified without omitting the ecosystem behaviour, which is indirectly considered when reproducing experimental trend curves.

Of course, the empirical approach needs a good knowledge of the investigated ecosystems in terms of atmospheric and environmental conditions, and fluxes.

As Mediterranean area is critical for future climate change scenarios, it is very important to study its most representative and widespread ecosystems and look at the climate feedback on them. The vegetation type that most represents the Mediterranean area is the Mediterranean maquis, composed by evergreen schlerophyllous species characterized by shrubs with small hight and sparse canopy. In addiction, vineyards ecosystems are one of the most

represented fruit crops worldwide, and the wine industry is one of the main important economic sectors. Also, the major producing countries are located in the Mediterranean basin (OIV, 2013).

The first aim of this study is to investigate these two different ecosystems, characterized by Mediterranean climate, and understand the link between the CO_2 flux and the environmental factors controlling it. These ecosystems are, in fact, more vulnerable to stress conditions, such as drought and elevated air temperature. The work is then carried out over two vineyards and one Mediterranean Maquis site, located in Italy, which have been monitored with the EC technique in order to measure the NEE flux.

The second objective of this analysis is to improve our knowledge on such Mediterranean ecosystems in terms of energy, water, and carbon budget calculated over long periods and their behaviour under stress conditions.

Finally, the third objective of the study is to model NEE flux and find out methods to partition it into the main components, GPP and R_{eco}. More in detail, the aim is to look for empirical relations to accurately reproduce CO_2 flux through measurements or estimates of environmental variables. EC and meteorological measurements collected over the three Mediterranean sites, characterized by different vegetation types and cover fraction, are used for this purpose.

The sections 2.1.1 and 2.1.2 describe the most widely used empirical equations to estimate GPP and R_{eco} during daytime and nighttime periods, and the section 2.2.7 reports the proposed empirical approach for the NEE estimation and partitioning over different ecosystems.

2.1.1 Gross primary production

Photosynthesis converts inorganic carbon to organic and the total energy produced in the unit of area and time is defined Gross Primary Production. Solar radiation (R_g) is the energy used by organism for their life processes. For plants, it represents the main driver for photosynthesis and growth. Plants use only a part of it, as leaves use wavelengths inside the visible spectrum range (0.4 μm $< \lambda <$ 0.7 μm). This fraction represents the so called Photosynthetically Active Radiation (PAR). During daytime, photosynthesis and respiration processes occur at the same time. Whereas, at night photosynthesis usually stops while R_{eco} processes are always ongoing. During daytime, in absence of other limiting environmental factors (e.g. soil water availability), plants processes are directly related to the amount of available energy. Photosynthetic light-response curves are therefore usually used to estimate the CO_2 flux as function of PAR.

In the literature, there are a wide range of different equations used to predict leaf photosynthesis response to PAR (Reichstein et al., 2012). One of the earliest was the *Blackman curve* (Blackman, 1905), constituted by two linear intersecting segments and, among the others, the most often used rectangular hyperbola (*Michaelis-Menten* function) (Ruimy et al., 1995):

$$NEE = \frac{\alpha\beta PAR}{\alpha PAR + \beta} \tag{2.3}$$

where α (μmol CO_2 μmol photons^{-1}) is the mean apparent ecosystem quantum yield and represents the initial slope of the light-response curve, and β (μmol CO_2 m^{-2} s^{-1}) is the light-saturated gross photosynthesis of the canopy (the plateau parameter, μmol CO_2 m^{-2} s^{-1}).

The lower root of the quadratic equation

$$\theta\,GPP^2 - (\alpha PAR + \beta)\,GPP + \alpha\beta\,PAR = 0 \tag{2.4}$$

is the non-rectangular hyperbola (NRH) (Rabinowitch, 1951):

$$GPP = \frac{1}{2\theta}\left(\alpha PAR + \beta - \sqrt{(\alpha PAR + \beta)^2 - 4\alpha\beta\theta PAR}\right) \qquad (2.5)$$

where α and β take the same meaning as in equation 2.3 and the additional parameter θ is the convexity of the curve at light saturation (adimensional bending parameter). When θ is zero, equation 2.4 simply becomes the Michaelis-Menten function.

For both equations 2.3 and 2.5, an ecophysiological interpretation of the coefficients (whose estimated values can be different) is possible, but it is well known the ability of the NRH in reproducing experimental data better than the simple rectangular hyperbola (Gilmanov et al., 2003). This is due to its additional curvature parameter (θ) on which the shape of the NRH equation depends. θ varies non linearly between 0 (when the equation becomes the Michaelis-Menten function) and 1 (when a Blackman response curve is reproduced) (Figure 2.1) but it is estimated that it performs well when ranging between 0.7 and 0.99 (Boote and Loomis, 1991; Gilmanov et al., 2003; Marshall and Biscoe, 1980; Ögren, 1993; Stoy et al., 2006).

Introducing the average ecosystem respiration as an intercept parameter at zero light (γ, μmol CO_2 m^{-2} s^{-1}) and changing sign to GPP, equation 2.5 becomes

$$NEE = R_{eco} + GPP =$$
$$= \gamma - \frac{1}{2\theta}\left(\alpha PAR + \beta - \sqrt{(\alpha PAR + \beta)^2 - 4\alpha\beta\theta PAR}\right) \qquad (2.6)$$

This equation can be used to partition the biogenic CO_2 flux into its components calculating GPP as a residual from measurements and γ (R_{eco}) estimates.
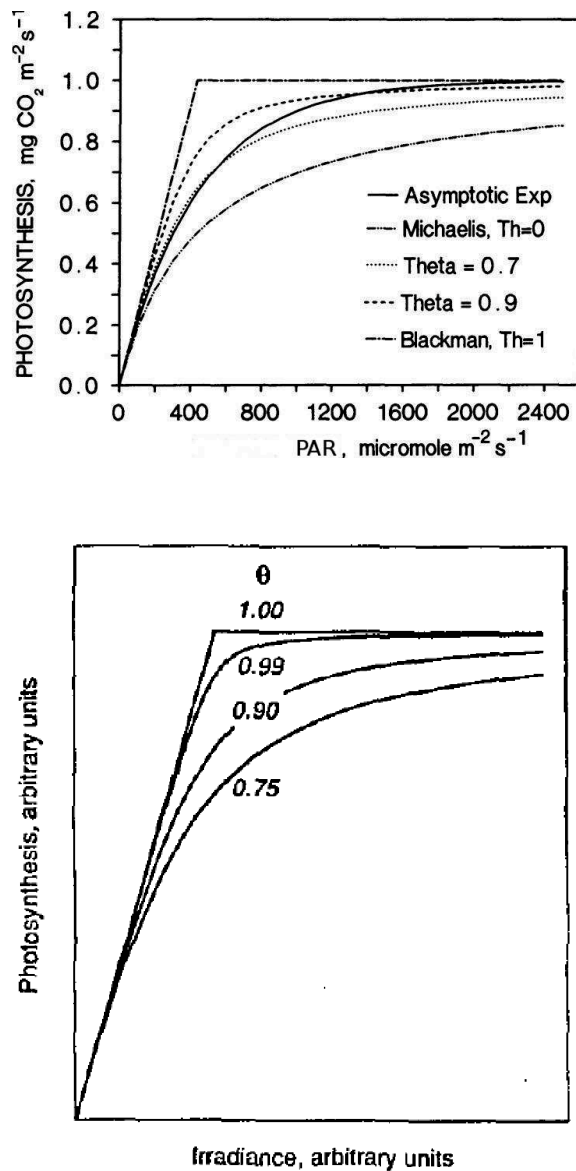
Figure 2.1: *Top: Gross Primary Production simulated by a non-rectangular hyperbola with different bending values (modified from Boote and Loomis, 1991). Bottom: non-rectangular hyperbola variation with theta values changing non-linearly (the curve with $\theta = 0.90$ is more similar to the one with $\theta = 0.75$ than to that with $\theta = 0.99$) (from Ögren, 1993)*

2.1.2 Ecosystem respiration

Total ecosystem respiration is the sum of autotrophic and heterotrophic respiration that, during daytime, occur simultaneously with photosynthesis processes. To exclude the contribution of photosynthesis when estimating R_{eco}, usually nocturnal measurements are considered. For deciduous ecosystems, in periods when leaves are not yet developed (winter season), the contribution of R_V to R_{eco} can be considered negligible, so nocturnal EC measurements are representative of R_S.

As nights often have more stable atmospheric conditions, it is important to select data when the assumptions underlying EC theory are still valid. When advective and storage terms can no more be considered negligible, EC measurements are systematically underestimated and this error can lead to inaccurate carbon balance estimates (Aubinet et al., 2000; Goulden et al., 1996; Gu et al., 2005; Moncrieff et al., 1996). Advection can affect both short and long-term budgets removing CO_2 from the ecosystem which is not detected by the measurement station. Storage has no impact on long periods but it becomes relevant on 30 minutes budgets, as the CO_2 stored during night is released all at once when turbulence begins again in the early morning (Aubinet et al., 2012). As shown in Figure 2.2, advection and storage effects can occur alone or at the same time.

Commonly, for nocturnal CO_2 fluxes, a friction velocity (u*) filter is employed (only valid when u* does not covary with environmental variables such as air temperature, T_{air}, and soil water content, SWC) to avoid overestimation of CO_2 fluxes due to low turbulence conditions (Aubinet et al., 2000; Goulden et al., 1996; Reichstein et al., 2005). By simply plotting the CO_2 flux against u*, the threshold can be detected as that value beyond which the flux remain constant and independent of u*. Typical u* threshold values
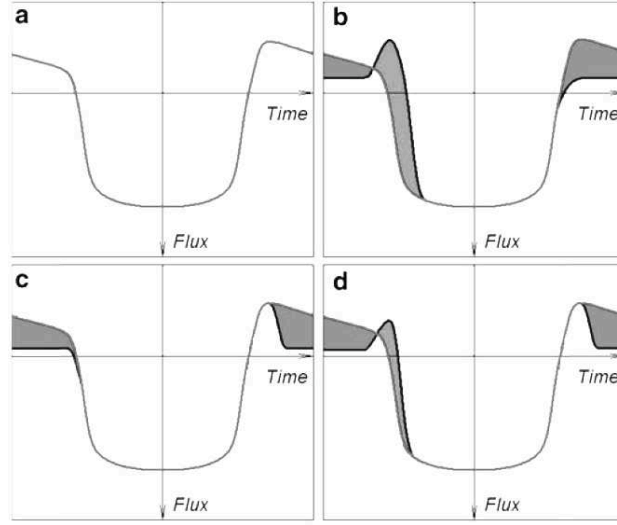
Figure 2.2: *Representation of the CO_2 flux time series: (a) ideal case with well developed turbulence conditions, (b) storage effect on Eddy Covariance flux (the underlying area offset the overlying one), (c) advection effect, (d) combined effect of storage and advection (the underlying area is not offset by the overlying one) (modified from Aubinet et al., 2012)*

range between 0.1 and 0.5 m s^{-1} (Aubinet et al., 2012). A more complex method is described in section 2.2.6.

Once nighttime datasets have been filtered by friction velocity, different equations to simulate R_{eco} response to environmental conditions can be used. The most used functions are the exponential, the Lloyd and Taylor (LLT) (Lloyd and Taylor, 1994), the Arrhenius and the logistic model (Richards, 1959). All these equations are temperature-driven (air or soil temperature). Among them, the LLT and the logistic model are described below.

The Lloyd and Taylor equation is an Arrhenius type equation given by:

$$R_{eco_{LLT}} = R_{ref}\, exp \left[E_0 \left(\frac{1}{T_{ref} - T_0} - \frac{1}{T_{soil} - T_0} \right) \right] \qquad (2.7)$$

where R_{ref} is the ecosystem respiration rate at a reference temperature (T_{ref}) and E_0 is an activation energy parameter that determines the temperature

sensitivity. In the original study (Lloyd and Taylor, 1994) T_{ref} and T_0 are set to 10°C and -46°C respectively and soil temperature (T_{soil}) is used as predictor.

The Lloyd and Taylor equation fits well to the experimental data during standard water availability conditions but in semi-arid ecosystems, where drought periods occur, the dependence of ecosystem respiration on soil water content has also to be considered for a higher sensitivity on water-stress conditions. Some models describe R_{eco} in semi-arid ecosystems by a multiplicative effect of temperature and moisture (Janssens et al., 2001; Reichstein et al., 2002). As an example, Reichstein et al. (2002) proposed a modified Lloyd and Taylor equation (LLT_{mod}), multiplying the original temperature-driven model (equation 2.7) by a moisture function:

$$R_{eco} = R_{eco_{LLT}} \cdot \frac{SWC - SWC_0}{(SWC_{1/2} - SWC_0) + (SWC - SWC_0)} \qquad (2.8)$$

where SWC_0 and $SWC_{1/2}$ are two parameters related to soil water content: the first is the residual soil water content at which respiration is zero and the second is the soil water content at which the half maximal respiration occurs.

As an alternative, the logistic function has also been used to simulate R_{eco} response to temperature in drought conditions. Because of its "S" shape, this model is indeed able to simulate soil respiration data characterized by an initial exponential growth followed by a saturation phase due to the effect of secondary limiting factors like water stress conditions, even without an explicit dependence on SWC (Rodeghiero and Cescatti, 2005):

$$R_{eco} = \frac{K}{1 + c\,e^{-a\,T_{soil}}} \qquad (2.9)$$

where K represents the maximum ecosystem respiration rate that the ecosystem is able to support over the long period under water deficit conditions,

c is an arbitrary constant determining the elongation along the x axis, and a is the initial R_{eco} growth rate (when $R_{eco} \ll K$), a parameter affecting the slope of the curve. The logistic model describes the ecosystem respiration increasing exponentially until an inflection point $(K/2)$, where the curvature changes decreasing asymptotically to $y = K$.

When available, chamber measurements of R_S are often used as an independent comparison to nocturnal EC flux (Reichstein et al., 2005).

2.2   Materials and Methods

Non gap-filled CO_2 flux measurements of three Mediterranean sites, characterized by having different vegetation types, were considered for the NEE biogenic flux partitioning: two vineyards and a Mediterranean maquis ecosystem (Figure 2.3, Table 2.1).

Table 2.1: *Sites characteristics.*

	Serdiana, Italy (Marras et al., 2012)	**Montalcino, Italy** (Marras, 2008)	**Capo Caccia, Italy** (Marras et al., 2011)
Area	Vineyard	Vineyard	Mediterranean Maquis
Latitude	39.36° N 9.12° E	43.08° N 11.80° E	40.61° N 8.15° E
Period	Jun-Jul-Aug (2009 - 2011)	Jun-Jul-Aug (2005 - 2006)	year (2005 - 2010)
% veg	~ 50 (grapevine)	~ 50 (grapevine)	~ 70 (shrubs)
T_{air} **(°C)**	16.2	12.4	15.9
Mean precipitation (mm)	426	691	488
LAI (m^2 m^{-2})	$1.2 - 3.2$	$1.26 - 1.55$	$2.7 - 3.0$

Figure 2.3: *Experimental sites location (http://www.bing.com/maps/)*

The EC method was used to monitor energy and mass fluxes over both maquis and vineyard ecosystems.

The analyzed period is the summer growing season for the vineyards (deciduous ecosystem), when vegetation cover is constant and about 50%. At the Mediterranean maquis site, plants are evergreen instead (schlerophyllous species) and the four season period is investigated as vegetation cover does not change during the year.

2.2.1   Serdiana vineyard

Serdiana territory is located in southern Sardinia, Italy ($39.36°$ N, $9.12°$ E, 112 m asl) at about 20 km north of Cagliari, Sardinian capital. The vineyard (Vermentino grapevine variety), managed by the Argiolas company, was planted in 2000 and extends for 8 ha. Also, it is trained in a Guyot system with rows oriented east-west and separated by 2.1 m whereas plants are 0.8 m apart. During the summer growing season, vegetation is at its maximum, reaching a height of about 2.0 m and an orthogonal projection of about 50% above the clay soil.

EC measurements have been collected since June 2009 and a meteorological and radiometric station (measurement height of 2.8 m above the ground), located within the vineyard, measured the main meteorological variables (air temperature, relative humidity, wind speed and direction, precipitation), incoming and outcoming solar radiation, and photosyntetically active radiation (PAR). Moreover, soil temperature and moisture were monitored at -0.20 m, -0.40 m, and -0.60 m in several vineyard locations.

The climate is typically Mediterranean. Sardinian Regional Agency for Environmental Protection (ARPAS) processed and provided climatic data indicating air temperature values ranging from a minimum of $11.3°C$ to a maximum of $21.2°C$ and a 30-year (1971-2000) annual average of $16.9°C$. Precipitation occurs mainly during spring and autumn seasons and annual mean value is 484 mm. During summer, drought conditions are frequent and a drip system is used to occasionally irrigate the vineyard. Dominant wind directions are from North-West (Mistral) and South-West (Sirocco) direction. During the growing season (May-September), measured Leaf Area Index (LAI) range is $1.2 – 3.2$ m^2 m^{-2}.

(a) Serdiana vineyard

(b) Eddy Covariance tower

(c) Meteorological station

(d) Net radiometer

(e) Rain gauge

Figure 2.4: *Serdiana vineyard experimental site and instruments*

(a) Col d'Orcia vineyard in the distance and surroundings

(b) Eddy Covariance tower over the vineyard

Figure 2.5: *Montalcino vineyard experimental site*

2.2.2   Montalcino vineyard

The area of Montalcino is located in a typical hilly countryside of Tuscany, central Italy, at about 40 km south of Siena. As the crow flies, it is about 40 km from the sea and 100 km from the Apennines. Montalcino territory is a square surrounded by Ombrone, Asso, and Orcia rivers. It extends for 24000 ha and, on the southern side, the Amiata mountain (1740 m) acts as a natural barrier often preventing Montalcino area from storms and abrupt atmospheric events. Only 29% of total surface cover is flat whereas 70% are hills and 1% mountain. Vineyards cover about 15% of the total area (Figure 2.5) and grapes variety tilled there (Sangiovese) are famous because of the Brunello wine production.

In 2005 and 2006, during the summer season (June, July and August), two field campaigns provided EC measurements of the 30-years old Sangiovese grapevines of Col d'Orcia (43.08° N, 11.8° E, 220 m asl). The vineyard is trained in a curtain system (Figure 2.5), it is not irrigated and rows are north-south oriented 3 m apart with plant separation of 1 m (Marras, 2008). During

the experimental campaign, measured LAI varied between 1.26 and 1.55 m^2 m^{-2}. The maximum vegetation cover is about 50% during the summer growing season with grapevines reaching a mean height of 2 m. The fetch was about 400 m in the upwind direction whereas measurement height was 2.8 m above the ground.

The climate is Mediterranean with some continental influence due to its position between the sea and the Apennines. Mean annual air temperature is 12.4°C and precipitation, occuring mainly in spring and late autumn, is 691 mm on average. During winter, snowfalls may occur above 400 m elevation. Fog and frosts rarely affect lower altitudes due to frequent windy conditions. Despite the small size of the area, due to the complexity of the terrain, microclimates are generated between valleys and mountain land.

2.2.3 Mediterranean maquis

Mediterranean maquis (schlerophyll species) is a typical evergreen ecosystem consisting of short shrubs with leathery leaves sparsely distributed. It is adapted to live in a semi-arid climate as that of Mediterranean coasts[1]

In this study, the monitored ecosystem is located in the Capo Caccia peninsula (municipal district of Alghero (SS), Italy) inside a natural reserve called *Prigionette*, also known as *Arca di Noé*, in the North-West Sardinia coast (40.61° N, 8.15° E, 74 m asl). The site extends for 1200 ha and, on the western side, the sea and a steep coastline with deep sea cliff (Pt. Cristallo, 326 m and Mt. Pegna, 271 m) mark its boundary whereas, on the northeastern side, Mt. Timidone, 361 m rises.

---

[1]Outside the Mediterranean basin this kind of ecosystem can be also found in California, Chile, South-Africa and southern-Australia in regions with similar climate (Spano et al., 2003b).

At this site, Mediterranean maquis appears as a shrub land of different species[2] (Figure 2.6), mainly juniper (53%) and lentisk (22%), randomly distributed in the measurement area.

At this site, geological substrate consists of Mesozoic limestone. The main soil type is Terra Rossa (Lithic Xerorthent and Typic Rhodoxeralfs), rocky and shallow with sandy loam texture in it. Soil depth is 30-40 cm and because of its consistency it is highly erodible (Spano et al., 2009).

In 1963 a fire destroyed vegetation and in 1970 the site was untended but the vegetation has now grown back. It has been monitored with an EC tower since April 2004. Measured total Leaf Area Index (LAI) ranges between $2.7 - 3.0$ m^2 m^{-2}. Maximum canopy height is around $2 - 2.5$ m and the discontinuous vegetation cover is 70% on average. EC measurement height is 3.5 m above the ground with a fetch of 800 m.

Climate is typically Mediterranean with mild winter seasons and warm summer when drought period occur (usually from May to September). Average annual air temperatures (1961-1990) is $15.9°$ ranging from a minimum of $7°C$ and a maximum of $28°C$ with an average annual thermal excursion of $14°C$ which is lower in early winter ($10°C$ in January) and higher in late summer ($24°C$ in August) (ARPAS data). Spring and autumn are the rainy seasons and mean annual rainfall are 588 mm. Strong predominant north-west (Mistral) and south-west winds blow in this area. Mediterranean maquis site is naturally well watered during the cold season and in the early spring, when the plants have greatest range of environmental conditions for physio-

---

[2]Juniper (*Juniperus Phoanicea* L.), lentisk (*Pistacia lentiscus* L.), tree phyllirea (*Phyllirea angustifolia* L.), dwarf fan palm (*Chamaerops humilis* L.), rosemary (*Rosmarinus officinalis* L.), *Genista corsica* (Loisel) DC., *Daphne gnidium* L., *Smilax aspera* L., *Euphorbia characias* L., *Helichrysum microphyllum* DC., *Asphodelus microcarpus* Salzm., and *Ferula communis* L. (Marras et al., 2011).

(a) View of Maquis vegetation at the site

(b) Location of the Eddy Covariance station in the Capo Caccia peninsula (red circle)

Figure 2.6: *Capo Caccia Mediterranean maquis site*

logical processes, whereas, in summer, water stress conditions occur due to reduced rain events frequency and increased, prolonged temperature values.

2.2.4 Micrometeorological measurements

The EC method was used to measure carbon and water exchanges between the Mediterranean ecosystems and the atmosphere. The instrumentation was the same for the three sites and powered by solar panels. For measurements of vertical wind speed and CO_2/H_2O concentration the instrumentation consisted of a 3D sonic anemometer (CSAT3, Campbell Scientific Inc., Logan, UT, USA), an open-path infrared gas analyzer (Li-7500, Li-Cor Biosciences, Lincoln, NE, USA) and a CR5000 and CR1000 datalogger (Campbell Scientific Inc., USA). All data were acquired at 10 Hz and fluxes determined for 30 minutes. Radiation balance components were measured at a frequency of 10 Hz using a four-component net radiometer (MR40, Eko Instruments, Tokyo, Japan) and stored in the CR23X datalogger (Campbell Scientific Inc., USA). PAR measurements were carried out by using the

quantum sensor Skye SKP 215 (range $400 - 700$ nm). Air temperature and humidity were hourly measured using the HMP45C probe (Campbell Scientific Inc., USA) whereas an aerodynamic rain gauge (ARG100, Environmental Measurements Limited, UK) was used to record precipitation data every hour.

To have a representative measure of soil heat flux (G) four heat plates (HFP01SC, Hukseflux, Delft, NL) were located at -0.07 m underground, along a transect between rows in the two vineyards and in four different positions to account for under canopy and bare soil conditions in the maquis ecosystem. In addition, for each plate, four thermocouples monitored soil temperature gradient between -0.07 m and the surface to account for heat storage and to estimate surface G flux. Also soil water content (SWC) was measured in both ecosystems by using the two Time-Domain Reflectometry probes (Model CS616-L, Campbell Scientific Inc., Logan, UT,USA). Instruments were buried at different depths: -0.20 m and -0.30 m in Maquis ecosystem and -0.20 m, -0.40 m and -0.60 m in the Sardinian vineyard. In this analysis, the shallow data (-0.20 m) are used. LAI measurements were carried out by using a LAI2000 (Li-Cor Biosciences, Lincoln, NE, USA) in Sardinian sites and an AccuPAR LP-80 (Decagon, Pullman, WA, USA) in Montalcino vineyard.

To obtain corrected energy and mass fluxes, collected data were processed using an in house software (EOLO) which was developed at the University of Sassari by the Agrometeorological laboratory of DipNET (Department of Science for Nature and Environmental Resources), according to the FLUXNET network protocol. For the three sites, data quality checks were made following the procedures of Aubinet et al. (2000), Baldocchi (1997), Papale et al. (2006), Schmid et al. (2000), Webb et al. (1980). They consisted in despik-

ing, double coordinate rotation, Webb correction for air density, stationarity test, and verification of turbulence integrity.

Data were gap filled and partitioned into NEE components (GPP and R_{eco}) using an algorithm developed following Falge et al. (2001a,b) and Reichstein et al. (2005) and available as an online tool (*http://www.bgc-jena.mpg.de/ MDIwork/eddyproc/*).

Latent (LE) and sensible (H) heat fluxes as well as net all wave radiation (R_n), and G were used to calculate the energy balance closure every 30-minute period (neglecting a small metabolic term):

$$R_n = H + LE + G \qquad (2.10)$$

the equality between $H + LE$ terms and $R_n - G$ terms is pursued with a 20-30% margin allowed by literature (Twine et al., 2000; Wilson et al., 2002). In this study, the energy balance closure calculations were in line with those reported in the literature.

Chamber measurements were carried out in Capo Caccia site, where 12 soil collars (20 cm in diameter) were placed underneath the canopy of the predominant species (70% of total land cover) and another 12 were placed in the bare soil (about 30% of total land cover) (Figure 2.7). Soil CO_2 efflux was measured once a month for about 1.5 years (April 2012 - November 2013) with a closed IRGA system (Li-8100, Li-Cor Biosciences, Lincoln, NE, USA). Soil water content and temperature were continuously measured at 5 cm depth close to two collars in the bare soil and two collars in the undecanopy.

2.2.5   Daytime measurements analysis

Diurnal CO_2 flux measurements were obtained filtering the datasets depending on global radiation and only data with $R_g > 5$ W m^{-2} were se-

Figure 2.7: *Chamber measurements location at Capo Caccia site (left) and overview of the measurements area (right).*

lected[3]. In addition, diurnal datasets were filtered excluding outliers and extreme conditions (10% of distribution tail) to focus on mean ecosystem behaviour, using variables and ranges indicated in Table 2.2.

Median values of CO_2 flux measurements, for bins of 50 $\mu mol\, m^{-2} s^{-1}$ of PAR, were used with Locally Estimated Scatterplot Smoothing (LOESS, Cleveland et al., 1992), a non-parametric regression, to determine the dominant trend of the photosynthetic light-response curve. LOESS, an extension of the Locally Weighted Scatterplot Smoothing (LOWESS, Cleveland, 1981), performs a local fit of points weighting them according to their distance from neighbours but without giving an equation. The parameter controlling the degree of smoothing, a proportion of points to be used as neighbourhood,

---

[3]All the analysis and fitting procedures described from now on, were carried out using R programming language and environment software.

Table 2.2: *Range of the selected variables used to filter datasets. A 10% threshold was used per each variable (see text for more details).*

Site	λ_V	$PAR\,(\mu mol\,m^{-2}s^{-1})$	$T_a\,(°C)$	$SWC\,(\%vol)$	$VPD\,(kPa)$
Serdiana, Italy (*Vineyard*)	≈ 0.5	< 1850	$13 - 36$	< 27	< 7
Montalcino, Italy (*Vineyard*)	≈ 0.5	< 1900	$18 - 35$	N.A.	< 5
Capocaccia, Italy (*Mediterranean Maquis*)	≈ 0.7	< 1900	$10 - 32$	< 38	< 4

was set to 0.4. As the LOESS curve approximated the NRH form (equation 2.6), non-linear least squares (nls) regression was used to calculate the best four values for the NRH coefficients (α, β, γ and θ).

Similarly, when SWC measurements were available (Serdiana and Capo Caccia sites), data were split into SWC classes and binned medians were used to establish photosynthetic light-response curves and to look at the influence of soil moisture on CO_2 flux measurements. Thus the variability of α, β, γ and θ coefficients with SWC was investigated for two different ecosystems. When the estimated θ values were not statistically significant, a fixed value was arranged. This was obtained directly from the fitting procedure per SWC classes (as for Capo Caccia) or considering the entire dataset (as for Serdiana).

2.2.6 Nighttime measurements analysis

During nighttime ($R_g < 5$ W m^{-2}), when diurnal photosynthesis processes are switched off, EC measurements are representative of R_{eco}. During the year, ecosystem respiration is affected by the seasonal change (for deciduous ecosystems) and vegetation response to environmental conditions,

especially temperature and water availability. Multiannual datasets were analyzed (for that reason Montalcino vineyard is not accounted in this analysis, as data were only measured for short periods during the summer season). Nocturnal measurements were filtered by an u* threshold detected according to Reichstein et al. (2005) methodology, briefly described below. As a first step, T_{air} quantiles were calculated in order to divide the complete dataset into six classes. For each of these temperature classes, CO_2 measurements were then binned into 20 u* intervals of 0.05 m s^{-1} and an average value for the highest u* bins was calculated. The lowest u* class, whose value (not correlated to T_{air}) was greater or equal to 95% of the average, was identified as local threshold. Finally, all six local thresholds were estimated and their median value was identified as the final one (Figure 2.8). Data below that threshold were rejected from further analysis.

Similarly to diurnal measurements analysis, highest and lowest variables values were omitted (10% of distribution tail) in order to focus on mean ecosystem behaviour, using variables and ranges reported in Table 2.3.

Table 2.3: *Range of the selected variables used to filter nocturnal datasets. A 10% threshold was used per each variable (see text for more details.*

Site	λ_V	SWC (% vol)	T_a (°C)	T_{Soil} (°C)	VPD (kPa)	u* (m s^{-1})
Serdiana (*Vineyard*)	≈ 0.5	≤ 27	$4 - 27$	$6 - 30$	$0 - 2$	$0.2 - 0.6$
Capo Caccia (*Mediterranean Maquis*)	≈ 0.7	$15 - 38$	$3 - 25$	$4 - 29$	$0 - 2$	$0.25 - 1$

Binned CO_2 flux medians were then calculated every degree Celsius of soil temperature, and R_{eco} multi-annual trend was detected by using LOESS regression. Finally, equations 2.7 – 2.9 were used to reproduce experimental curves, with some parameters (T_{ref} and T_0) fixed to constant values as in the
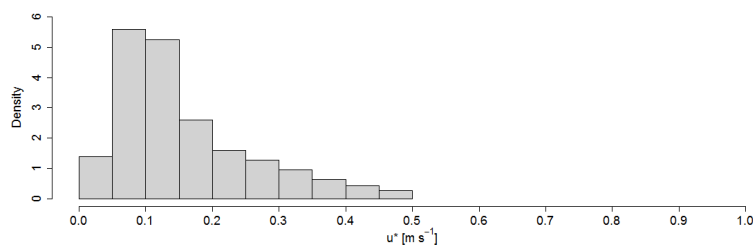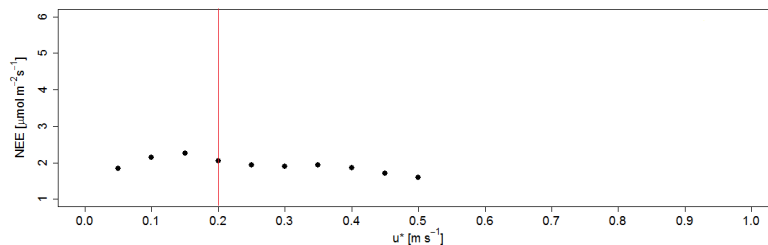
(a) Serdiana
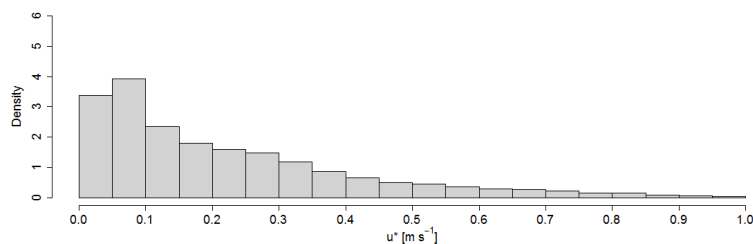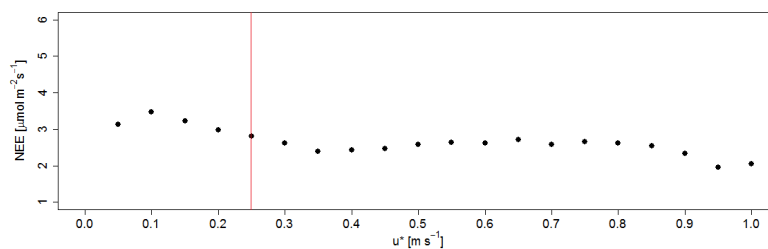
(b) Capo Caccia

Figure 2.8: *Binned CO_2 flux measurements as function of friction velocity (u*) and u* density distribution at the sites of Serdiana ((a) top and bottom, respectively) and Capo Caccia ((b) top and bottom, respectively). Friction velocity threshold (red line) was calculated and was equal to 0.2 m s^{-1} at Serdiana and 0.25 m s^{-1} at Capo Caccia.*

original study (see section 2.1.2) and the others being free and estimated by
using non-linear least squares regression.

2.2.7   Combined analysis

Through the analysis of the NEE measured fluxes (five years in the
Mediterranean maquis ecosystem and three years in the vineyard), it was
possible to find a combined approach to quantify NEE as a result of GPP
and R_{eco} models. As reported in sections 2.1.1 and 2.1.2, different equations
can be used to estimate GPP and R_{eco} from environmental variables, such
as PAR, T_{soil}, and SWC.

In the hyperbolic light-response curve, ecosystem respiration can be calcu-
lated both by a constant intercept parameter (γ) or as function of T_{air}, T_{soil},
and SWC (equations 2.7 – 2.9). A soil temperature-dependent equation was
used by Gilmanov et al. (2006) and Lasslop et al. (2010). Gilmanov et al.
(2006) combined the NRH (equation 2.6) with a simple exponential function
by using daytime and nighttime data, whereas Lasslop et al. (2010) used
the Michaelis and Menten function (Ruimy et al., 1995) together with the
Lloyd and Taylor model (Lloyd and Taylor, 1994) (equation 2.7) considering
daytime data.

In this study, the proposed approach is a combination of the two above
mentioned methods, that is a combination of the NRH (equation 2.6) together
with the LLT (equation 2.7) model. The Lloyd and Taylor model is, then,
introduced into the NRH as follows:

$$
\begin{aligned}
NEE = R_{ref}\, exp &\left[E_0 \left(\frac{1}{T_{ref} - T_0} - \frac{1}{T_{soil} - T_0} \right) \right] - \\
&- \frac{1}{2\theta} \left(\alpha PAR + \beta - \sqrt{(\alpha PAR + \beta)^2 - 4\alpha\beta\theta PAR} \right)
\end{aligned}
\tag{2.11}
$$

This generalized NEE model is applied to diurnal multiannual data, binned

Veronica Bellucco, *Empirical estimations of CO$_2$ flux components over different ecosystems*, Tesi di Dottorato in
"Scienze e Biotecnologie dei Sistemi Agrari e Forestali e delle Produzioni Alimentari", Indirizzo "Agrometeorologia ed
Ecofisiologia dei Sistemi Agrari e Forestali", Università degli Studi di Sassari.

and fit with methods described in section 2.2.5. Some parameters of the proposed model (equation 2.11) were kept constant to avoid overparameterization: T_0 and T_{ref} were fixed to original values (see section 2.1.2), whereas θ was fixed to the value estimated through the analysis of measured data as described in section 2.2.5. E_0 was fixed from the analysis of both daytime data (section 2.2.5) and nighttime (section 2.2.6), whereas the other parameters (α, β, and R_{ref}) were estimated only using daytime measurements.

2.3   Results and discussion

This section is divided in two parts. The subsection 2.3.1 reports the main results related to EC flux measurements recorded over the two Sardinian sites (Mediterranean Maquis and vineyard). Per each site, it gives information about the environmental conditions, energy, water, and CO_2 measured fluxes with the aim of highlighting the different physiological and environmental processes over the two ecosystems. The subsection 2.3.2 describes the results obtained through the empirical approach developed to estimate and partition the NEE into its main components. It also analyzes the relation between the CO_2 flux and drought conditions in order to understand the behaviour of the studied ecosystems under Mediterranean climate condition.

2.3.1   Flux measurements

Before presenting the observed fluxes[4], a brief description on the environmental conditions in the Mediterranean Maquis site (2005 – 2010) and in the Sardinian vineyard (2009 – 2011) will be presented, that can help to

---

[4]Raw data were processed by the Agrometeorological laboratory of DipNET (University of Sassari), whereas further data analysis is part of this study.

Veronica Bellucco, *Empirical estimations of CO_2 flux components over different ecosystems*, Tesi di Dottorato in "Scienze e Biotecnologie dei Sistemi Agrari e Forestali e delle Produzioni Alimentari", Indirizzo "Agrometeorologia ed Ecofisiologia dei Sistemi Agrari e Forestali", Università degli Studi di Sassari.

understand the observed fluxes dynamics and budgets.

Both sites are characterized by Mediterranean climate, with drought summer periods and precipitation mainly concentrated in spring and fall.

Measurements showed that mean air temperature ranged from 14.9°C in 2010 to 16.7°C in 2006 and 2007 in the Maquis site, while in the Sardinian vineyard the main air temperature varied from 15.8°C in 2010 to 17.5°C in 2009 (Table 2.4). Maximum air temperature values occurred during summer, both over maquis vegetation (40°C in July 2009) and over the vineyard (42°C in July 2009), whereas minimum values ranged from -4.7°C in February 2009 in the maquis site to -2.60°C in January 2010 in the vineyard.

The main differences in environmental conditions were due to the amount of precipitation during the years, whereas the seasonal trend, characterized by rainfall mostly concentrated from November through March, was similar.

At both sites, the year 2010 was characterized by lower air temperature and more precipitation amount (Table 2.4), whereas years 2006, 2007, and 2009 showed annual precipitation values lower than climate data. In particular, years from 2006 to 2009 were also characterized by air temperature values warmer than normal.

Measured variations in soil water content were mainly related to precipitation patterns. In the maquis site, values of volumetric soil water content (SWC) were the mean of data measured at 0.20 m and 0.30 m (Figure 2.9,top), while in the vineyard they correspond to the mean of measurements collected at 0.20 m and 0.40 m (Figure 2.9, bottom). At both sites, SWC pattern shows a clear decrease in SWC during summer and an increase after the first rainfall events in the early fall. In the maquis site, SWC values ranged between about 13% in September 2005 to about 80% in September 2010 due to a rainy event with a total amount of more than 88 mm of precip-

Table 2.4: *Climate data and mean annual values of air temperature (°C) and precipitation (mm) measured by a nearby weather station.*

Capo Caccia (Medit. maquis)	T_{mean} (°C)	Precipitation (mm)	Serdiana (vineyard)	T_{mean} (°C)	Precipitation (mm)
Climate (1961-1990)	15.9	588	Climate (1971-2000)	16.2	426
2005	15.7	596			
2006	16.7	442			
2007	16.7	395			
2008	16.4	656			
2009	16.6	454	2009	16.6	385
2010	14.7	576	2010	15.7	457
			2011	16.2	366

itation (Figure 2.9, top). In 2010, SWC values were in general higher than other years, due to the more precipitation occurred during the year.

In the vineyard, minimum SWC value occurred in November 2010, while maximum values (more than 30%) were registered during the winter and spring in 2011, mainly associated to precipitation. During summer, SWC varied between 20 and 30% due to irrigation events. Consecutive peaks in SWC values clearly revealed the irrigation applied by the company. Only in summer 2011, SWC reached more than 35% because of both irrigation and precipitation occurred during the summer months.

Ecosystems behavior in terms of energy and mass fluxes was investigated to understand the ecosystem function in relation to the environmental characteristics. Figure 2.10 shows the energy balance trend in the maquis (top) and vineyard (bottom) site. Specifically, daily trend of net radiation (R_n), sensible heat (H), latent heat (LE), and soil heat (G) fluxes are shown.

R_n represents the energy used by the ecosystem for the different processes: to heat/cool the air (as sensible heat flux, H), for water evapotranspiration/condensation (as latent heat flux, LE), and to heat/cool the soil
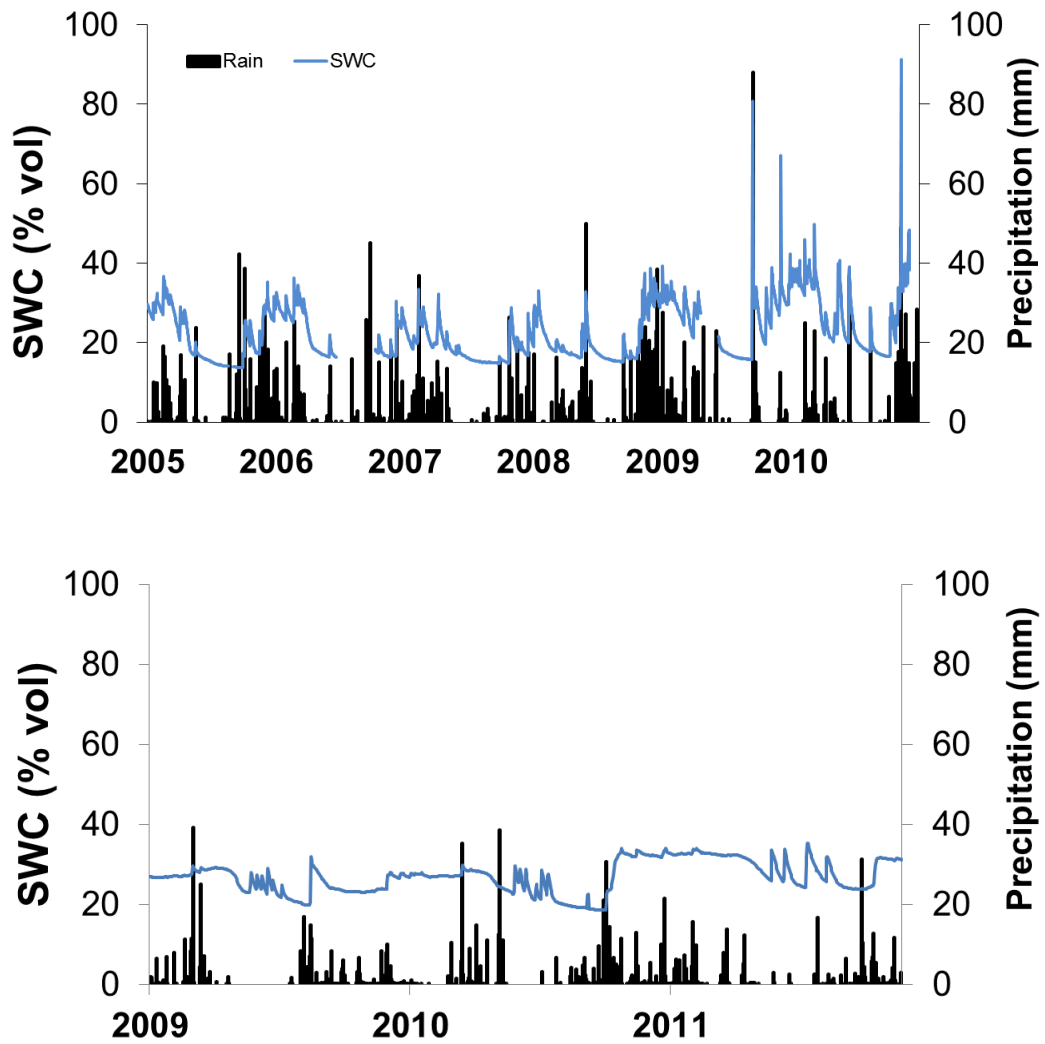
Figure 2.9: *Interannual variation in daily precipitation and mean volumetric soil water content (SWC) measured in the Capo Caccia maquis site (top) and in Serdiana vineyard (bottom). See text for details about measurements depth.*
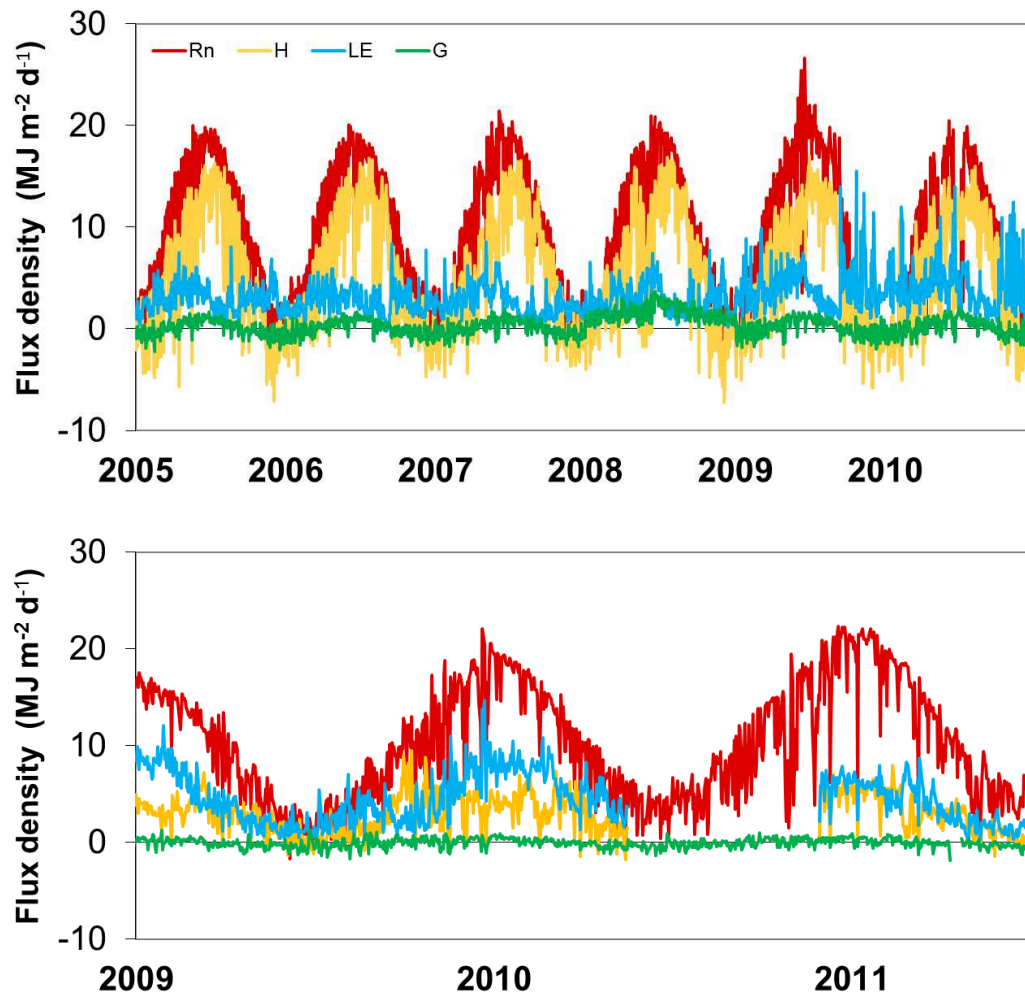
Figure 2.10: *Daily trend of net radiation (R_n), sensible heat (H), latent heat (LE), and soil heat flux (G) during 2005-2010 in the maquis site (top) and during 2009-2011 in the vineyard site (bottom). Half-hourly gap-filled data were used to obtain the daily budget.*

(as soil heat flux, G). A clear seasonal pattern is evident in both sites, with higher R_n values during summer and lower in winter. Maximum values are around 20 MJ m^{-2} d^{-1}, except in 2009 for maquis and 2011 for the vineyard, where some days with $R_n > 20$ MJ m^{-2} d^{-1} occurred.

In the maquis site, H values were higher than LE, indicating that most

of the energy was used to heat the air. LE values were clearly related to the precipitation amount and patterns, showing higher values during spring and fall and a decrease during summer periods. Only in 2010, LE showed values similar or higher to H in some days, due to the more precipitation amount occurred during that year (Figure 2.10, top). The maquis ecosystem was then characterized by water deficit conditions, which affected the amount of evapotranspiration. Maquis species, however, have mechanisms to adapt to drought condition, so vegetation still continued to be active, even at a small rate. This behavior was similar along the years, showing the typical ecosystem behavior at Mediterranean climate. Soil heat flux (G) generally showed a similar trend during the five years, with lower values during November and December and higher values during summer (Figure 2.10, top).

The R_n partitioning in the vineyard site showed a different pattern (Figure 2.10, bottom). More available energy $(R_n - G)$ was partitioned to LE than to H during summer, presumably because there was adequate water availability from irrigation. In some case, LE was higher than H, for example during summer months in 2010, when precipitations were higher than other years. From late August to the end of the year, energy was approximately equally partitioned between H and LE. Also in this ecosystem, G pattern was similar along the years.

Eddy Covariance stations allowed measuring carbon fluxes over the two Mediterranean ecosystems and provided the quantification of the carbon sequestered or released from each site. The NEE could be positive or negative.

Negative values of NEE imply that the ecosystem is a *sink* for carbon (uptake by photosynthesis is greater than losses by respiration), while positive values mean that the ecosystem is a *source* of carbon. The analysis of measured NEE fluxes is, therefore, useful to understand the role of ecosystems

in the global carbon balance.

NEE values were expressed in μmol m^{-2} s^{-1} and converted to g C m^{-2} for each 30-minute period. In addition, daily, monthly, and annual sums were calculated. Moreover, measured NEE was partitioned between Gross Primary Production (GPP) and ecosystem respiration (R_{eco}) following the Reichstein et al. (2005)[5].

The general trend of NEE values measured over maquis ecosystem showed negative fluxes (C sink) from January to July and positive fluxes from August to October (respiration processes greater than photosynthesis). At the end of the year, the ecosystem returned to be a carbon *sink* even at a reduced rate (Figure 2.11, top). During spring the ecosystem showed the highest physiological activity, mainly due to the absence of limiting factors. Both the controlling variables for this kind of vegetation (energy and water) were at the optimum level. Drought periods, instead, occurred every summer, negatively controlling the physiological processes. Photosynthesis is reduced and respiration increased, leading to positive NEE values.

At daily scale, the mean carbon uptake was -0.66 g C m^{-2} d^{-1}, whereas the maximum value was observed in May 2010 (-6.81 g C m^{-2} d^{-1}). This value is lower than observed in deciduous forests (-10 g C m^{-2} d^{-1}), but similar to other coniferous forests (-6 or -7 g C m^{-2} d^{-1}) (Granier et al., 2007). In the Mediterranean area, maximum uptake of about -3 or -4 g C m^{-2} d^{-1} was observed for South European forests (Papale and Valentini, 2003).

The monthly trend in GPP showed high variability between months, mainly due to environmental conditions. Higher values of GPP occurred during spring (May), when plants found better conditions for growing (-186

---

[5]*http://www.bgc-jena.mpg.de/ MDIwork/eddyproc/*
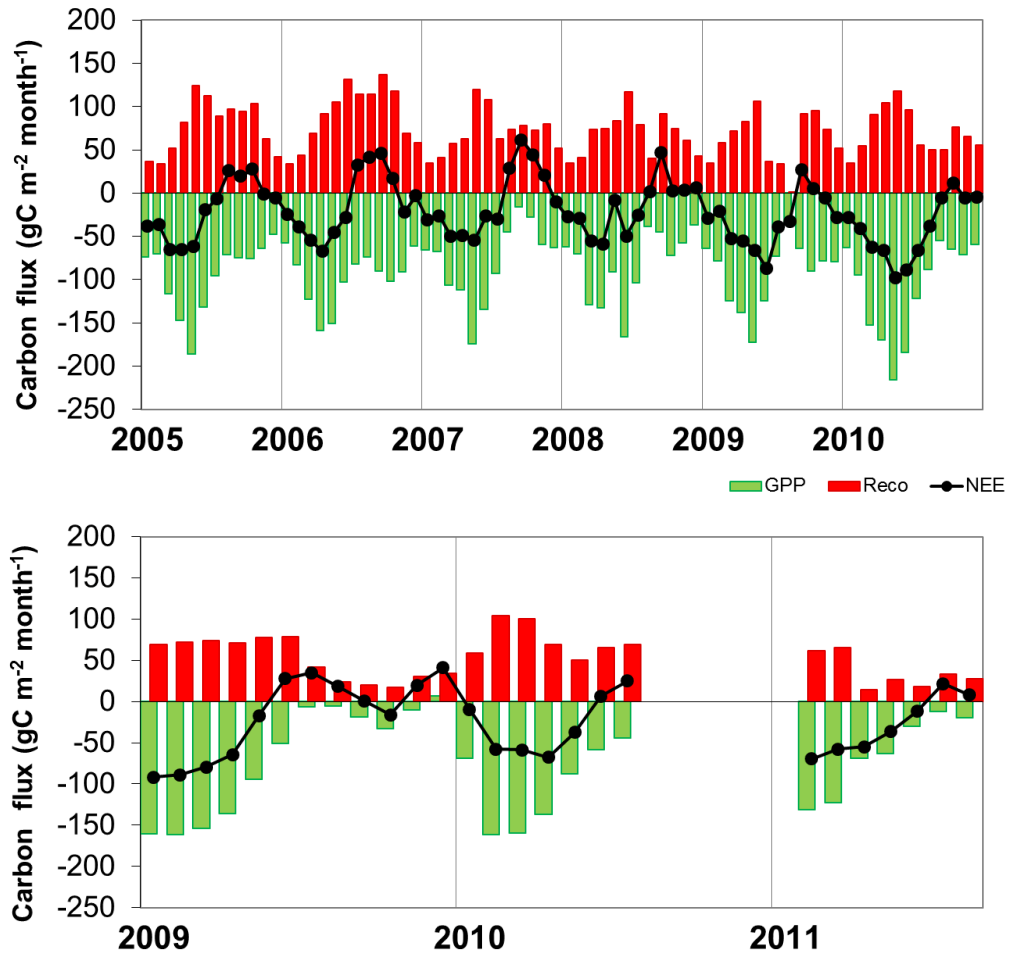
Figure 2.11: *Monthly variation in carbon flux (g C m^{-2} month^{-1}) at the maquis site (top) and the Sardinian vineyard site (bottom). Red bars represent R_{eco}, green bars represent GPP, and the black line reports NEE values.*

g C m^{-2} month^{-1} in May 2005, -174 g C m^{-2} month^{-1} in May 2009, and -216 g C m^{-2} month^{-1} in May 2010). In 2006 and 2008, the maximum GPP was registered in April (-156 g C m^{-2} month^{-1}) and June (-167 g C m^{-2} month^{-1}), respectively. Minimum GPP values occurred during winter (December and January each year), except in 2007, when -16 g C m^{-2} month^{-1} and -20 g C m^{-2} month^{-1} of GPP were observed in September and October, due to peaks in ecosystem respiration (R_{eco}).

The year 2007 was characterized by higher air temperature values and lower precipitation amount than the climate mean (see Table 2.4), so the ecosystem experienced a pronounced drought summer. The first rainfall events after summer stimulated mibrobes and plants activity resulting in R_{eco} peaks (Figure 2.11, top). The average R_{eco} during the five years was 2.42 g C m^{-2} month^{-1}.

Chamber measurements carried out at the maquis site, both underneath the shrubs canopy (UC) and on the bare soil (BS), provided an indirect comparison to nocturnal EC results. Nocturnal EC flux measurements are indeed representative of ecosystem respiration whereas chamber measurements represent only the soil efflux contribution (R_S). As a consequence, from EC and chamber results comparison it is possible to understand how much the soil contributes to ecosystem respiration.

In Figure 2.12 (top and central picture) R_S and soil temperature (T_{soil}) time histories are compared for both UC and BS data. The temporal trend of R_S and soil water content is also shown in Figure 2.12 (bottom). Both UC and BS measurements revealed the presence of a limiting factor and a double dependence of soil respiration on temperature and SWC. In particular, a reduction of soil respiration processes occurred when soil temperature values exceeded 20°C. At the same time, water availability also affected R_S both at
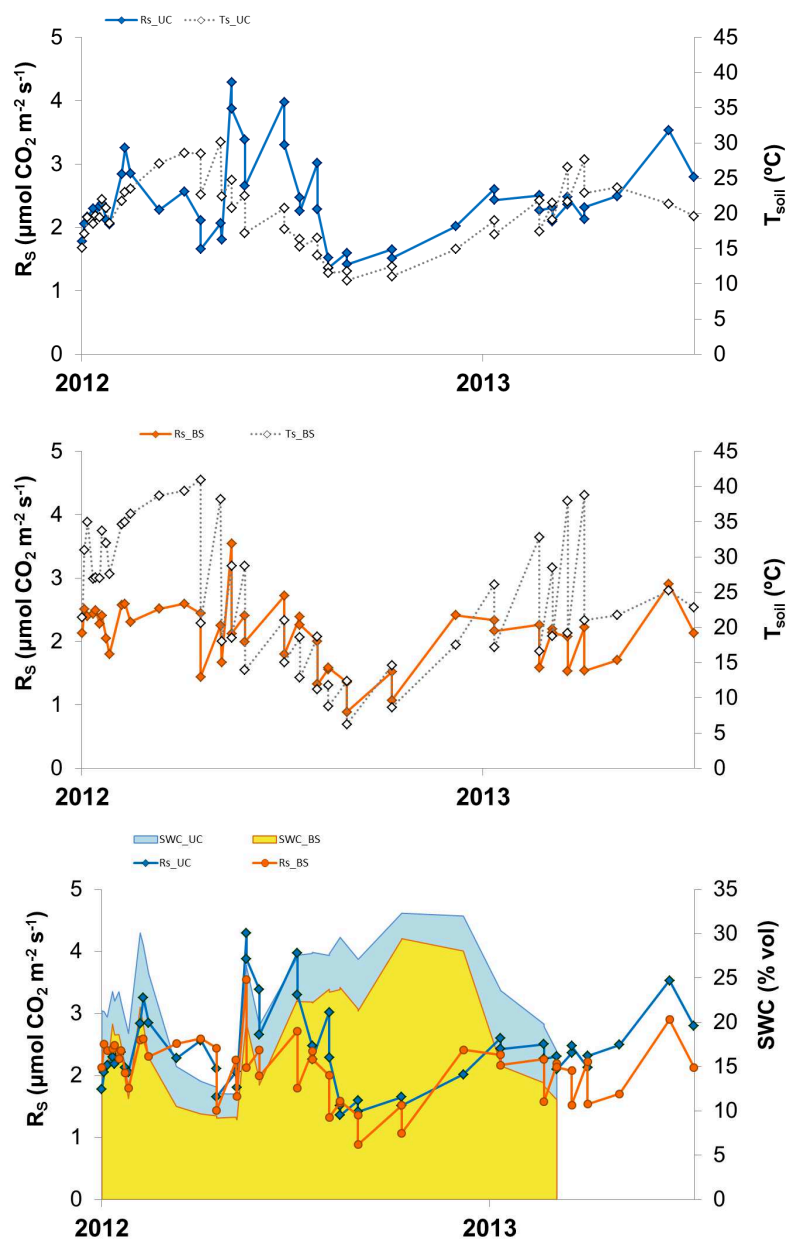
Figure 2.12: *Daily data of soil respiration R_S and soil temperature (T_{soil} collected by chamber measurements during the field campaign period (April 2012 - November 2013) at Capo Caccia site. Underneath the shrubs canopy (UC) measurements are reported in the top panel, whereas measurements on the bare soil (BS) are reported in the central panel. The bottom panel shows R_S data, both UC and BS, and soil water content (SWC) measurements.*

highest and lowest SWC. Therefore, soil respiration decreased at high T_{soil} and water stress conditions but also when temperatures were low and water availability was high. The scatterplot in Figure 2.13 shows the comparison between EC and chamber measurements. R_S is plotted as function of soil temperature and binned in 1°C intervals. On average, soil respiration was about 75% of ecosystem respiration, with UC being more influential (about 80%) than BS soil efflux (about 70%). Because the bare soil corresponds to only about one third of total soil cover, scaling previous results, the UC soil efflux contributed for about 55% and BS only for about 20%, being together 75% of total ecosystem respiration. As a residual, vegetation respiration was therefore 25% influential.

At annual scale, the maquis ecosystem acted as a carbon *sink* even if large variability was observed between years. Annual NEE values ranged from -123 g C m^{-2} y^{-1} in 2007 to -494 g C m^{-2} y^{-1} in 2010, whereas on average the maquis site was able to annually sequester -262 g C m^{-2} y^{-1} (Table 2.5). These values are higher than other shrub land ecosystems. For example, Mexican shrub ecosystem showed mean carbon uptake around -45 g C m^{-2} y^{-1} due to low annual precipitation (Hastings et al., 2005), whereas a mature semiarid chaparral ecosystem sequestered less than -200 g C m^{-2} y^{-1} in California during seven years (Luo et al., 2007). Similar annual NEE values (-107 < NEE < 407 g C m^{-2} y^{-1}) were found by Powell et al., 2006 for a scrub oak ecosystem in Florida, whereas higher values were found for European forests: NEE greater than 700 g C m^{-2} y^{-1} in the North of Italy (Marcolla et al., 2005) and NEE around 400 g C m^{-2} y^{-1} was observed in Mediterranean pine forests in Tuscany (Tirone et al., 2003).

Agriculture ecosystems show a different behavior regarding carbon sequestration and release. So far, only a few studies focused on measuring CO_2
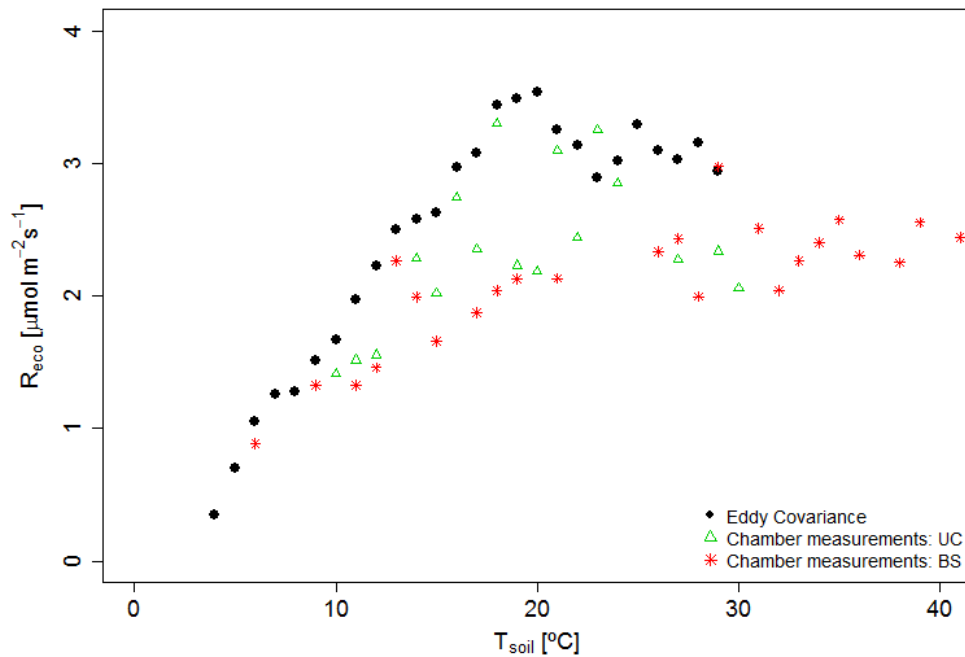
Figure 2.13: *Respiration curves as function of soil temperature at Capo Caccia site. Black dots represent u* filtered nocturnal eddy covariance data (2005 – 2011), green triangles represent chamber measurements (April 2012 – November 2013) underneath the canopy, and red stars represent bare soil chamber measurements. All data were binned in 1°C intervals.*

fluxes over grapevine ecosystems with the aim to investigate the role of this ecosystem in the carbon balance. In addition, previous studies only showed NEE measured in short-term periods (Spano et al., 2003a, 2008), whereas a three years period was analyzed by Guo et al. (2014) in arid northwest China.

Measured NEE values at Serdiana site showed an average daily value of -0.65 g C m^{-2} d^{-1} during the three years. Maximum daily carbon uptake occurred on 21 June 2010 (-3.47 g C m^{-2} d^{-1}), whereas maximum emissions

Table 2.5: *Annual cumulated values of NEE during the five years at the maquis site.The percentage of gap-filled data ranged from 20% (in 2010) to 50% (in 2007).*

Year	NEE (g C m^{-2} y^{-1})
2005	-226.29
2006	-147.17
2007	-123.03
2008	-195.13
2009	-384.45
2010	-493.79
Average	-261.64

were registered on 26 March 2010 (2.19 g C m^{-2} d^{-1}). The average carbon uptake was lower than the other vineyard ecosystem (Montalcino, Tuscany) analyzed in this thesis where Eddy Covariance measurements showed that the vineyard acted as a carbon *sink* with an average daily value of about -2 g C m^{-2} d^{-1} (Spano et al., 2003a, 2008). Moreover, a vineyard located in the North of Sardinia showed an average value of -4.32 g C m^{-2} d^{-1} (Spano et al., 2003a), whereas in the South of Italy average daily carbon exchanges of about -2 g C m^{-2} d^{-1} were obtained by Rossi et al. (2004).

Monthly NEE values revealed a clear pattern in carbon flux. The vineyard was a net carbon *sink* during the growing period (May-October), when vegetation is present (Figure 2.11, bottom). Maximum carbon uptake was in July and August (-79.69 g C m^{-2} month^{-1} and -64.42 g C m^{-2} month^{-1} in July and August 2009, respectively; -58.63 g C m^{-2} month^{-1} and -67.80 g C m^{-2} month^{-1} in July and August 2010), whereas in 2011 the highest NEE values were registered in June and July (-69.54 g C m^{-2} month^{-1} and -57.71 g C m^{-2} month^{-1}, respectively). These months were probably char-

acterized by better environmental conditions (more precipitation and lower air temperature) than in 2009 and 2010.

Every year, net carbon emissions occurred in winter and early spring, with values ranging from 6.54 g C m^{-2} month^{-1} in October 2010 to 40.81 g C m^{-2} month^{-1} in April 2010. The soil between rows is covered by grass during winter and early spring, and this clearly mitigated the release of carbon in absence of plant leaves. Lower values of carbon emissions are, in fact, observed in January and October 2010. In addition, the vineyard is usually managed and soil tillage practices directly affected soil carbon emissions. The negative trend in carbon emissions from December 2009 to February 2010 was clearly interrupted by the use of tractors to till the soil, resulting in peaks in carbon emissions in March and April 2010 (R_{eco} greater than GPP) (Figure 2.11, bottom). From June to the end of 2009, the vineyard was a net C *sink*, with a cumulated NEE value of -169 g C m^{-2} period^{-1}. From January to October 2010 the *sink* was about 180 g C m^{-2} period^{-1} and from late May to December 2011 the vineyard accumulated about 214 g C m^{-2} period^{-1}.

Each year, a certain degree of variability was observed in the carbon accumulated during the growing period (June-September), probably depending on weather conditions. As an example, in 2010, C sequestrated by the vineyard was higher than during the other two years (Table 2.6).

The total carbon sequestered by the vineyard during the measurement period was about 616 g C m^{-2} period^{-1}. In order to have the carbon balance for a complete year with direct measurements, the sum of NEE from October 2009 to September 2010 was calculated. At annual scale, the vineyard acted as a carbon *sink* absorbing 105 g C m^{-2} y^{-1}.

In China, the three years study conducted by Guo et al. (2014), showed

Table 2.6: *NEE monthly values during the growing period (June-September) at the Sardinian vineyard. The percentage of gap-filled data ranged from 2 % to 30 %.*

Growing period	NEE		
	g C m^{-2} month^{-1}		
	2009	**2010**	**2011**
June	-89	-58	-70
July	-80	-59	-58
August	-64	-68	-55
September	-17	-37	-36
Tot.	-250	-222	-218

an annual mean of 868 g C m^{-2} y^{-1}, clearly higher than the Sardinian site. In addition, other forest sites (Valentini et al., 1996), and agricultural ecosystems (Hollinger et al., 2005; Schmidt et al., 2012) showed higher carbon sequestered at annual scale, while the Sardinian vineyard showed values similar to grassland ecosystems (Mudge et al., 2011; Peichl et al., 2012; Zenone et al., 2013), showing that vineyard could have a strong carbon sink efficiency.

The analyses of carbon exchange fluxes over the two Mediterranean sites showed the ability for both ecosystems to act as a carbon *sink* at annuals scale, even if large variability was observed between years and during the growing period in the vineyard ecosystem, mainly attributed to the environmental conditions. Regressions analysis indicated that air temperature and water availability are the main factors affecting C uptake. In dry climate, as Mediterranean climate, water resources are limited, especially during summer and can affect the ecosystem functioning.

2.3.2   NEE empirical estimation

Daytime

Daytime EC measurements account for the uptake of atmospheric CO_2 by vegetation photosynthesis. As described in section 2.1.1, solar radiation (R_g) is plants primary energy source and it is used to drive all ecosystem processes. Plants sequestration of CO_2 due to photosynthetic activity increases with increasing PAR values until a plateau is reached due to a light-saturation effect. At high PAR values, associated with clear skies and high air temperatures, plant stomata may close to limit water loss, thus limiting also the CO_2 uptake.

The light-response curves of binned CO_2 flux medians values, together with their interquartile range, are shown in Figure 2.14 in which the LOESS regression curve and the non-rectangular hyperbolic fit at the three Mediterranean sites are also plotted.

The vineyard ecosystems show a similar behaviour with narrower interquartile range for the spread of data, whereas maquis ecosystem show a broader one due to the NEE response to seasonality environmental conditions.

The photosynthetic light-response curves fit with the non-rectangular hyperbola (equation 2.6) and α, β, γ, and θ coefficients were estimated using the R software environment following the methodology described in section 2.2. Non-linear regression results are shown in Table 2.7 and Figure 2.14.

In agreement with the expectation of constant mean ecosystem quantum efficiency for standard CO_2 concentration conditions and temperature (Boote and Loomis, 1991), the α parameter has little variability among the sites (0.005 μmol CO_2 μmol photons^{-1}) and it is similar at Capo Caccia and

Veronica Bellucco, *Empirical estimations of CO_2 flux components over different ecosystems*, Tesi di Dottorato in "Scienze e Biotecnologie dei Sistemi Agrari e Forestali e delle Produzioni Alimentari", Indirizzo "Agrometeorologia ed Ecofisiologia dei Sistemi Agrari e Forestali", Università degli Studi di Sassari.
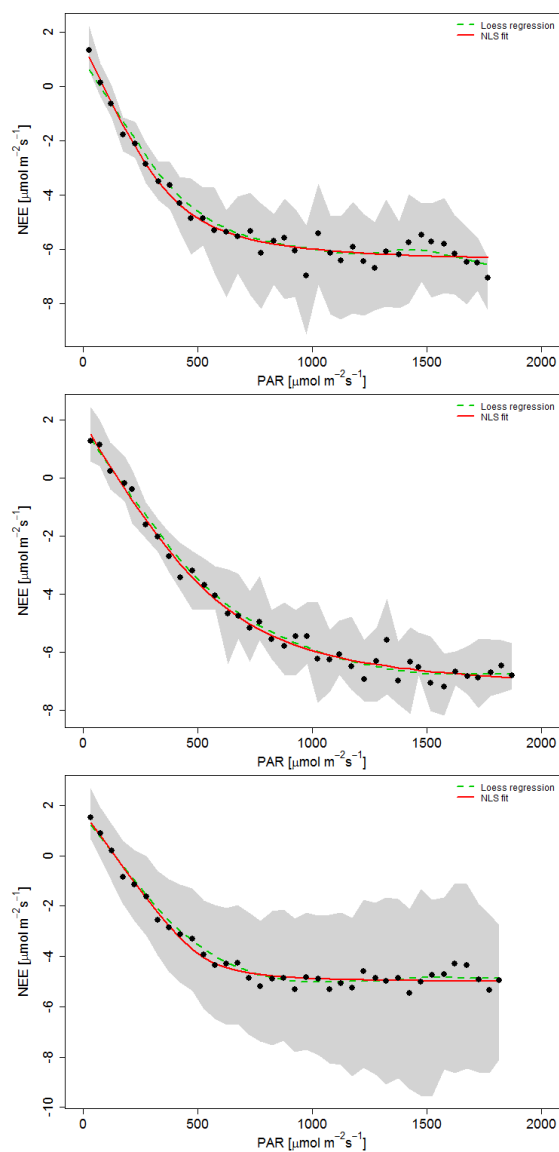
Figure 2.14: *Photosynthetic light-response curves in the Mediterranean sites during the photosynthetically active period. Trends of daytime ($R_g > 5\,W\,m^{-2}$) multi-year CO_2 fluxes as function of PAR. Data are sorted in bins of $50\,\mu mol\,m^{-2}s^{-1}$ and fitted using LOESS regression and non-rectangular hyperbolae (equation 2.6) by non linear least squares. The shaded area is the interquartile range. From top to bottom: Serdiana ($R^2 =0.97$) and Montalcino ($R^2 =0.99$) vineyards, and Capo Caccia Mediterranean maquis ($R^2 =0.98$). Different scales for NEE representation are used in the figures.*

Montalcino (0.013 μmol CO_2 μmol photons^{-1}) whereas it takes a higher value at Serdiana (0.018 μmol CO_2 μmol photons^{-1}).

The gross photosynthetic assimilation (β) varies from about 7 μmol CO_2 m^{-2} s^{-1} in maquis ecosystem to about 9 μmol CO_2 m^{-2} s^{-1} in Serdiana vineyard. An estimate of the ecosystem respiration is provided by the intercept (γ) which varies from about 1.6 μmol CO_2 m^{-2} s^{-1} at Serdiana to about 1.9 μmol CO_2 m^{-2} s^{-1} at Montalcino. The bending parameter, θ, does not drop below 0.7 and its range (0.86-0.97) is in accordance with Boote and Loomis (1991), Gilmanov et al. (2003), Marshall and Biscoe (1980) and Ögren (1993).

The fitting procedure of the light-response curves at different SWC, carried out in sites where SWC measurements were available (Serdiana and Capo Caccia ecosystems), provided significative (P < 0.0001 from F-test) estimates of the NRH coefficients (Table 2.8, Figure 2.15).

In both sites, it is evident a range of variability in the coefficients related to SWC. The variation of β shows that the more the soil is watered, the more CO_2 the ecosystem is able to sequester.

Table 2.7: *Non linear regression results for the non rectangular hyperbola equation (equation 2.6) coefficients. In brackets approximated standard errors of the estimates are indicated. All the parameter estimates are significant with P < 0.0001.*

Site	α [$\mu mol\, CO_2$ $\mu mol\, photons^{-1}$]	β [$\mu mol\, CO_2$ $m^{-2}s^{-1}$]	γ [$\mu mol\, CO_2$ $m^{-2}s^{-1}$]	θ dimensionless
Serdiana (*Vineyard*)	0.018 (0.003)	8.207 (0.486)	1.597 (0.355)	0.881 (0.063)
Montalcino (*Vineyard*)	0.013 (0.001)	9.469 (0.475)	1.917 (0.241)	0.862 (0.058)
Capo Caccia (*Mediterranean Maquis*)	0.013 (0.001)	6.814 (0.285084)	1.74 (0.228945)	0.972 (0.017780)
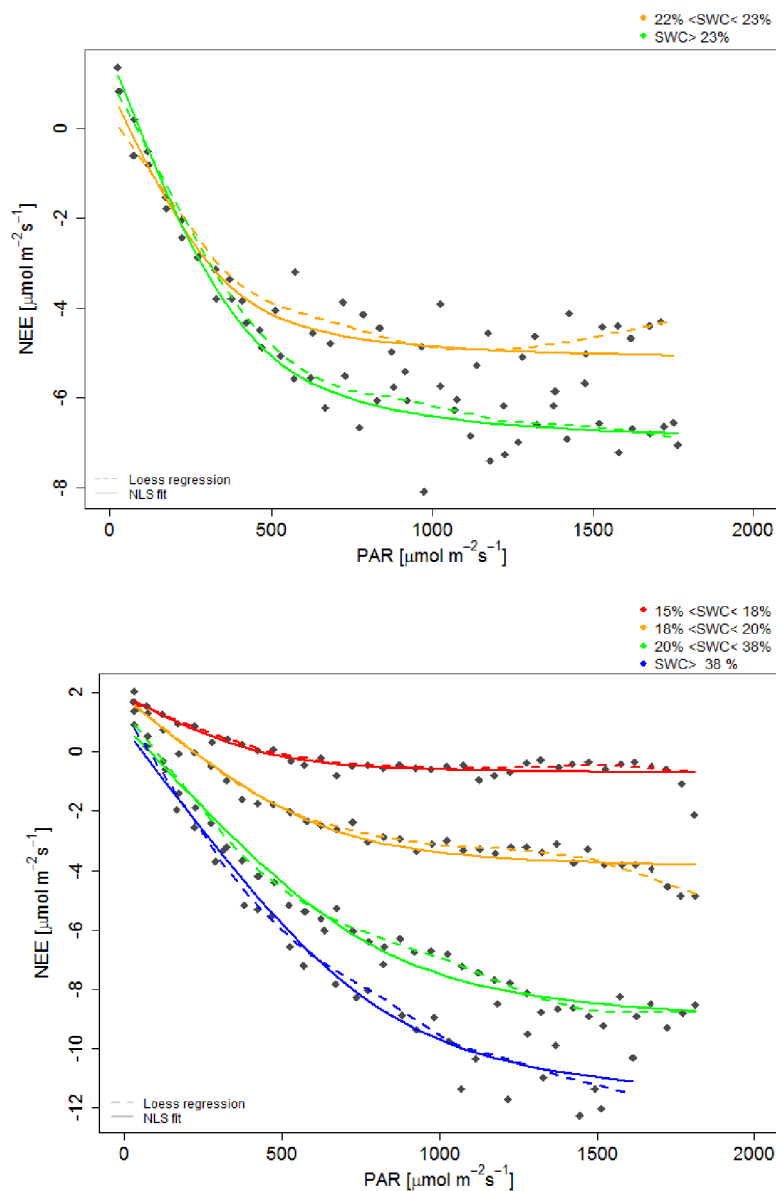
Figure 2.15: *Photosynthetic light-response curves at the Serdiana vineyard (top) and Capo Caccia Mediterranean maquis (bottom) sites. Trends of daytime ($R_g >$ $5\,W\,m^{-2}$) multi-year CO_2 fluxes as function of PAR. Data are sorted in bins of $50\,\mu mol\,m^{-2}s^{-1}$ and split into SWC intervals. Measurements are fitted using LOESS regression and non-rectangular hyperbolae (equation 2.6) by non linear least squares. Different scales for NEE representation are used in the figures.*

In Table 2.8, it is also evident the difference between the irrigated (Serdiana) and the unmanaged (Capo Caccia) site. In the vineyard ecosystem, as the dry summer season was assisted by irrigation, the extension of the SWC variability interval was limited (from 22 to 33% vol). Whereas, the Mediterranean maquis experienced drought periods (15-18% vol) and reduced physiological functions during the summer season as well as during during the late spring and the early fall (20-38% vol) but well watered and optimum conditions (>38% vol) occurred during the cold months.

Trends of the light-response curves in Figure 2.15 are consistent with the expectation that water availability plays an important role in semiarid ecosystems where typically the more the water availability is, the more plants ability to gain carbon increases (Huxman et al., 2004).

From the literature, it is observed that GPP is more responsive to well watered conditions than R_{eco}, as plants reach their optimum carbon uptake at high SWC levels but, in water stress conditions, they use the carbon previously stored (Adams et al., 2009).

Table 2.8: *Coefficients of the non rectangular hyperbola equation (equation 2.6) depending on soil water content (SWC) estimated by non linear least squares. In brackets approximated standard errors of the estimates are indicated. All the parameters estimates were significant with P < 0.0001.*

Site	SWC	α	β	γ	θ
	[% vol]	[$\mu mol\,CO_2$	[$\mu mol\,CO_2$	[$\mu mol\,CO_2$	dimensionless
		$\mu mol\,photons^{-1}$]	$m^{-2}s^{-1}$]	$m^{-2}s^{-1}$]	
Serdiana	22 − 23	0.016 (0.004)	6.192 (0.610)	0.932 (0.618)	0.881 (fixed)
	> 23	0.019 (0.002)	8.804 (0.373)	1.657 (0.376)	0.881 (fixed)
Capo Caccia	15 − 18	0.005 (0.002)	2.648 (0.376)	1.861 (0.271)	0.910 (0.125)
	18 − 20	0.008 (0.001)	5.918 (0.251)	1.809 (0.247)	0.910 (fixed)
	20 − 38	0.012 (0.001)	10.394 (0.274)	0.929 (0.257)	0.910 (fixed)
	> 38	0.015 (0.001)	13.055 (0.547)	0.838 (0.476)	0.910 (fixed)

R_S response to soil moisture is a rapid increase at low SWC, an effect also known as the *pulse response* (Huxman et al., 2004), that slows down at higher values when, on the contrary, GGP is favoured. During a drought period, however, because photosynthesis processes reduce and are more reactive to soil moisture than R_{eco} ones, the result can be a positive carbon balance with emissions of CO_2 also when water availability is again restored (Reichstein et al., 2002).

Nighttime

Ecosystem respiration processes are always active and usually nocturnal measurements are investigated to observe them without the confusing effect of photosynthesis.

Multiannual nocturnal CO_2 flux measurements of the Sardinian sites[6] were analyzed as function of soil temperature. Anyway, the strong correlation ($R^2 \approx 0.9$) between soil and air temperature, found at both sites (Table 2.9), indicates that, whenever T_{soil} is not available, T_{air} can be used as predictor.

Table 2.9: *Soil and air temperature correlation at Sardinian sites during nighttime (five years of measurements in the Mediterranean Maquis ecosystem and three years of measurements in the vineyard). Soil temperature was collected at -0.07 m in the Maquis site and -0.20 m in the vineyard. Non gap-filled u* filtered data were used for the analysis.*

	linear relation	R^2	N
Serdiana	$y = 0.75\,x + 2.90$	0.86	1758
Capo Caccia	$y = 0.75\,x + 4.30$	0.87	7451

---

[6]For Montalcino vineyard, EC measurements were only available during short summer periods and are not considered in this analysis
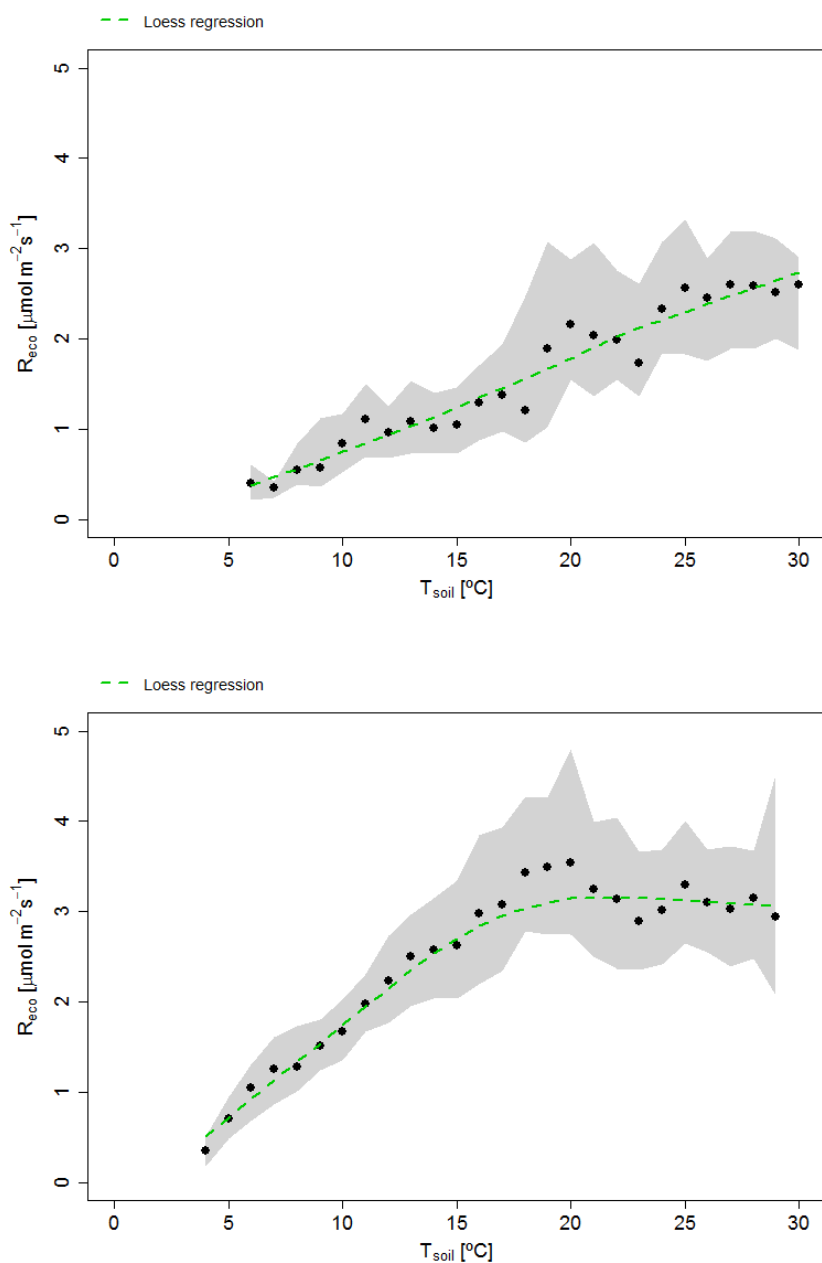
Figure 2.16: *Respiration curves of Serdiana vineyard (top) and Capo Caccia (bottom) as function of soil temperature. Shaded area indicates the interquartile ranges. Dashed line is the LOESS regression trend. Binned data by 1°C from 2005 to 2010 and from 2009 to 2011 were used in the Maquis and vineyard sites, respectively.*
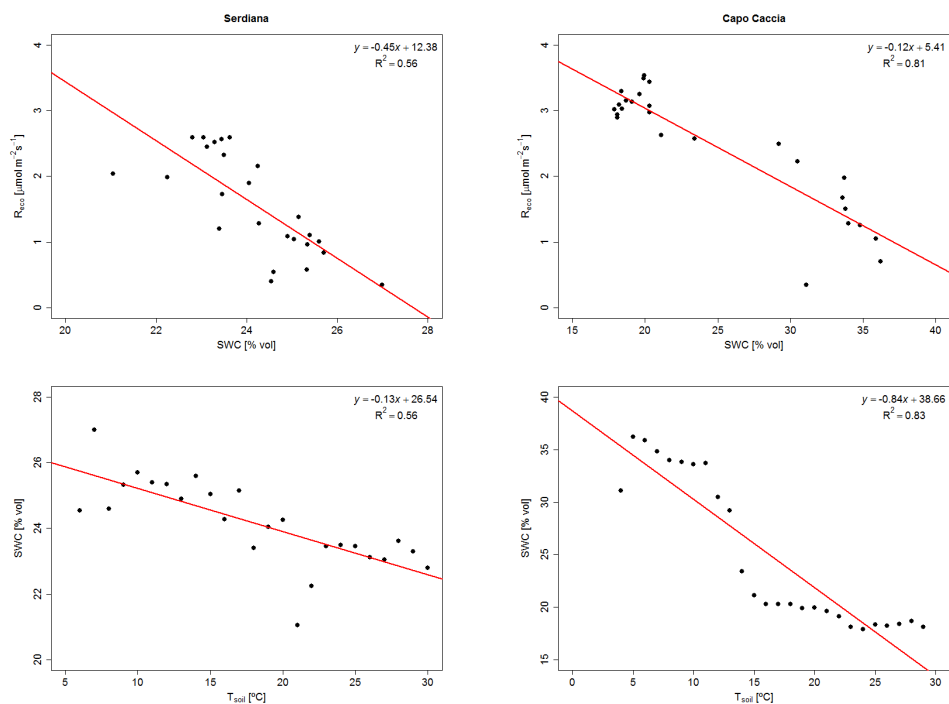
Figure 2.17: *Nocturnal CO_2 binned medians (by 1°C intervals). On the right-hand side: Serdiana vineyard. On the left-hand side: Capo Caccia Mediterranean maquis. Top: ecosystem respiration as function of soil water content (SWC). Bottom: SWC as function soil temperature. From the F-test results, linear regressions are significant at 99.9% probability*

Binned CO_2 flux medians values with their interquartile range and LOESS regression trends are shown in Figure 2.16. A seasonality effect is evident at both sites with R_{eco} reaching maximum values during wetter periods (winter, early spring, and late autumn) and showing reduced emissions during drought (summer). The LOESS regression curve highlights indeed a decrease of the exponential trend at higher temperatures corresponding to the warmest and driest season. This behaviour is typical of water-limited and semi-arid ecosystems indicating how the ecosystems (particularly Mediterranean maquis) respond to local climate conditions (Anderson-Teixeira et al., 2011). Under water stress conditions, the ecosystems fight to survive inhibit-

ing GPP processes during the hot and dry periods, when on the contrary respiration processes, particularly soil respiration, can be favoured and loss of carbon can occur also beyond that stress conditions (Reichstein et al., 2002). When wetter conditions restores, carbon uptake increases and it is favoured over R_{eco} making the ecosystem behave as a carbon *sink* (Huxman et al., 2004).

The scatterplot of CO_2 binned medians (by 1°C intervals) versus soil water content (Figure 2.17, top) reveals that, during summer, at the water assisted vineyard R_{eco} is weakly correlated with water availability ($R^2 = 0.56$). Whereas, at the unmanaged Mediterranean maquis, multiannual R_{eco} bins decreases linearly with increasing soil water content ($R^2 = 0.81$).

In literature it is observed that, in semi-arid ecosystems, as Mediterranean sites, water availability affects ecosystem respiration (particularly soil respiration) response to temperature, because of the interaction between moisture and temperature. Soil water content and temperature are indeed generally correlated (Anderson-Teixeira et al., 2011). At our sites, soil water content (in bins of 1°C) is related to soil temperature (Figure 2.17, bottom) decreasing linearly with increasing T_{soil}. Again, a weak correlation is observed at Serdiana vineyard ($R^2 = 0.56$) whereas at Capo Caccia a stronger relation is found ($R^2 = 0.83$).

Three models, whose driving variable is the soil temperature, were tested on nocturnal datasets: the original Lloyd and Taylor (equation 2.7), its modified version to account for SWC (equation 2.8), and the logistic function (equation 2.9). The results of the fitting procedure are shown in Figure 2.18 and Table 2.10.

The LLT model performs better over the vineyard ($R^2 = 0.93$), since no pronounced drought occurred at Serdiana, than over the unmanaged Capo
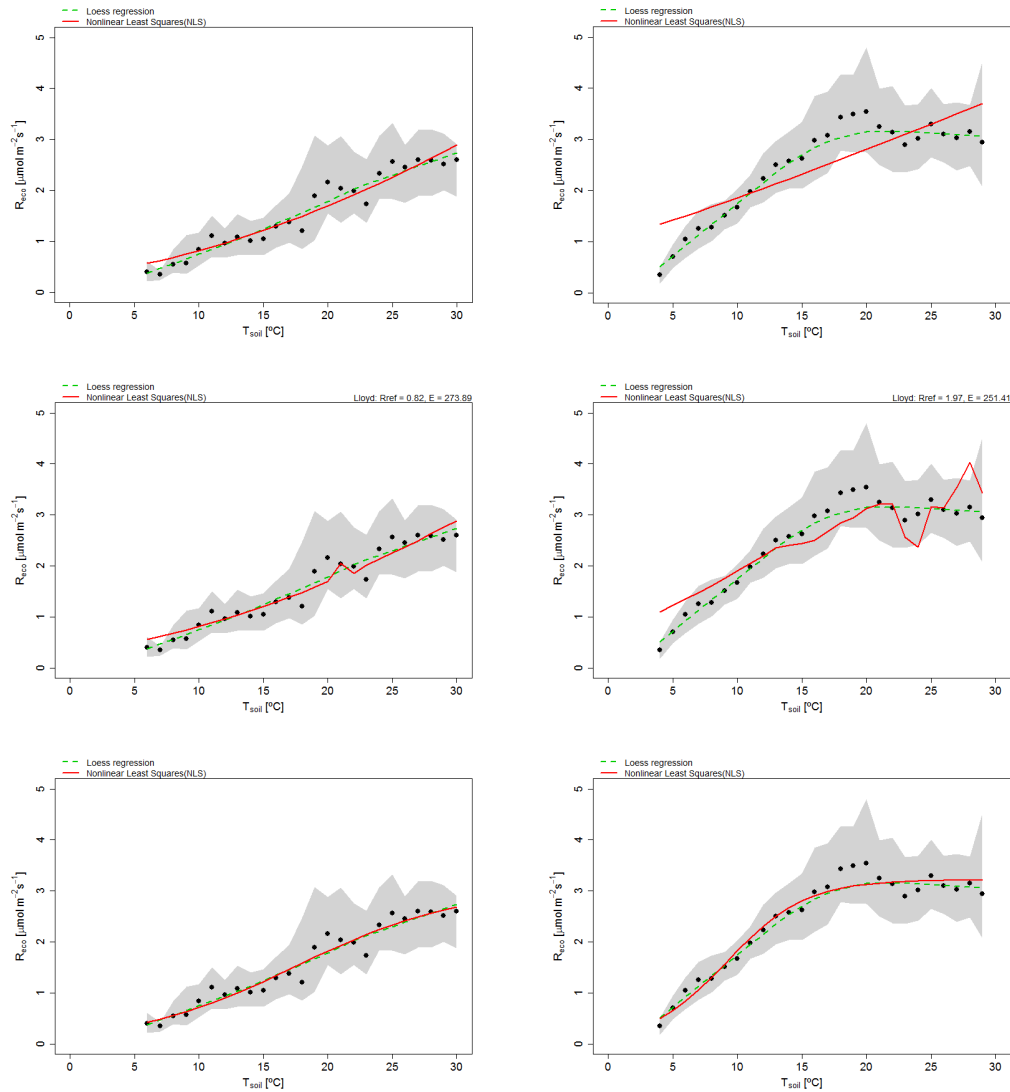
Figure 2.18: *Respiration curves of Serdiana vineyard (left panels) and Capo Caccia (right panels) as function of soil temperature. Shaded area indicates the interquartile ranges. Dashed line is the LOESS regression trend, whereas the red line indicates the three models fit: Lloyd and Taylor (top) (equation 2.7); modified version of the Lloyd and Taylor model (center) (equation 2.8); logistic equation fit (bottom) (equation 2.9). Binned data by 1°C from 2005 to 2010 and from 2009 to 2011 were used in the Maquis and vineyard sites, respectively.*

Table 2.10: *Non-linear regression results of multiannual ecosystem respiration curves: Lloyd and Taylor (LLT) (equation 2.7); modified version of the Lloyd and Taylor model (LLT_{mod}) (equation 2.8); logistic equation (equation 2.9). In brackets approximated standard errors of the parameter estimates are indicated. All the parameter estimates are significant with $P < 0.0001$. Root Mean Squared Error (RMSE) and Index of Agreement (IOA) are calculated.*

LLT	R_{ref}	E_0			R^2	RMSE	IOA
	$[\mu mol\, m^{-2} s^{-1}]$	[K]					
Serdiana	0.82 (0.06)	269.34 (19.47)			0.93	0.21	0.98
Capo Caccia	1.85(0.14)	152.80 (23.40)			0.72	0.49	0.90
LLT_{mod}	R_{ref}	E_0	SWC_0	$SWC_{1/2}$			
	$[\mu mol\, m^{-2} s^{-1}]$	[K]	[%vol]	[%vol]			
Serdiana	0.82 (0.06)	273.89 (22.38)	21.41 (1.08)	21.45 (1.17)	0.93	0.20	0.98
Capo Caccia	1.97 (0.23)	251.41 (74.40)	17.27 (0.71)	17.93 (0.47)	0.81	0.41	0.94
Logistic	K	c	a				
	$[\mu mol\, m^{-2} s^{-1}]$						
Serdiana	3.05 (0.29)	15.97 (3.91)	0.16 (0.02)		0.95	0.18	0.99
Capo Caccia	3.22 (0.07)	20.44 (6.49)	0.33 (0.04)		0.96	0.19	0.99

Caccia site ($R^2 = 0.72$), where the exponential ecosystem respiration response to soil temperature is restricted to lower temperature values. The better performance over Serdiana is also confirmed by the other statistical indices, which indicate there both a higher Root Mean Square Error (RMSE) and Index Of Agreement (IOA) ($RMSE = 0.21\ \mu mol\, m^{-2} s^{-1}$ and $IOA = 0.98$) than at the Maquis site ($RMSE = 0.49\ \mu mol\, m^{-2} s^{-1}$ and $IOA = 0.90$).

No improvement is reached by using the modified LLT model (LLT_{mod}) on Serdiana vineyard ($R^2 = 0.93$, $RMSE = 0.20\ \mu mol\, m^{-2} s^{-1}$ and $IOA = 0.98$) but it performs better than the simpler model version over the maquis site ($R^2 = 0.81$, $RMSE = 0.41\ \mu mol\, m^{-2} s^{-1}$ and $IOA = 0.94$)

Under conditions of drought, a good fit is obtained at both sites by using the more flexible logistic model which provides $R^2 = 0.95$ at the vineyard

and $R^2 = 0.96$ at the Mediterranean maquis, capturing the impact of water stress on ecosystem respiration better than an exponential model, such that of Lloyd and Taylor (1994). Also the other statistical indices confirm this better performance of the logistic model, showing lower RMSE and IOA values at both sites: $RMSE = 0.18~\mu mol\,m^{-2}s^{-1}$ and $IOA = 0.99$ at Serdiana and $RMSE = 0.19~\mu mol\,m^{-2}s^{-1}$ and $IOA = 0.99$ at Capo Caccia.

These results are consistent with other works that try to understand the effects of water stress on ecosystem respiration (Anderson-Teixeira et al., 2011; Rodeghiero and Cescatti, 2005; Walle et al., 2007): when R_{eco} is affected by water stress, the ecosystem respiration decreases at high temperatures assuming a "S" shaped trend typical of the logistic equation (Figure 2.16). On the contrary, in standard condition of water availability, the R_{eco} exponential increase with temperature is reproduced, and exponential-type models are able to fit experimental data.

Combined estimation

The combination of previous daytime and nighttime functions (see section 2.2.7) is proposed here as a combined model (equation 2.11). It is applied on multiannual light-response curves of diurnal binned CO_2 flux measurements (by 50 $\mu mol\,m^{-2}s^{-1}$ PAR intervals) in order to simultaneously describe the dependence of NEE biogenic components on its main driving factors, such as T_{soil} and PAR.

θ parameter, indicating the curvature of the light-response curve, was fixed to the values obtained at each site from daytime analysis (Table 2.7). When available, E_0, the temperature sensitivity parameter, was fixed to the nighttime estimated value (as for Serdiana site) otherwise it was estimated from diurnal binned values together with the other two parameters (α, the

apparent quantum efficiency, and β, the maximum photosynthesis at light saturation).

Table 2.11: *Non-linear regression results of light-response curves with the combined models. θ parameter was fixed from daytime analysis. When statistically significant, E_0 parameter was fixed from nighttime analysis or estimated together with the other coefficients using daytime data. In brackets approximated standard errors of the parameter estimates are indicated. $*$ indicates non-significative parameter estimate. $**$ indicates $P < 0.01$ by T-test whereas all the other parameter estimates are significant with $P < 0.0001$. Root Mean Squared Error (RMSE) and Index of Agreement (IOA) are calculated.*

		Serdiana	Serdiana	Capo Caccia
θ		0.881 **(fix)**	0.881 **(fix)**	0.972 **(fix)**
R_{ref}	$[\mu mol\, CO_2\, m^{-2} s^{-1}]$	0.562 (0.101)	1.023 (0.451)$**$	1.196 (0.193)
E_0	[K]	269.341 **(fix)**	128.957 (105.7)$*$	204.259 (55.220)
α	$[\mu mol\, CO_2\, \mu mol\, photons^{-1}]$	0.017 (0.001)	0.018 (0.002)	0.013 (0.001)
β	$[\mu mol\, CO_2\, m^{-2} s^{-1}]$	8.552 (0.344)	8.451 (0.356)	7.532 (0.293)
R^2		0.968	0.969	0.981
RMSE	$[\mu mol\, CO_2\, m^{-2} s^{-1}]$	0.359	0.350	0.254
IOA		0.992	0.992	0.995

Non-linear least squares results for the parameter estimates and related statistic are shown in Table 2.11, whereas in Figure 2.19 the light-response curves, the LOESS regression trend, and the combined model fit are represented.

At Serdiana site, when the E_0 value is fix from multiannual nighttime data analysis (Table 2.10, left top panel of Figure 2.18), all the other free parameter estimates are statistically significant (P<0.0001) and a good simulation is reproduced (R^2=0.97).

Whereas, the estimation of all parameters from daytime binned values did not provide significant values for E_0. This is probably related to the different period considered for the analyzed curves: the whole year for R_{eco}
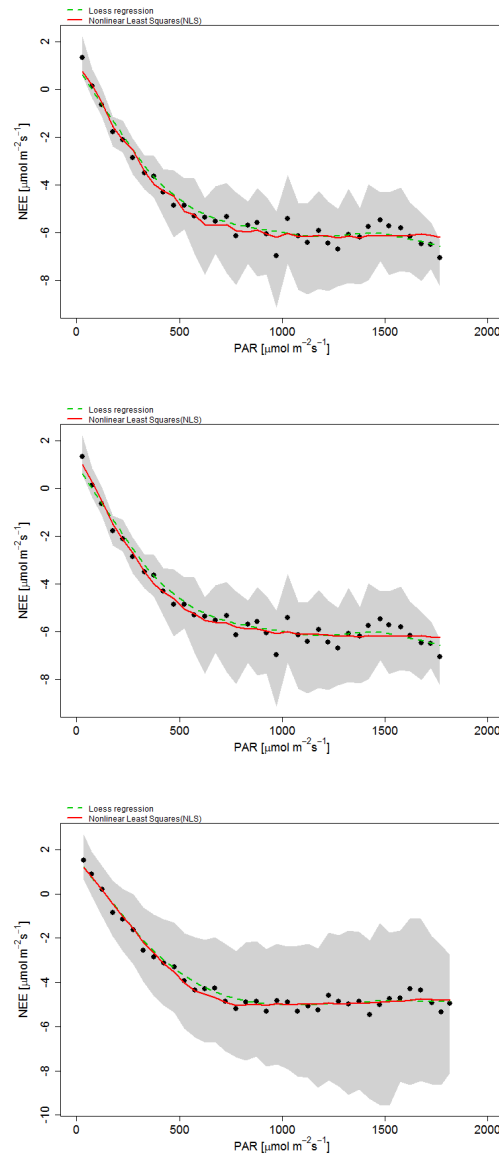
Figure 2.19: *Photosynthetic light-response curves in Serdiana and Capo Caccia. Trends of daytime $(R_g > 5\,W\,m^{-2})$ multi-year CO_2 fluxes as function of PAR. Data are sorted in bins of $50\,\mu mol\,m^{-2}s^{-1}$ and fitted using LOESS regression (green dashed line) and the combined models fit (red line) (equation 2.11) by non linear least squares. The shaded area is the interquartile range. Top panel: Serdiana CO_2 measurements with fixed E_0 and θ parameter values; Central and bottom panels: Serdiana and Capo Caccia CO_2 measurements with a θ parameter fix value. Different scales for NEE representation are used in the figures.*

as function of T_{soil}, and the summer season for the light-response curves. Therefore, when estimating E_0 for the whole year, that value is representative of a annual average, which accounts both for cold and warm seasons and different levels of vegetation stages, whereas when the estimations derives from daytime summer data, the R_{eco} saturation effect at high temperatures is more pronounced, thus affecting the parameters estimation.

In order to understand results obtained for the Capo Caccia site, it is necessary to look back to the Table 2.10 and the right top panel of Figure 2.18. At the Mediterranean Maquis ecosystem, the water-stress saturation effect prevailed on respiration processes after about 20° C, thus changing the typical exponential trend. The LLT estimated coefficients are therefore assumed to be not representative of the real processes. For this reason, E_0 at this site was only estimated from daytime data together with the other coefficients. Results for this simulation, shown in Table 2.11, indicate a good fit of experimental binned data with $R^2 = 0.98$, $RMSE = 0.25$, and $IOA \approx 1$.

Despite two different methods were used to simulate biogenic processes at the two Sardinian sites, the combined model performances were similar in accurately reproduce the mean trend of CO_2 fluxes: R^2 values ranged between 0.97 (vineyard ecosystem) and 0.98 (Maquis ecosystem), and IOA between 0.99 (Serdiana) and ≈ 1 (Capo Caccia). Only the RMSE was lower at Capo Caccia (0.25 $\mu mol\, m^{-2} s^{-1}$), when E_0 was estimated together with the other coefficients from diurnal measurements, than at Serdiana (0.35 – 0.36 $\mu mol\, m^{-2} s^{-1}$), when E_0 was fix from nighttime or diurnal measurements.

From this analysis, both methods are therefore considered able to reproduce the mean trend of CO_2 fluxes over a long period.

2.4 Conclusions

The general aim of this work was to develop an empirical approach to estimate and partition NEE flux over different ecosystems. Different equations to estimate GPP and R_{eco} used by authors were reported and a new combined approach was here proposed. As Mediterranean area is critical for future climate change scenarios, three Mediterranean sites (two vineyards and one Maquis ecosystems) were selected for this purpose and to investigate the relations between the CO_2 flux and the environmental factors controlling it, in particular drought conditions.

Eddy covariance multiannual measurements at three Mediterranean sites were analyzed (data for five years over Maquis ecosystems and for more than three years over vineyard ecosystems). The analysis improves our knowledge on the behaviour of such different vegetation types, which are characterized by Mediterranean climate conditions, both in terms of energy, water, and carbon fluxes. In the Sardinian sites, photosynthesis and respiration processes were affected by soil water deficit conditions.

The analysis of diurnal and nocturnal observations, per each ecosystem, confirmed that the more the water availability is, the more the ecosystem is able to photosynthesize. At the same time, R_{eco} is limited during drought conditions whereas it increases exponentially in non water-stressed conditions.

In addition, this analysis allowed to separately investigate the behaviour of GPP and R_{eco} through different empirical relations: the Non-Rectangular Hyperbola (NRH) model (equation 2.6), the Lloyd and Taylor (LLT) equation (equation 2.7), the modified LLT (LLT_{mod}) to account for SWC (equation 2.8), and the logistic model (equation 2.9). The logistic model gave the best performances in simulating experimental data coming from Mediter-

ranean area, even without explicitly taking into account the soil water content as an independent variable. It is then useful to reproduce the influence of water deficit on respiration processes. However, its parameters have not an ecophysiological representation, whereas the LLT and the LLT_{mod} model include this aspect.

Finally, a new approach was developed and proposed here, which consists of a combination between the LLT and the NRH models, to estimate the NEE flux in the Mediterranean environment. The LLT model was preferred both to avoid an overparameterization and to allow a broader application under non-water stress conditions.

The combined model was tested over the two Sardinian sites (the vineyard and the Maquis ecosystems) both with the E_0 parameter obtained from diurnal and nocturnal data. Results showed that the proposed model accurately reproduce the mean trend of CO_2 flux over the two sites, with R^2 values greater than 97%.

However, further investigations are still needed to understand the role of soil water content at the different sites. Future efforts are oriented at testing and developing a new equation (that explicitly considers ecosystem respiration dependence on temperature and soil water content) able to simulate ecosystem respiration both in well watered and in water-limited ecosystems.

References

Adams, H. D., Guardiola-Claramonte, M., Barron-Gafford, G. A., Villegas, J. C., Breshears, D. D., Zou, C. B., Troch, P. A., and Huxman, T. E. (2009). Temperature sensitivity of drought-induced tree mortality portends increased regional die-off under global-change-type drought. *Proceedings of the National Academy of Sciences*, 106(17):7063–7066.

Anderson-Teixeira, K. J., Delong, J. P., Fox, A. M., Brese, D. A., and Litvak, M. E. (2011). Differential responses of production and respiration to temperature and moisture drive the carbon balance across a climatic gradient in new mexico. *Global Change Biology*, 17(1):410–424.

Aubinet, M., Feigenwinter, C., Heinesch, B., Laffineur, Q., Papale, D., Reichstein, M., Rinne, J., and Van Gorsel, E. (2012). Nighttime flux correction. In *Eddy Covariance*, pages 133–157. Springer.

Aubinet, M., Grelle, A., Ibrom, A., Rannik, Ü., Moncrieff, J., Foken, T., Kowalski, A. S., Martin, P. H., Berbigier, P., Bernhofer, C., et al. (2000). Estimates of the annual net carbon and water exchange of forests: the EUROFLUX methodology. *Advances in ecological research*, 30:113–175.

Baldocchi, D. (1997). Flux footprints within and over forest canopies. *Boundary-Layer Meteorology*, 85(2):273–292.

Blackman, F. F. (1905). Optima and limiting factors. *Annals of Botany*, 19(2):281–296.

Boote, K. J. and Loomis, R. S. (1991). The prediction of canopy assimilation. *Modeling Crop Photosynthesis–from Biochemistry to Canopy*, 19:109–137.

Falge, E., Baldocchi, D., Olson, R., Anthoni, P., Aubinet, M., Bernhofer, C., Burba, G., Ceulemans, R., Clement, R., Dolman, H., et al. (2001a). Gap filling strategies for defensible annual sums of net ecosystem exchange. *Agricultural and forest meteorology*, 107(1):43–69.

Falge, E., Baldocchi, D., Olson, R., Anthoni, P., Aubinet, M., Bernhofer, C., Burba, G., Ceulemans, R., Clement, R., Dolman, H., et al. (2001b). Gap filling strategies for long term energy flux data sets. *Agricultural and Forest Meteorology*, 107(1):71–77.

Gilmanov, T. G., Svejcar, T. J., Johnson, D. A., Angell, R. F., Saliendra, N. Z., and Wylie, B. K. (2006). Long-term dynamics of production, respiration, and net CO_2 exchange in two sagebrush-steppe ecosystems. *Rangeland ecology & management*, 59(6):585–599.

Gilmanov, T. G., Verma, S. B., Sims, P. L., Meyers, T. P., Bradford, J. A., Burba, G. G., and Suyker, A. E. (2003). Gross primary production and light response parameters of four Southern Plains ecosystems estimated using long-term CO_2-flux tower measurements. *Global Biogeochemical Cycles*, 17(2).

Goulden, M. L., Munger, J. W., FAN, S.-M., Daube, B. C., and Wofsy, S. C. (1996). Measurements of carbon sequestration by long-term eddy covariance: Methods and a critical evaluation of accuracy. *Global change biology*, 2(3):169–182.

Granier, A., Reichstein, M., Bréda, N., Janssens, I., Falge, E., Ciais, P., Grünwald, T., Aubinet, M., Berbigier, P., Bernhofer, C., et al. (2007). Evidence for soil water control on carbon and water dynamics in Euro-

pean forests during the extremely dry year: 2003. *Agricultural and Forest Meteorology*, 143(1):123–145.

Gu, L., Falge, E. M., Boden, T., Baldocchi, D. D., Black, T., Saleska, S. R., Suni, T., Verma, S. B., Vesala, T., Wofsy, S. C., et al. (2005). Objective threshold determination for nighttime eddy flux filtering. *Agricultural and Forest Meteorology*, 128(3):179–197.

Guo, W., Kang, S., Li, F., and Li, S. (2014). Variation of nee and its affecting factors in a vineyard of arid region of northwest china. *Atmospheric Environment*, 84:349–354.

Hastings, S. J., Oechel, W. C., and Muhlia-Melo, A. (2005). Diurnal, seasonal and annual variation in the net ecosystem CO_2 exchange of a desert shrub community (Sarcocaulescent) in Baja California, Mexico. *Global Change Biology*, 11(6):927–939.

Hollinger, S. E., Bernacchi, C. J., and Meyers, T. P. (2005). Carbon budget of mature no-till ecosystem in north central region of the united states. *Agricultural and Forest Meteorology*, 130(1):59–69.

Huxman, T. E., Snyder, K. A., Tissue, D., Leffler, A. J., Ogle, K., Pockman, W. T., Sandquist, D. R., Potts, D. L., and Schwinning, S. (2004). Precipitation pulses and carbon fluxes in semiarid and arid ecosystems. *Oecologia*, 141(2):254–268.

Janssens, I. A., Kowalski, A. S., and Ceulemans, R. (2001). Forest floor CO_2 fluxes estimated by eddy covariance and chamber-based model. *Agricultural and Forest Meteorology*, 106(1):61–69.

Lasslop, G., Reichstein, M., Papale, D., Richardson, A. D., Arneth, A., Barr, A., Stoy, P., and Wohlfahrt, G. (2010). Separation of net ecosystem

exchange into assimilation and respiration using a light response curve approach: critical issues and global evaluation. *Global Change Biology*, 16(1):187–208.

Le Quéré, C., Peters, G. P., Andres, R. J., Andrew, R. M., Boden, T. A., Ciais, P., Friedlingstein, P., Houghton, R. A., Marland, G., Moriarty, R., et al. (2014). Global carbon budget 2013. *Earth System Science Data*, 6(1):235–263.

Lloyd, J. and Taylor, J. (1994). On the temperature dependence of soil respiration. *Functional ecology*, pages 315–323.

Luo, H., Oechel, W. C., Hastings, S. J., Zulueta, R., Qian, Y., and Kwon, H. (2007). Mature semiarid chaparral ecosystems can be a significant sink for atmospheric carbon dioxide. *Global Change Biology*, 13(2):386–396.

Marcolla, B., Cescatti, A., Montagnani, L., Manca, G., Kerschbaumer, G., and Minerbi, S. (2005). Importance of advection in the atmospheric CO_2 exchanges of an alpine forest. *Agricultural and Forest Meteorology*, 130(3):193–206.

Marras, S. (2008). *Evaluation of the Advanced Canopy-Atmosphere-Soil Algorithm (ACASA) model performance using micrometeorological techniques.* PhD thesis, Agrometeorology and Ecophysiology of Agricultural and Forest Ecosystems, University of Sassari.

Marras, S., Pyles, R. D., Sirca, C., Paw U, K. T., Snyder, R. L., Duce, P., and Spano, D. (2011). Evaluation of the Advanced Canopy-Atmosphere-Soil Algorithm (ACASA) model performance over Mediterranean maquis ecosystem. *Agricultural and Forest Meteorology*, 151(6):730–745.

Marras, S., Sirca, C., Duce, P., Arca, A., Zara, P., Bacciu, V., and D, S. (2012). Carbon sequestration monitoring in a typical Mediterranean vineyard. 30th American Meteorological Society Conference on Agricultural and Forest Meteorology, Boston, May 26th-June 2nd.

Marshall, B. and Biscoe, P. V. (1980). A model for c3 leaves describing the dependence of net photosynthesis on irradiance. *Journal of Experimental Botany*, 31(1):29–39.

Moncrieff, J., Malhi, Y., and Leuning, R. (1996). The propagation of errors in long-term measurements of land-atmosphere fluxes of carbon and water. *Global change biology*, 2(3):231–240.

Mudge, P. L., Wallace, D. F., Rutledge, S., Campbell, D. I., Schipper, L. A., and Hosking, C. (2011). Carbon balance of an intensively grazed temperate pasture in two climatically contrasting years. *Agriculture, Ecosystems & Environment*, 144(1):271–280.

Ögren, E. (1993). Convexity of the photosynthetic light-response curve in relation to intensity and direction of light during growth. *Plant Physiology*, 101(3):1013–1019.

OIV (2013). International Organization of Vine and Wine, Statistical report on world vitiviniculture.

Papale, D., Reichstein, M., Canfora, E., Aubinet, M., Bernhofer, C., Longdoz, B., Kutsch, W., Rambal, S., Valentini, R., Vesala, T., et al. (2006). Towards a more harmonized processing of eddy covariance CO_2 fluxes: algorithms and uncertainty estimation. *Biogeosciences Discussions*, 3(4):961–992.

Papale, D. and Valentini, R. (2003). A new assessment of European forests carbon exchanges by eddy fluxes and artificial neural network spatialization. *Global Change Biology*, 9(4):525–535.

Peichl, M., Carton, O., and Kiely, G. (2012). Management and climate effects on carbon dioxide and energy exchanges in a maritime grassland. *Agriculture, Ecosystems & Environment*, 158:132–146.

Powell, T. L., Bracho, R., Li, J., Dore, S., Hinkle, C. R., and Drake, B. G. (2006). Environmental controls over net ecosystem carbon exchange of scrub oak in central Florida. *Agricultural and Forest Meteorology*, 141(1):19–34.

Rabinowitch, E. I. (1951). *Photosynthesis and related processes*, volume 2. Interscience Publisher, New York.

Reichstein, M., Falge, E., Baldocchi, D., Papale, D., Aubinet, M., Berbigier, P., Bernhofer, C., Buchmann, N., Gilmanov, T., Granier, A., et al. (2005). On the separation of net ecosystem exchange into assimilation and ecosystem respiration: review and improved algorithm. *Global Change Biology*, 11(9):1424–1439.

Reichstein, M., Stoy, P. C., Desai, A. R., Lasslop, G., and Richardson, A. D. (2012). Partitioning of net fluxes. In *Eddy Covariance*, pages 263–289. Springer.

Reichstein, M., Tenhunen, J. D., Roupsard, O., Ourcival, J.-M., Rambal, S., Dore, S., and Valentini, R. (2002). Ecosystem respiration in two Mediterranean evergreen Holm Oak forests: drought effects and decomposition dynamics. *Functional Ecology*, 16(1):27–39.

Richards, F. (1959). A flexible growth function for empirical use. *Journal of experimental Botany*, 10(2):290–301.

Rodeghiero, M. and Cescatti, A. (2005). Main determinants of forest soil respiration along an elevation/temperature gradient in the italian alps. *Global Change Biology*, 11(7):1024–1041.

Rossi, F., Facini, O., Georgiadis, T., and Nardino, M. (2004). Bilancio energetico, bilancio radiativi e flussi di carbonio in un vigneto ad uva da tavola allevato a tendone. *Quad. Vitic. Enol. Univ. Torino, 27*, pages 177–199.

Ruimy, A., Jarvis, P., Baldocchi, D., and Saugier, B. (1995). Co2 fluxes over plant canopies and solar radiation: a review. *Advances in Ecological Research (United Kingdom)*.

Schmid, H. P., Grimmond, C. S. B., Cropley, F., Offerle, B., and Su, H.-B. (2000). Measurements of CO_2 and energy fluxes over a mixed hardwood forest in the mid-western United States. *Agricultural and Forest Meteorology*, 103(4):357–374.

Schmidt, M., Reichenau, T. G., Fiener, P., and Schneider, K. (2012). The carbon budget of a winter wheat field: An eddy covariance analysis of seasonal and inter-annual variability. *Agricultural and Forest Meteorology*, 165:114–126.

Spano, D., Duce, P., and Snyder, R. L. (2003a). Estimate of mass and energy fluxes over grapevine using eddy covariance technique. In *IV International Symposium on Irrigation of Horticultural Crops 664*, pages 631–638.

Spano, D., Sirca, C., Marras, S., Duce, P., Zara, P., Arca, A., and Snyder, R. L. (2008). Mass and energy flux measurements over grapevine using micrometeorological techniques. *Acta Horticulturae*, 792:623–662.

Spano, D., Snyder, R. L., and Cesaraccio, C. (2003b). Mediterranean climates. In *Phenology: an integrative environmental science*, pages 139–156. Springer.

Spano, D., Snyder, R. L., Sirca, C., and Duce, P. (2009). ECOWAT - A model for ecosystem evapotranspiration estimation. *Agricultural and forest meteorology*, 149(10):1584–1596.

Stoy, P. C., Katul, G. G., Siqueira, M., Juang, J.-Y., Novick, K. A., Uebelherr, J. M., and Oren, R. (2006). An evaluation of models for partitioning eddy covariance-measured net ecosystem exchange into photosynthesis and respiration. *Agricultural and Forest Meteorology*, 141(1):2–18.

Tirone, G., Manca, G., Valentini, R., and Seufert, G. (2003). Assorbimento di carbonio negli ecosistemi forestali mediterranei: confronto tra una lecceta ed una pineta. In De Angelis, P., Macuz, A., Bucci, G., and Scarascia Mugnozza, G., editors, *Alberi e Foreste per il Nuovo Millennio, Atti del III Congresso Nazionale della Societa' Italiana di Selvicoltura ed Ecologia Forestale (SISEF Atti III)*, pages 99–104, Viterbo.

Twine, T. E., Kustas, W., Norman, J., Cook, D., Houser, P., Meyers, T., Prueger, J., Starks, P., and Wesely, M. (2000). Correcting eddy-covariance flux underestimates over a grassland. *Agricultural and Forest Meteorology*, 103(3):279–300.

Valentini, R., Angelis, P. d., Matteucci, G., Monaco, R., Dore, S., and Mucnozza, G. S. (1996). Seasonal net carbon dioxide exchange of a beech forest with the atmosphere. *Global Change Biology*, 2(3):199–207.

Walle, I. V., Samson, R., Looman, B., Verheyen, K., and Lemeur, R. (2007).

Temporal variation and high-resolution spatial heterogeneity in soil CO_2 efflux in a short-rotation tree plantation. *Tree physiology*, 27(6):837–848.

Webb, E. K., Pearman, G. I., and Leuning, R. (1980). Correction of flux measurements for density effects due to heat and water vapour transfer. *Quarterly Journal of the Royal Meteorological Society*, 106(447):85–100.

Wilson, K., Goldstein, A., Falge, E., Aubinet, M., Baldocchi, D., Berbigier, P., Bernhofer, C., Ceulemans, R., Dolman, H., Field, C., et al. (2002). Energy balance closure at fluxnet sites. *Agricultural and Forest Meteorology*, 113(1):223–243.

Zenone, T., Gelfand, I., Chen, J., Hamilton, S. K., and Robertson, G. P. (2013). From set-aside grassland to annual and perennial cellulosic biofuel crops: Effects of land use change on carbon balance. *Agricultural and Forest Meteorology*, 182:1–12.

Chapter 3

NEE anthropogenic flux partitioning

3.1 Introduction

In recent years, more attention has been dedicated to study the role of cities in global climate change due to the increasing growth of urban population and the consequent increase of energy demand and carbon emissions (Pataki et al., 2006). In urban areas, anthropogenic contributions such as fossil fuel combustion, cement production, and replacement of natural or agricultural ecosystems by impervious surfaces (dwellings, roads, roofs etc.) are, in fact, the main responsible of carbon emissions and add to the natural processes of urban vegetation (Canadell et al., 2009).

A rapid urbanization process has occurred over the past sixty years (Figure 3.1). Whereas in 1950 the proportion of people living in urban areas was 70% rural and 30% urban, global urban population has been exceeding global rural population since 2007, being nowadays 54%. This growth trend will continue and it is estimated that, by 2050, the proportion will be almost
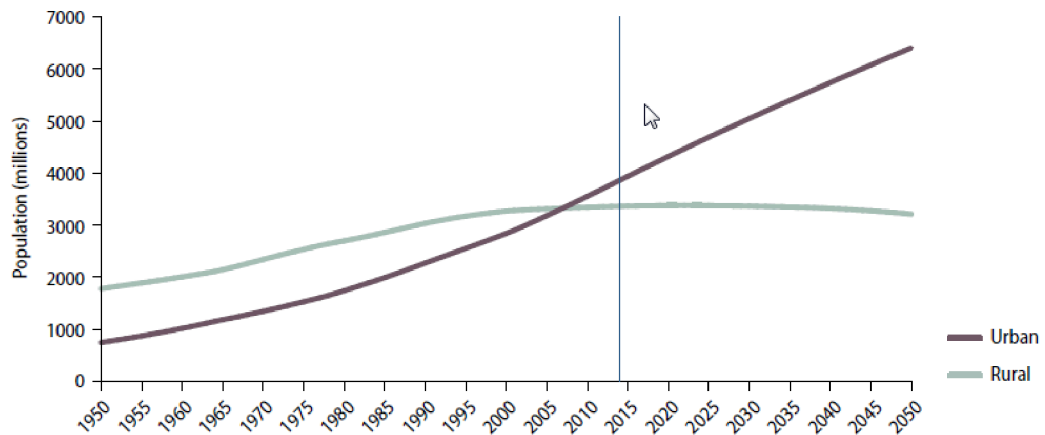
Figure 3.1: *Urban and rural population of the world, 1950 - 2050 (from UN, 2014).*

reversed: the world will be 34% rural and 66% urban with urban population increasing more than two thirds (UN, 2014).

In general, climate and people priorities are the major driving forces of an urban area (Churkina, 2008). Since 2000, some cities, the majority located in low fertility country of Asia and Europe, are depopulating (UN, 2014), and nowadays, most people live in temperate and tropical climates (44.6% and 28%, respectively) (Grimmond and Christen, 2012) and in fertile lands, near the main roads.

In addition to this, cities have become widely recognized as major contributors to global greenhouse gas (GHG) emissions: although their small percentage (2% of Earth surface) they emit 30-40% of green house anthropogenic emissions (Satterthwaite, 2008) and more than 70% of CO_2 anthropogenic fluxes (Canadell et al., 2009; Koerner and Klopatek, 2002). The urban flows of energy, water, and carbon have an important impact on climate change (Mills 2007). Moreover, the higher temperatures (urban heat island) and the increased CO_2 concentrations that occur within an urban center, make cities a look-out point to study the impact of future global processes on a

local scale. Hence, further studies on urban carbon exchanges are crucial to better understand the interaction between natural and anthropogenic processes (Walsh et al., 2004) as well as to develop strategies to mitigate future emissions.

The urban site can be thought as an organism consuming material and energy inputs (electricity, fuel, water, and food), processing them into usable forms, and producing waste as outputs of the process (pollutants, greenhouse gases, heat, ect.). This urban metabolism concept, defined as the exchange and transformation of energy and matter (water, carbon, and other substances) between a city and its environment, was first coined by Wolman (1965), and, since then, the metabolic approach to study city systems has been proposed several times. Both Decker et al. (2000) and Kennedy et al. (2007) reviewed studies conducted around the globe and described how the urban metabolism of cities is changing. The urban carbon emissions are closely linked to the energy demand and burning of fossil fuel (Kennedy et al., 2007), and a conceptual scheme of the urban carbon budget is shown in Figure 3.2 (Churkina, 2008).

Carbon exchanges occurring within cities are the result of the interaction among lateral and vertical fluxes, and carbon pools (Churkina, 2008). Lateral fluxes can be directed into the urban system or outside it, as a consequence of human activities importing and exporting fossil fuel, food, construction materials, and waste products. In the same way, vertical fluxes can be positive (towards the atmosphere) or negative (towards the surface, by micrometeorological convention) originating both from natural (ecosystem respiration and photosynthesis) and anthropogenic processes (burning of fossil fuel, traffic, heating, household activities, and human respiration). At the same time, cities store carbon both in natural and anthropogenic pools through vegeta-
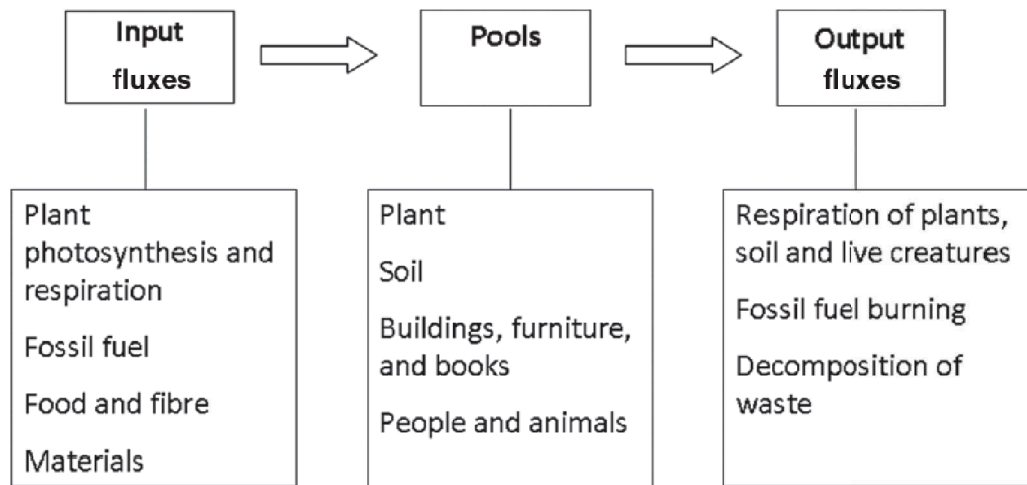
Figure 3.2: *Schematic representation of carbon inputs, pools and emissions (modified from Churkina, 2008).*

tion, soil, buildings, landfills, clothing, people, and animals (Churkina, 2008).

Whereas natural ecosystems are self-supporting, urban areas are not, as they require energy from outside to supply human needs (heating, food, electric power, fossil fuel burning, ect.) (Churkina, 2008).

In urban areas, CO_2 fluxes are almost always positive both on a daily and seasonal scale (Moriwaki and Kanda, 2004) and for this reason, cities are considered as net sources of CO_2 (Coutts et al., 2007; Grimmond et al., 2004; Hom et al., 2003; Velasco and Roth, 2010; Vogt et al., 2003). In addition, at local scale the magnitude of CO_2 fluxes shows high variability (Bergeron and Strachan, 2011; Crawford et al., 2011; Järvi et al., 2012; Ramamurthy and Pardyjak, 2011) though seasonal and diurnal pattern are similar for both Southern and Northern Hemisphere (Coutts et al., 2007). Vegetation cover offsets urban sources of CO_2 fluxes to the atmosphere and, similarly to vegetated ecosystems, cities are able to sequester large amounts of carbon, perhaps as much as tropical forests on a per unit area basis (Churkina

et al., 2010; Coutts et al., 2007). Negative CO_2 fluxes are, for example, generally observed during the growing season in suburban areas having a greater amount of vegetation and a lower population density (Bergeron and Strachan, 2011; Crawford et al., 2011; Vesala et al., 2008). Seasons affect CO_2 exchanges and reduced urban emissions during summer are the result of the increased uptake by urban vegetation (Moriwaki and Kanda, 2004; Soegaard and Møller-Jensen, 2003).

Likewise in natural ecosystems, since '90s, the Eddy Covariance (EC) technique has been more and more used to measure energy and mass fluxes in urban areas at local (or neighborhood) scale (Velasco and Roth, 2010). Ever since, the number of urban sites monitored with the EC technique has increased and more than 60 measurement towers, operating both for long or short periods, have been employed, especially in temperate and continental climates (Grimmond and Christen, 2012).

Measurements are crucial to test and improve models ability to predict urban fluxes. So far, different types of models have been developed with the aim to study the ecosystems behaviour under different environmental conditions, in terms of energy, water and CO_2 exchanges. Moreover, through models it is possible to study the impact of climate change over ecosystems, and investigate the modification of carbon budget over urban areas in order to identify mitigation strategies.

The aim of this chapter is to review empirical methods used to estimate the urban CO_2 flux components and to show results obtained by the new urban implementation of the SVAT model ACASA (Advanced Canopy-Atmosphere-Soil Algorithm).

Veronica Bellucco, *Empirical estimations of CO₂ flux components over different ecosystems*, Tesi di Dottorato in "Scienze e Biotecnologie dei Sistemi Agrari e Forestali e delle Produzioni Alimentari", Indirizzo "Agrometeorologia ed Ecofisiologia dei Sistemi Agrari e Forestali", Università degli Studi di Sassari.

3.2 Modelling the urban carbon cycle

Atmospheric CO_2 emissions together with uptake from urban vegetation, represent the net exchange of vertical fluxes between the urban surfaces and the upper atmosphere. The most important and difficult task for EC observation, especially in urban area, is to partition CO_2 flux into its main components. In this context, models are helpful and they can also reproduce experimental data whenever direct measurements are not available. Two different approaches can be employed and combined to model CO_2 emissions: top-down and bottom-up. The top-down method is used to elaborate and separate aggregated data (inventories, consumption surveys, population data, long term trends) for a temporal and spatial downscaling, from a higher to a lower scale (Heiple and Sailor, 2008; Puliafito, 2006). Conversely, the bottom-up approach is used to analyze information and generalize emissions scaling-up from local to higher scales. It generally includes intracity detailed studies, such as in situ measurements or consumption/emission data concerning individuals elements of the urban systems (e.g. buildings, vehicles, people), and restricted temporal and spatial scales, which can be then aggregated to the desired resolution.

Different ecosystem process-based models, originally developed for natural ecosystems, were used in urban systems, focusing on the surface energy budget estimation to study the carbon balance. Such models simulate the response of vegetation in cities and the urban footprint to urban pollution, enhanced levels of atmospheric CO_2, and to changes in urban climate, on the half hourly to daily scales. They can be applied at local scale as well as at larger scale to provide regional and global estimates. As an example, the biogeochemical model BIOME-BGC, was used to simulate carbon balance of turf grasses of the USA (Milesi et al., 2005) whereas the CASA model, used

by Imhoff et al. (2004), estimated the effect of urban land cover change on Net Primary Production (NPP) of the USA. However, this kind of models completely omit carbon emissions associated with anthropogenic activities and are run on daily to monthly or longer scales.

To improve estimates of the urban carbon cycle, modeling efforts have been oriented toward integrated models, where both biophysical and human related fluxes, as well as their integration, are considered. For instance, an urban metabolism approach has been proposed by Christen et al. (2010) and, during the last decade, many authors (Christen et al., 2011; Crawford and Christen, 2014; Crawford et al., 2011; Moriwaki and Kanda, 2004; Nemitz et al., 2002; Soegaard and Møller-Jensen, 2003) tried to understand and model the various contributions to the vertical CO_2 flux in urban areas. Briefly, partitioning CO_2 flux into its main components is the result of a combination of sub-models able to simulate individual carbon emission sources and sinks. According to Soegaard and Møller-Jensen (2003), the CO_2 vertical flux measured with the Eddy Covariance technique, is the Urban Net Exchange (UNE), likewise the Net Ecosystem Exchange for natural ecosystem. UNE can be then thought as the sum of six principal components:

$$UNE = E_T + E_B + R_A + (R_S + R_V - P_V) \qquad (3.1)$$

The first three terms are the anthropogenic contributes, namely vehicular traffic (E_T) and buildings (E_B) emissions, and human and animal respiration (R_A), whereas the last three terms are related to urban vegetation and represents below-ground autotrophic and heterotrophic respiration (R_S), above-ground vegetation respiration (R_V), and CO_2 uptake by photosynthesis process (P_V) (Crawford et al., 2011) (Figure 3.3).

New technologies development are allowing a quick improvement in modelling techniques and approaches. In particular remote sensing technology,
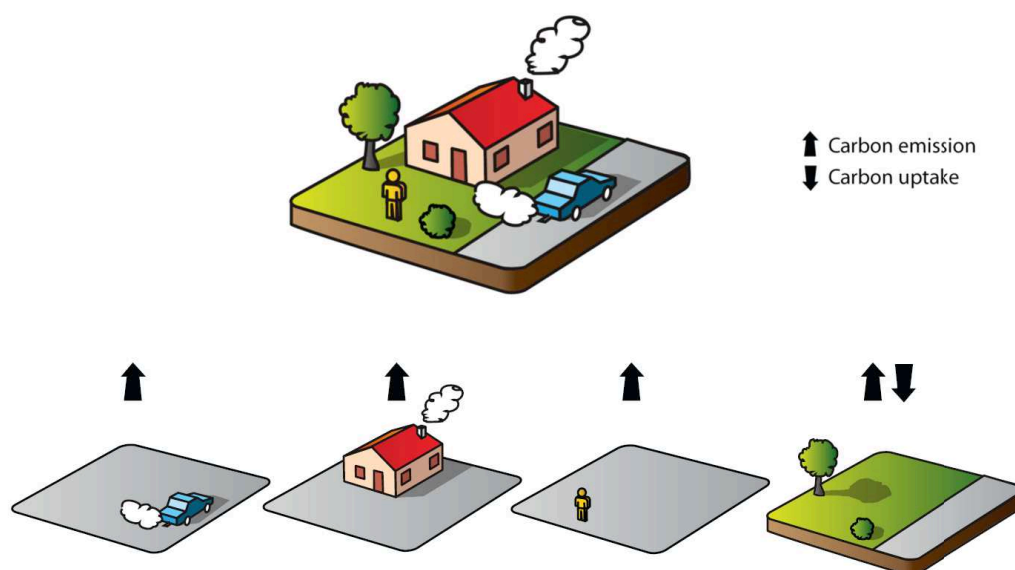
Figure 3.3: CO_2 *flux components in urban areas (modified from Christen et al., 2010).*

such as Light Detection and Ranging (LiDAR) and satellite data, is helpful in providing detailed and accurate information about urban structure, buildings and land cover. These information together with meteorological, vehicles, census and statistical data about population, land use and employment are combined and used as input information to models. On average, modeled annual emissions vary from 9.2 μmol m^{-2} s^{-1} in the city center of Copenhagen (Soegaard and Møller-Jensen, 2003) to 14.7 μmol m^{-2} s^{-1} for the Montreal urban site (Bergeron and Strachan, 2011), and 15.2 μmol m^{-2} s^{-1} in the suburban neighbourhood of Vancouver (Christen et al., 2011). With remote sensing and new technologies, differences between modelled and measured fluxes are generally in order of 10% of the mean flux density. A brief description on how to model each CO_2 flux emission source is reported below.

3.2.1 CO_2 emissions from traffic

Traffic is the most important source of CO_2 vertical fluxes in urban areas showing a bimodal daily profile associated with traffic rush hours especially during weekdays (Bergeron and Strachan, 2011; Coutts et al., 2007; Hiller et al., 2011; Nemitz et al., 2002; Velasco et al., 2005). In Figure 3.4, Bergeron and Strachan (2011) showed measurements of CO_2 fluxes collected in an urban and a suburban area of Montreal. They are hourly binned and split into the four seasons to highlight differences both between a residential site and the city center, and among different periods of the year. In addition, emissions due to vehicular traffic are also considered for the cold and the warm season. As expected, two peaks related to traffic rush hours are evident: one in the early morning, and the other one in the evening. This behaviour is evident at all seasons and more pronounced at the urban site. In addition, highest values of CO_2 fluxes are observed in the winter season.

The number of vehicles is generally almost constant throughout the year (Moriwaki and Kanda, 2004), even if a little inflection of about -20% is observed in some cities during the summer holidays (Gioli et al., 2012; Järvi et al., 2012; Soegaard and Møller-Jensen, 2003). However, measurements in other sites have highlighted that traffic is the most important source of CO_2 fluxes during the summer season. As an example, in Copenhagen traffic was found to be responsible of 51% in summer and 39% in winter of total CO_2 emissions (Soegaard and Møller-Jensen, 2003) whereas it was estimated to be about 40% of observed annual total fluxes in Florence (Gioli et al., 2012).

In the urban areas of Edinburgh, Copenhagen, Montreal, Helsinki, Mexico city, and Minneapolis–Saint Paul, UNE and vehicular traffic volumes, as well as related emissions, are linearly dependent and differ among sites. Figure 3.5 shows, for Montreal, the difference of the linear dependence of CO_2 fluxes
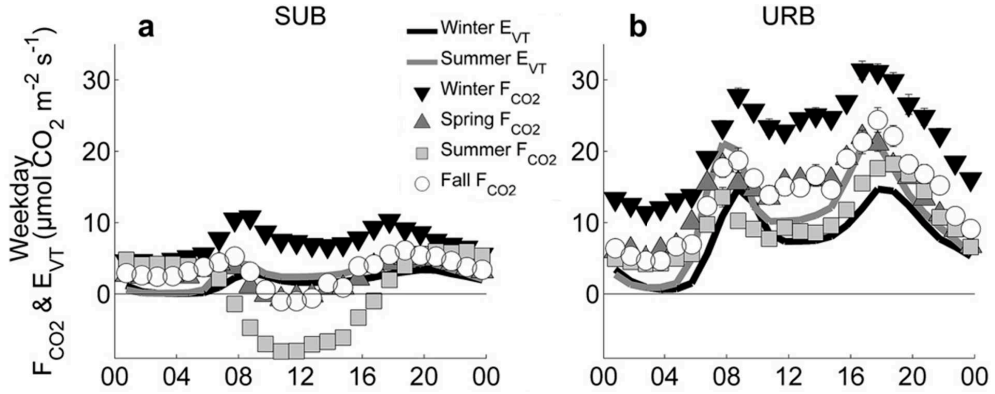
Figure 3.4: *Weekday summer and winter profiles of vehicular CO_2 emissions (E_{VT}) compared to daily CO_2 emissions for an urban (URB) and suburban (SUB) area of Montreal (modified from Bergeron and Strachan, 2011).*

and vehicular emissions between an urban and a suburban neighborhood. Intercepts (representing the estimated flux in absence of traffic) increase with urbanization, and, the urban site shows indeed a higher intercept value. Since the slope of the two linear relations are similar, the differences between urban and suburban sites confirm the presence of other non-traffic sources (i.e. winter local heating) (Bergeron and Strachan, 2011; Nemitz et al., 2002; Soegaard and Møller-Jensen, 2003; Velasco et al., 2005; Vesala et al., 2008).

When local traffic count datasets are available, E_T is estimated considering total consumption of fuel and emission coefficients (Moriwaki and Kanda, 2004). The knowledge of vehicle type, mean distance travelled by each vehicle, fuel type, and operating mode information can give more accurate estimates (Bergeron and Strachan, 2011; Christen et al., 2011; Matese et al., 2009). In accordance to Bergeron and Strachan (2011), E_T can be calculated as follows:

$$E_T = pvDVD \cdot N_V \cdot F_t \cdot \rho_{pop} \cdot EF \qquad (3.2)$$

where $pvDVD$ is the per vehicle daily vehicle distance (km vehicle^{-1} day^{-1}),

N_V is the number of vehicle per person (vehicle person^{-1}), F_t is the fraction of daily traffic per hour (day hour^{-1}), ρ_{pop} is the hourly population density (person m^{-2}) and EF is the emission factor corresponding to the amount of CO_2 released per vehicle per distance travelled (μmol CO_2 km^{-1}).

In addition, different top-down approaches have been used to estimate vehicular traffic emissions: (1) through a linear relation between CO_2 emissions and traffic measurements; (2) as a power-law of traffic counts (Contini et al., 2012; Gioli et al., 2012); (3) as residual derived from the difference between the total CO_2 flux, measured by the EC technique, and the other summed estimated contributions (Nemitz et al., 2002); (4) as function of number and type of vehicles, emission factors, and travelled distance (Christen et al., 2011); (5) through empirical footprint models (Hiller et al., 2011).

As an example, in a specific study area of Vancouver, vehicles were divided in four categories (light, transit, medium and heavy freight vehicles) based on their task and travelled distance, and estimates of total annual carbon and fuel consumption for each type of vehicle and fuel are shown in Table 3.1 (Christen et al., 2011). Whereas in Minneapolis-Saint Paul, Hiller et al. (2011) used an empirical footprint model, based on the road influence on the footprint area and on the number of vehicles.

Table 3.1: *Carbon emissions factors and fuel consumption per vehicle and fuel type (from Christen et al., 2011*

| Vehicle type	Fuel	Fuel efficiency	
		(l km^{-1})	(g C km^{-1})
Light	Gasoline	0.115	75.6
Medium freight	Gasoline	0.265	174.3
Heavy freight	Diesel	0.390	296.0
Transit	Diesel	0.390	296.0

Different studies showed that modeled daily traffic emission values vary

from 11.7 μmol m^{-2} s^{-1} in Edinburgh (Nemitz et al., 2002) to 7.5 μmol m^{-2} s^{-1} in Tokyo (Moriwaki and Kanda, 2004), whereas an annual value of 7.7 μmol m^{-2} s^{-1} was found in Vancouver (Christen et al., 2011).

3.2.2 CO_2 emissions from buildings

CO_2 emissions from buildings can be thought as the combination of two contributions: local natural gas combustion for heating and household services (Soegaard and Møller-Jensen, 2003). During daytime, E_B is in general the second most important CO_2 source (Christen et al., 2011; Nemitz et al., 2002). As reported in the previous section, Bergeron and Strachan (2011) have found a gap in intercepts, with increased CO_2 non-vehicular source emissions at higher urbanized areas (Figure 3.5). This gap accounts for 6.7 μmol m^{-2} s^{-1}, with the city center having more than double values (11.5 μmol m^{-2} s^{-1}) than the suburban area (4.8 μmol m^{-2} s^{-1}). This difference was partially explained by the household heating emissions. In addition, domestic heating also explained the winter-summer gap (2.2 μmol m^{-2} s^{-1}) observed in Copenhagen (Soegaard and Møller-Jensen, 2003).

A method recently used to estimate E_B is proposed by Crawford and Christen (2014). They have shown that building emissions have a negative linear relation with air temperature (T_{air}) expressed as Heating Degree Days (HDD), when it is below a certain threshold, whereas E_B is almost constant at higher temperatures. Christen et al. (2011) have shown that, in Vancouver, monthly CO_2 emissions are linearly dependent on HDD, increasing about 0.35 g C m^{-2} month^{-1} every HDD unit. Below a T_{air} threshold, air temperature values themselves are considered an indicator of heating demand.
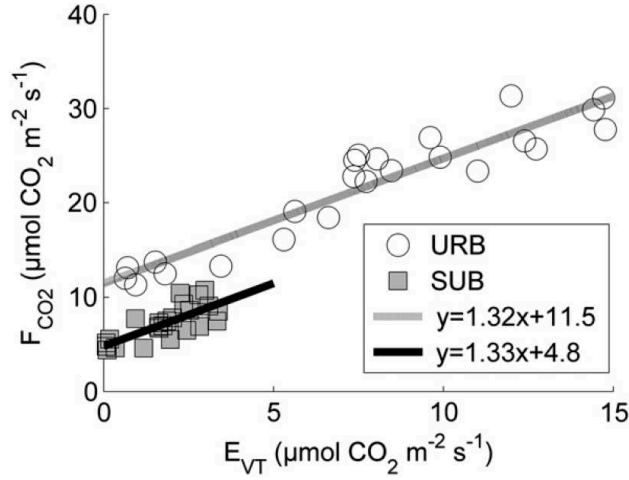
Figure 3.5: *Total winter CO_2 emissions as function of vehicular traffic emissions (E_{VT}) (from Bergeron and Strachan, 2011).*

Building emissions are then estimated by the following equation:

$$E_B = \frac{m\,T_{air} - b}{\lambda_B \cdot z_B} \qquad (3.3)$$

which is the ratio between the before mentioned linear relation below a certain threshold, and the product between the percentage of building land cover (λ_B) and building height (z_B) to account for different building volumes. However, this empirical method is biased toward residential buildings neglecting other building energy consumption profiles (Crawford and Christen, 2014).

Other approaches estimate emissions from buildings based on: (1) local fossil fuel consumption statistics (Nemitz et al., 2002); (2) energy use data multiplied by the density of dwellings (Moriwaki and Kanda, 2004); (3) building energy models Christen et al. (2011, 2010).

As an example, Christen et al. (2011, 2010) classified buildings based on their use, form, date of construction, and energy consumption determined by remote sensing (LiDAR) and statistical data. Thus, two building energy models, based on building volume and typology attributes, were used to

estimate building CO_2 emissions separately for residential dwellings (95% of total buildings) and "other" buildings (5% of total buildings).

Literature data showed, on average, a daily contribution from natural gas combustion of 12.6 μmol m^{-2} s^{-1} (52% of total net CO_2 flux) for the city of Edinburgh (Nemitz et al., 2002). Moriwaki and Kanda (2004) reported seasonal estimated emissions from buildings of 8.0 μmol m^{-2} s^{-1} (62%) in winter and 2.2 μmol m^{-2} s^{-1} (39%) in summer, whereas in Vancouver, Christen et al. (2011) estimated an annual value of 6.5 μmol m^{-2} s^{-1} (40% of total), 5.7 μmol m^{-2} s^{-1} coming from residential dwellings and 0.8 μmol m^{-2} s^{-1} due to non-residential dwellings.

3.2.3 CO_2 emissions from human respiration

Human respiration can be considered the third most important contribution to UNE, after traffic and buildings emissions (Christen et al., 2010; Moriwaki and Kanda, 2004; Nemitz et al., 2002). The contribution of human respiration to UNE is calculated by multiplying the estimated CO_2 human emission factor by population density. The distribution of population can be assumed homogeneous over the study area (Moriwaki and Kanda, 2004; Nemitz et al., 2002) or estimated based on residential floor area by using Li-DAR volume and land use data (Christen et al., 2010). Velasco et al. (2013) considered age, gender, weight, and the labour force rate of population from Singapore census data and local experience, to account for differences in human respiration rate.

Human exhalation rate varies from 201.5 μmol CO_2 person^{-1} s^{-1} (Moriwaki and Kanda, 2004) to 280 μmol CO_2 person^{-1} s^{-1} (Nemitz et al., 2002).

As a result, mean daily R_A values of about 2 μmol m^{-2} s^{-1} were found in Edinburgh (Nemitz et al., 2002) and Tokyo (Moriwaki and Kanda, 2004)

whereas an annual contribution of 1.3 μmol m^{-2} s^{-1} was found in the suburban area of Vancouver (Christen et al., 2011).

3.2.4 CO_2 emissions and uptake from vegetation

Daytime uptake due to vegetation photosynthesis can reduce emissions generated from other CO_2 sources. However, estimates of uptake by urban vegetation are difficult both because of the complexity of urban ecosystem and the different distribution of species and trees (Velasco et al., 2013).

Emissions and uptake from soil and vegetation can be modelled together, as ecosystem respiration (R_{eco}), or separately following the equation 3.1 for the total carbon dioxide flux estimation. For instance, according to Lloyd and Taylor (1994) (equation 2.5 in chapter 2), both the respiration of non-sealed surfaces (R_S) and R_{eco} can be estimated as function of soil (or air) temperature and on volumetric water content. Then, to up-scale for example the R_S flux estimate, the calculated respiration can be multiplied by the non-sealed area fraction (Christen et al., 2011; Soegaard and Møller-Jensen, 2003). Another approach was applied by Velasco et al. (2013), who used the empirical Q10 equation (Hoff van't, 1898) to simulate emissions from soil respiration in Singapore.

However, when the soil cover extension is only a small percentage of the total area, R_S is considered to be negligible (Gioli et al., 2012; Moriwaki and Kanda, 2004).

On the other hand, emissions from vegetation respiration (R_V) can be estimated from measurements of dark respiration in leaves or needles of representative trees species in the study area, or calculated as function of air temperature, based on literature data for similar vegetation. In addition, vegetation cover fraction or, recently, satellite-estimated Leaf Area Index

(LAI), as well as climatic data, are used to up-scale R_V (Christen et al., 2011; Nemitz et al., 2002).

Finally, the uptake from photosynthesis (P_V) can be modelled in different ways:

- as function of light response curves (Bergeron and Strachan, 2011; Christen et al., 2011; Crawford and Christen, 2014; Nemitz et al., 2002)

- using meteorological data and satellite LAI estimates as input of a "leaf level photosynthesis" model (Soegaard and Møller-Jensen, 2003)

- from literature data for similar vegetation type and scaling up the flux depending on vegetation cover fraction (Moriwaki and Kanda, 2004)

- using allometric equations, biomass and growth rates (Velasco et al., 2013)

Christen et al. (2011) reported, for the city of Vancouver, annual values for each of the three components (R_S, R_V, and P_V) representing a total net contribution to CO_2 flux of -0.42 μmol m^{-2} s^{-1}.

3.3   ACASA CO_2 flux modeling in urban areas

ACASA (Advanced Canopy-Atmosphere-Soil Algorithm) is a process-based model which has been developed for over the past twenty years by the University of California Davis (Meyers and Paw U, 1986; Meyers, 1985; Meyers and Paw U, 1987; Pyles, 2000; Pyles et al., 2004, 2000).

This model has been used both for stand-alone (in situ) simulations (Marras et al., 2011b; Staudt et al., 2010, 2011) and for regional scale modeling purposes when linked to the fifth-generation Pennsylvania State University-National Center for Atmospheric Research (NCAR) Mesoscale Model (MM5)

(Pyles et al., 2003) or to the Weather Research and Forecasting (WRF) numerical mesoscale weather model (Blečić et al., 2014; Casula, 2013; Falk et al., 2014; Marras et al., 2012). In all these works, it has been found that the model is able to adequately simulate turbulent fluxes in different environmental conditions and ecosystems.

Hereinafter, new numerical implementations used for the urban carbon exchange parametrization are described. The model was applied, at local scale, over the European city of Helsinki (Finland), and in situ EC measurements were used to evaluate ACASA main modifications in simulating the CO_2 flux over cities.

3.3.1 ACASA model description

This Soil-Vegetation-Atmosphere (SVAT) model simulates energy, mass and momentum vertical turbulent fluxes, as well as vertical wind profiles, temperatures, humidity, and CO_2 concentration within and above canopy. The prognostic equations are used to describe kinematic turbulent fluxes, and fourth, third, and second order turbulence closure parameterizations are calculated (Meyers and Paw U, 1986, 1987; Paw U and Gao, 1988). The ecosystem and the related fluxes are also described as an interconnected system where the atmosphere, the surface and the soil are represented as a multi-layer system (10 levels above the canopy, 10 levels within the canopy, and 10 levels within the soil) (Figure 3.6). 10 second order and 17 third order closure equations are calculated at each layer.

Multiple leaf/surface element angle classes (nine sunlight and one shaded) and direct as well as diffuse radiation absorption, reflection, transmission and emission, are considered to estimate energy fluxes per each layer. For each angle class, the flux sources and sinks are estimated per each canopy element
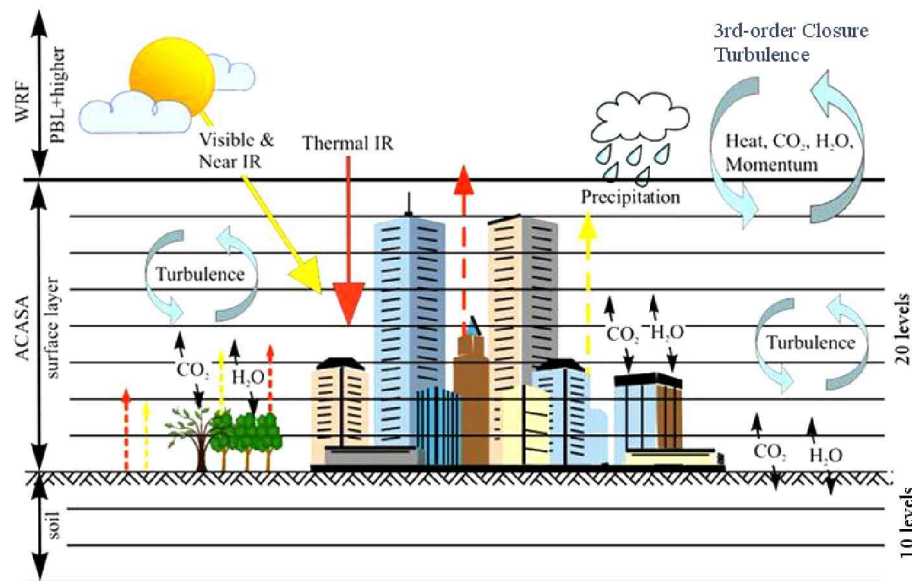
Figure 3.6: *Schematic representation of the ACASA multi-layer system.*

type (leaf, stem, building wall) and surface state (dry, wet, ice/snow-covered). Building surfaces and stems are assumed always dry. Flux calculation requires accurate computation of surface temperatures for leaf, stem, soil, and wall, even when they significantly differ from ambient air temperature.

The total carbon dioxide flux (UNE) in ACASA includes CO_2 flux from vegetation and soil, in addition to the anthropogenic sources (Falk et al., 2012).

In the vegetation scheme, a combination of the Ball-Berry stomatal conductance (Collatz et al., 1991) and the Farquhar and Von Caemmerer (1982) and Harley et al. (1992) equations for photosynthesis, as described by Su et al. (1996), is used to represent the plant physiological responses to changing micro-environmental conditions, including changes to carbon dioxide concentrations.

Vegetation can be specified with a leaf area index (LAI), which is defined

as the leaf or canopy element area per unit horizontal area of ground below the elements. This allows for the case of LAI > 0 in cities that have significant amounts of vegetation. LAI is used in ACASA for scaling up leaf energy and mass exchange, radiation transfer, and precipitation interception. A more detailed description can be found in Marras et al. (2011b), and Pyles et al. (2000, 2003).

To simulate local scale fluxes at a half-hourly time scale, the model is driven by measured meteorological variables, such as relative humidity (%), air temperature (K), wind speed (m s^{-1}), shortwave and longwave downward radiation (W m^{-2}), precipitation (mm), and air pressure (hPa) (Table 3.2). In addition to these, also hourly measured traffic counts are considered in urban environment. All values can be easily measured in a city or can derive, as boundary conditions, from mesoscale models, like WRF, in the WRF-ACASA coupled model version (Falk et al., 2010).

Table 3.2: *Meteorological input driving variables in the ACASA model.*

Input variables	Units
Fractional day	
Precipitation	mm
Relative humidity	%
Wind speed	m s^{-1}
Downward shortwave radiation	W m^{-2}
Downward longwave radiation	W m^{-2}
Air temperature	K
Atmospheric pressure	hPa
CO_2 concentration	ppmv
Vehicle counts	vehicle

The soil type is specified by modifying the USDA classification used by

Clapp and Hornberger (1978). There are 16 classes of soil type in the model code, from sandy to clay soil, accounting for organic matter content, presence of rocks, ice or open water. The sensitivity analysis was performed to investigate how the choice of soil type class and values of population density affect flux simulations (Marras et al., 2011a).

When population density is nonzero, urban modifications are reckoned in ACASA and urban fluxes are parameterized as proportional to population density. As a default, vegetation density is assumed to decrease linearly with population density above 1000 people km^{-2}, with zero values for population densities exceeding 10,000 people km^{-2}.

In this study, the model was modified to account for the anthropogenic contributions of carbon emissions and include fuel combustion due to transportation (E_T), household heating (E_B), and human respiration rate (R_A).

ACASA simulates CO_2 traffic emissions depending on the availability of measured traffic data. When measured vehicle counts (V) are available, they are normalized for the timestep (dt) and the footprint area (A) to infer a vehicle density measure (vehicle m^{-2} s^{-1}). Then, they are multiplied by the mean road length (l_r, km) travelled into the footprint and an averaged emission factor (EF, μmol CO_2 vehicle^{-1} km^{-1}):

$$E_T = \frac{V \cdot l_r \cdot EF}{dt \cdot A} \tag{3.4}$$

When vehicle data are not available, ACASA calculates carbon traffic flux from measured averages of the composite-diurnal carbon monoxide exposure, which varies throughout the diurnal cycle, used as a proxy for vehicle flux density. Emissions are then normalized to the population density.

Building contribution (E_B) to urban carbon balance is calculated as:

$$E_B = b_V \cdot H_p \cdot f \cdot f_{CO_2} \tag{3.5}$$

where b_V (m^3 m^{-2}) is a building volume-area index which consider a mean building volume with respect to the area of the footprint, H_p (W m^{-3}) is the building heating power for unite of volume, f (kg$_{diesel}$ m^{-3} s^{-1}) is the fuel consumption for heating, and f$_{CO_2}$ (μmol CO_2 kg$_{diesel}^{-1}$) represents the fuel CO_2 emission.

Human respiration rate (h_{CO_2}) is set to 201.5 μmol CO_2 person^{-1} s^{-1} (Christen et al., 2011; Moriwaki and Kanda, 2004) and multiplied by the nighttime resident population density (ρ_{pop}, person m^{-2}) to obtain the human respiration term (R_A):

$$R_A = h_{CO_2} \cdot \rho_{pop} \qquad (3.6)$$

As a result, UNE is simulated in ACASA by summing the biogenic carbon fluxes, as described in Marras et al. (2011b) and equations 3.4-3.6.

3.3.2   Case study: Helsinki

In this study, the city of Helsinki was selected to evaluate the ACASA performances over an urban environment. This urban site is part of the Helsinki Metropolitan area located on the Gulf of Finland. A 31 m high Eddy Covariance triangular lattice mast is placed at the Station for Measuring Ecosystems - Atmosphere Relations (SMEAR) III (60° 12' N, 24° 58' E, 26 m above sea level), at about 5 km north-east from the city center (Figure 3.7). It has been measuring urban turbulent fluxes since late 2004, and raw data were collected at 10 Hz and saved for later postprocessing. Commonly accepted procedures were then used in the calculation of 30-min fluxes and to assure data quality (Järvi et al., 2009b).

The area enclosing the EC tower is highly variable, and three wind sectors characterize the three main land uses, that are urban, road, and vegetation (see Järvi et al., 2009a, 2012 and Vesala et al., 2008 for more details). Within
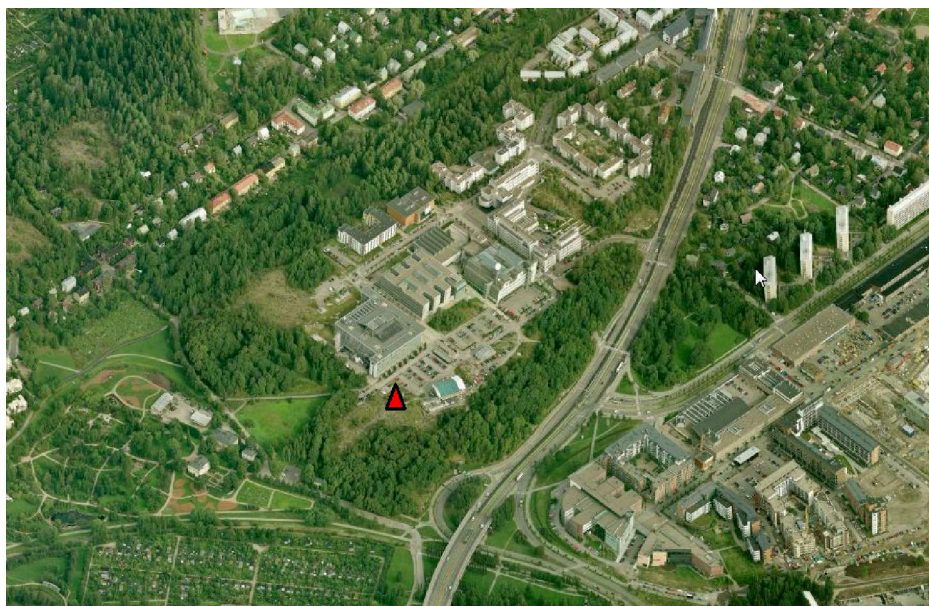
Figure 3.7: *Location of the Eddy Covariance tower (red triangle) at the SMEAR III station in Helsinki, Finland.*

a radius of 500 m, the surface is however 13% covered by buildings, 35% by impervious, and 52% by vegetation (Table 3.3) (personal communication).

Table 3.3: *Surface cover fractions within a radius of 500 m and 1000 m around the Eddy Covariance tower. All the wind sectors are considered.*

Distance (m)	Buildings	Impervious	Water	Vegetation
500	0.134	0.345	0.002	0.521
1000	0.148	0.383	0.003	0.469

Vegetation height is estimated to be 9 m on average and constituted both by gardens and grass, and deciduous trees[1] (Vesala et al., 2008). On the other hand, buildings typology is mainly commercial and their mean height is 20 m. Most of them, use district heating which is generated outside the footprint area by power plants (Järvi et al., 2012). For this reason, in this

---

[1] *Betula, Acer platanoides, Populus tremulus, Salix caprea, Prunus padus.*

study, emissions from buildings are considered negligible with respect with the other CO_2 emission sources.

A major road, with a traffic flow of 44,000 vehicles per workday (Lilleberg and Hellman, 2011), is located 150 m from the EC tower, and vehicular traffic is estimated to be the most important emission source in that area (Vesala et al., 2008). According to Järvi et al. (2012), a typical Helsinki traffic distribution is constituted by 83% passenger cars, 10% vans, 3% trucks and 4% buses (Lilleberg and Hellman, 2011), which leads to a mixed fleet CO_2 emission factor of 285 g km^{-1}.

ACASA was calibrated by using measured data of years 2008 – 2009 and selecting the best parameterization. The model was then run for a one year period (January – December 2010) and EC measurements were used to validate new implementations.

Two files are required in input, that are meteorological and traffic (30 minute) data (Table 3.2), and vegetation (plant and soil) and urban canopy information (Table 3.4). Whenever possible, in situ measurements were used to initialize the model.

Values of parameters related to vegetation (such as LAI and V_{cmax}) have been selected according to the vegetation species present in the study area. As LAI experimental measurements were not available, a combination of deciduous forest (such as birch trees) and grasslands was considered when estimating a LAI value for the city of Helsinki. LAI for birch ranges between 1.92 and 4.13 m^2 m^{-2} (Wang et al., 1995) whereas for grass values are between 0.3 and 5.0 (Asner et al., 2003). After model calibration, a mean LAI value of 1.4 m^2 m^{-2} was set to initialize ACASA.

In this work, the model vertical resolution was set to ten layers within the canopy and ten above-canopy, even if variations in the height or density

Table 3.4: *Biotic and urban parameterization used to run the ACASA model in the city of Helsinki.*

Description	Units	Helsinki
Year		2010
Latitude	decimal degrees	60.2
LAI	$m^2\ m^{-2}$	1.4
EC tower height	m	31
Canopy element drag coefficient		0.05
Wilting point	$m^3\ m^{-3}$	0.2
Soil type		3
Reflectivity (Visible)	μm	0.2
Reflectivity (Near Infrared)	μm	0.3
Tot. number of active root layers		7
Initial soil temperature	K	270
Initial soil moisture	$m^3\ m^{-3}$	0.35
Maximum carboxylation rate (V_{cmax})	$\mu mol\ CO_2\ m^{-2}\ s^{-1}$	62
population density	people km^{-2}v	2700
Human respiration	$\mu mol\ CO_2\ person^{-1}\ s^{-1}$	201.5
Mean CO_2 vehicle emission	$g\ CO_2\ km^{-1}\ vehicle^{-1}$	285
Mean road length into the footprint	km	1.4

of vegetation existed. The number of soil layers was set to 8, each of which is 0.20 m thick. The soil was classified as "sandy – loam" which corresponds to class 3 in the USDA classification. Wilting point, initial soil moisture and temperature must also be input (Table 3.4).

Assuming to have a long-term static footprint area, with 80% of isopleths, within a radius of 600 m, the mean road length travelled by a vehicle would be roughly equal to the footprint size (almost the length of the major road

into the footprint area) plus a small fraction due to minor roads. Therefore, the value of 1.4 m was set as mean road length.

3.3.3 Model results and statistical analysis

CO_2 fluxes simulated by the ACASA model were compared with in situ Eddy Covariance measurements. For the analysis, three weeks of the summer season, when the effect of vegetation is evident, were chosen. As a result, the selected periods are 11 – 18 June 2010 (DOY 162–169), 26 June – 2 July 2010 (DOY 177 – 184), and 19 – 26 July 2010 (DOY 200–207). The comparison was made both between simulated and observed fluxes at half hourly time step (Figure 3.8) and with data sorted and averaged by time (Figure 3.9).

Linear regression was used as a first assessment for the agreement of simulated (y_{sim}) and measured (y_{meas}) CO_2 fluxes, and the F statistic was used to test the significance of the model. Then, four statistical indices were calculated to check ACASA simulations accuracy: the Root Mean Square Error (RMSE), the Mean Absolute Error (MAE), the Mean Bias Error (MBE), and the Index Of Agreement (IOA).

The RMSE is the square root of the mean squared error and returns an average magnitude of the error. It is given by

$$RMSE = \sqrt{\frac{\sum_{i=1}^{N}(y_{sim,i} - y_{meas,i})^2}{N}} \tag{3.7}$$

where N is the number of data. Individual differences take not the same weight because they are squared and therefore RMSE is more sensitive by larger than small errors.

A similar equation is used to calculate the MAE, an average of the absolute errors between simulated and observed fluxes:

$$MAE = \frac{\sum_{i=1}^{N}|y_{sim,i} - y_{meas,i}|}{N} \tag{3.8}$$
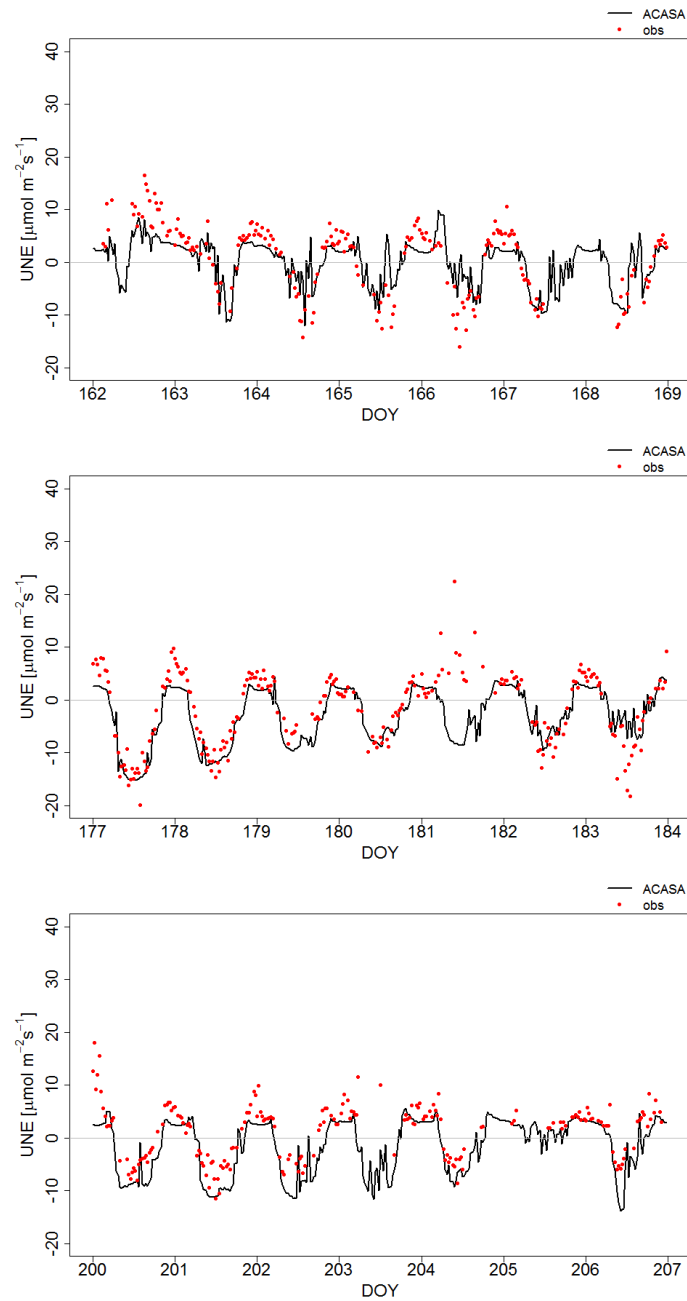
Figure 3.8: *Time histories showing measured (flux tower, red dots) and modelled (ACASA, black line) carbon flux for Helsinki, Finland. From top to bottom, the selected periods are 11 – 18 June 2010 (DOY 162–169) (R^2=0.67), 26 June – 2 July 2010 (DOY 177–184) (R^2=0.62), and 19 – 26 July 2010 (DOY 200–207) (R^2=0.7).*

Here, all the individual errors are instead equally weighted. As a consequence, MAE values are generally similar but slower than RMSE. In both cases, the more these indices are small, the more the model is accurate.

When also the sign of the errors is taken into account, the previous equation becomes the MBE:

$$MBE = \frac{\sum_{i=1}^{N}(y_{sim,i} - y_{meas,i})}{N} \tag{3.9}$$

which gives an indication of the tendency of the model to bias predictions. Underestimations are indicated by negative values whereas overestimation by numbers of positive sign.

Finally, the last statistical index is the IOA, which is calculated as follows:

$$IOA = 1 - \frac{\sum_{i=1}^{N}(y_{sim,i} - y_{meas,i})^2}{\sum_{i=1}^{N}(|y_{sim,i} - \bar{y}_{meas}| + |y_{meas,i} - \bar{y}_{meas}|)^2} \tag{3.10}$$

It can vary between 0 and 1, with 1 indicating a perfect fit between simulated and measured data.

In Table 3.5 the calculated statistic for the three summer weeks is shown.

Table 3.5: *Statistical indices for the ACASA modelled CO_2 flux during three summer weeks of 2010 in Helsinki. MAE and MBE values are expressed as $\mu mol \ m^2 \ s-1$.*

DOY (1 week period)	R^2	RMSE	MAE	MBE	IOA
162–169	0.67	4.21	3.25	-0.49	0.85
177–184	0.62	4.51	3.00	-1.48	0.87
200–207	0.70	4.19	3.22	-2.85	0.85

The model was able to capture the diurnal trend of CO_2 flux (Figure 3.8). The two typical peaks due to the traffic rush hours, a weak one in the morning and a major one in the late afternoon, can be observed. Moreover, UNE is affected by vegetation uptake during daytime both in the observations and the modelled time series.
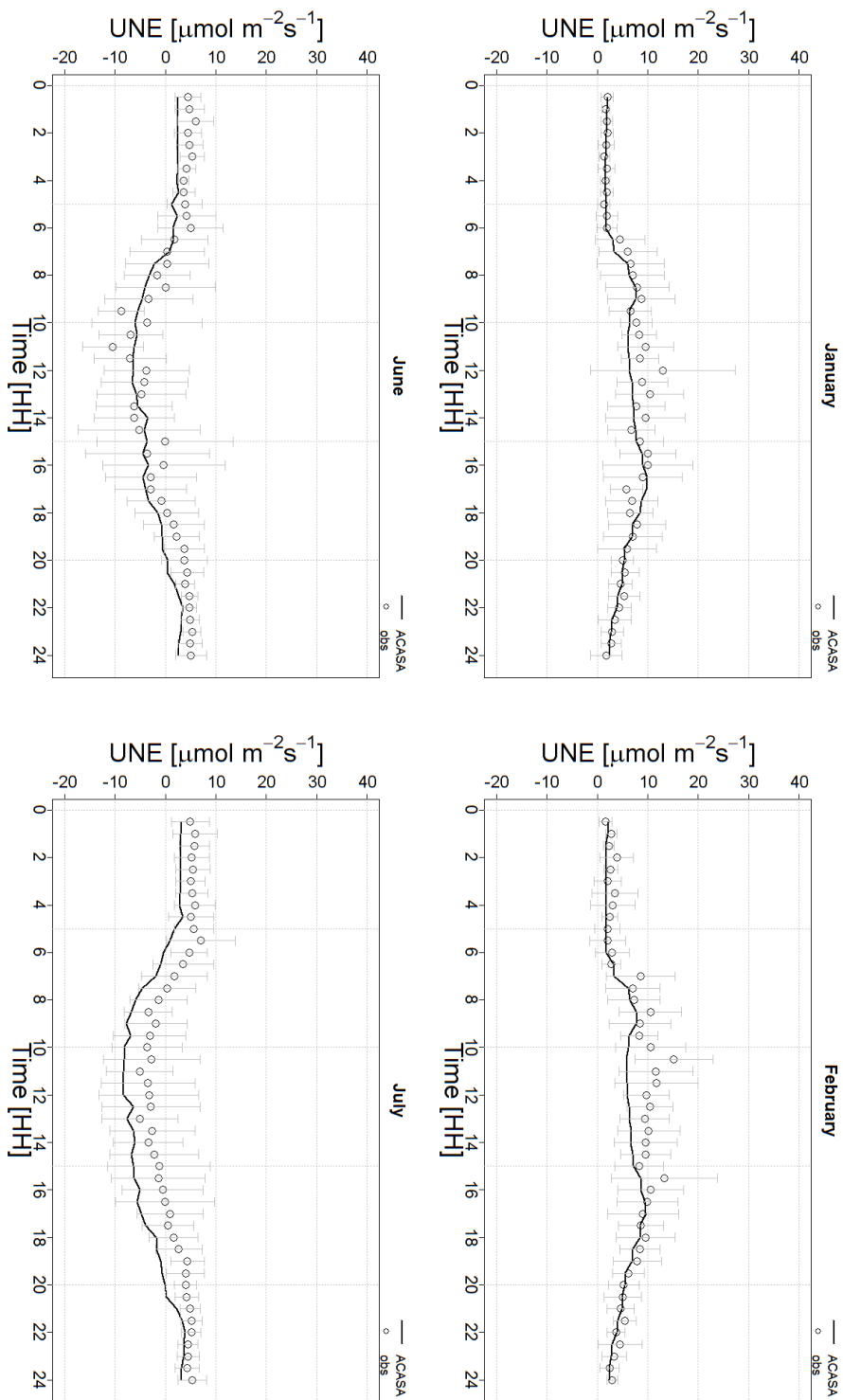
Figure 3.9: *Comparison between simulated (solid line) and mean half-hourly observed binned CO_2 flux (UNE) data (dots) in Helsinki. Standard deviation bars are also shown.*
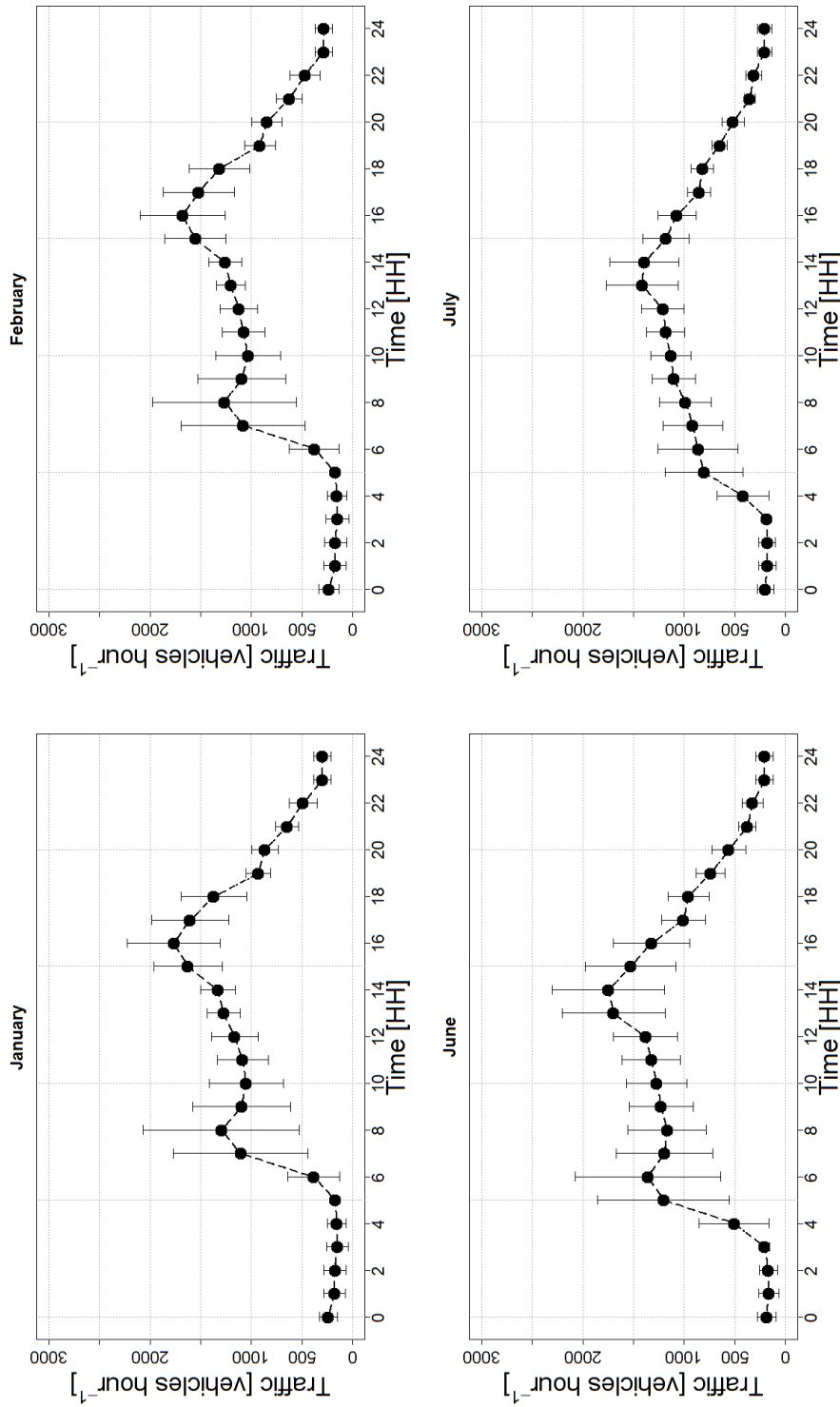
Figure 3.10: *Measured traffic counts in Helsinki during four months of 2010. Data are binned into 1 hour intervals and monthly averaged. Standard deviation bars are also shown.*

Increased emissions during the night period and reduced CO_2 fluxes during the day are related to the intense plants ecophysiological activity during the summer growing season. Diurnal peaks are due to locally emission sources (e.g. vehicular traffic).

The model explains up to 70% (R^2) of the weekly time history of half hourly CO_2 measured fluxes reproducing the daily trend. The other statistical indices (Table 3.5) are similar for the three weeks, with RMSE ranging between 4.19 μmol m^2 s^{-1} and 4.51 μmol m^2 s^{-1}, and MAE varying from 3.00 μmol m^2 s^{-1} and 3.25 μmol m^2 s^{-1}. Whereas, the MBE varies between -0.49 μmol m^2 s^{-1} and -2.85 μmol m^2 s^{-1}, thus highlighting a less model underestimation for the week 11 – 18 June 2010. The IOA is also mainly constant among weeks with values ranging from 0.85 and 0.87. A tendency to a model underestimation (negative MBE in Table 3.5) is related to uncertainties in measurements of traffic counts, traffic composition, vehicle emission factor and footprint definition, as discussed in Järvi et al. (2012), as well as assumptions related to the mean road length, LAI and other non-measured parameters.

Better model performances (R^2 up to 92% in July) are reached when considering UNE sorted and averaged by time over longer periods. In Figure 3.9 and Table 3.6 results are shown for the months of January, February, June, and July. Moreover, in Figure 3.10, the typical mean daily traffic trend for the simulated months is shown for comparison. ACASA is able to catch the UNE daily mean trend on a monthly scale with simulations falling within the interval range of standard deviations and reproducing the combined effects of the considered emissions sources and sink. High R^2 (0.70 – 0.92) and IOA (0.81 – 0.91) values in Table 3.6 highlight the general good performances of the model during winter and summer months. The RMSE

varied from 1.67 μmol m^2 s^{-1} in January to 3.88 μmol m^2 s^{-1} in July, and
MAE from 1.10 μmol m^2 s^{-1} to 3.62 μmol m^2 s^{-1}. Finally, the MBE showed
a lower model underestimation during January and June whereas in July the
model underestimation was more than 3 μmol m^2 s^{-1}.

Table 3.6: *Statistical indices for the ACASA modelled CO_2 flux sorted and averaged
by time during four months of 2010 in Helsinki.MAE and MBE values are expressed
as μmol m^2 s-1.*

Month	R^2	RMSE	MAE	MBE	IOA
January	0.74	1.67	1.10	-0.62	0.91
February	0.70	2.67	1.85	-1.77	0.82
June	0.86	2.45	2.23	-1.63	0.90
July	0.92	3.88	3.62	-3.62	0.81

Vehicular traffic in Helsinki is the most important contributor to the UNE
flux (Vesala et al., 2008). Especially in winter traffic and human respiration
are the main CO_2 contributors while the vegetation activity is at its mini-
mum and sinks of CO_2 are negligible. This is confirmed by the two typical
peaks due to the traffic rush hours, clearly distinguishable during that sea-
son, around 8 am and 4 pm (January and February in Figure 3.10). The
model was able to follow this trend as showed in Figure 3.9.

The model perfectly matched the nocturnal measured fluxes, the morn-
ing increase and the evening decrease in CO_2 flux related to traffic. A slight
model underestimation is instead evident during the central part of the day,
when a greater variability in anthropogenic sources is reported in measure-
ments. On the other hand, in summer months, peaks are early in the morning
(around 6 am) and in the afternoon (around 14 pm) both in simulated and
observed fluxes (June and July in Figures 3.10 and 3.9). Especially in July,

traffic rates are reduced due to the holiday period (Järvi et al., 2012) and the morning peak is not evident as in the other months. Therefore, the observed CO_2 exchange is mainly due to vegetation contribution than to traffic rates (Järvi et al., 2012). The contribution of vegetation is well reproduced by the model as shown by the higher R^2 values during these months (Table 3.6).

Greater differences between observations and model arose during the spring and fall seasons, when changes in vegetation conditions and anthropogenic contributions are not taken into account by the model, thus resulting, for example, in an overestimation of vegetation uptake in simulated UNE fluxes (data not shown). Improvements can be obtained by setting a variable LAI value during the year. In addition, further analysis per wind direction sectors could help in understanding some of the differences between model and observations.

3.4   Conclusion

So far, many efforts have been done to understand the impact of cities on the climate system. Results from Eddy Covariance flux measurements, sampled worldwide in the last ten years in different urban areas, have shown that cities are a net source of CO_2, both over short and long periods (Coutts et al., 2007; Grimmond et al., 2004; Hom et al., 2003; Velasco and Roth, 2010; Vogt et al., 2003). An exception to this is represented by residential sites with a percentage of vegetation cover greater than 70% during the summer growing season (Crawford et al., 2011; Velasco and Roth, 2010).

Emissions due to traffic are the greatest source, followed by those generated by building local heating and household activities, and by human and vegetation respiration. By contrast, vegetation uptake can offset these emis-

sions during the growing period, particularly within residential areas where vegetation represents at least the 34% total land cover (Velasco and Roth, 2010).

Urban systems are extremely complex and the interaction of carbon emissions with the environment and local meteorology make it a non-trivial task to quantify and predict CO_2 fluxes.

In the first part of this chapter, a scrupulous literature research was carried out in order to review different empirical and statistical methods used to simulate anthropogenic and biogenic components of urban CO_2 vertical exchanges. This review was recently published as part the book chapter "Urban carbon budget modeling", in "Understanding Urban Metabolism: A Tool for Urban Planning" (Spano et al., 2014).

The literature analysis led, in the second part of this work, to the implementation of the ACASA model for urban CO_2 flux simulations. The previous ACASA code was improved by new parameterizations to simulate traffic and human respiration emissions, whereas a new module to simulate emissions from building was proposed. The new ACASA version was tested over the city of Helsinki by using Eddy Covariance flux measurements from January to December 2010.

Results have shown a good agreement during three typical summer weeks and better performances are obtained when simulating mean daily trends (for bins of 30 minutes) on a monthly time scale. The traffic mark is distinguishable especially during the winter period rather than in summer, when traffic rates are reduced. Moreover, photosynthesis processes greatly affect summer fluxes and they are clearly reproduced by the model.

Greater discrepancies were found between modeled and observed fluxes during spring and fall, probably due to a fix LAI value entered as input into

the model. The inclusion of a monthly, or seasonal, variable LAI could improve the vegetation contribution estimation by the model especially during the early and final stage of the growing season. In addition, measurements of heating and cooling processes, as well as other household activities, could be important to include these sources into the model.

However, the use of ACASA to simulate urban fluxes is promising and future applications for studies at both local and meso-scale spatial resolution are planned.

References

Asner, G. P., Scurlock, J. M., and A Hicke, J. (2003). Global synthesis of leaf area index observations: implications for ecological and remote sensing studies. *Global Ecology and Biogeography*, 12(3):191–205.

Bergeron, O. and Strachan, I. B. (2011). CO_2 sources and sinks in urban and suburban areas of a northern mid-latitude city. *Atmospheric Environment*, 45(8):1564–1573.

Blečić, I., Cecchini, A., Falk, M., Marras, S., Pyles, D. R., Spano, D., and Trunfio, G. A. (2014). Urban metabolism and climate change: A planning support system. *International Journal of Applied Earth Observation and Geoinformation*, 26:447–457.

Canadell, J., Ciais, P., Dhakal, S., Le Quéré, C., Patwardhan, A., and Raupach, M. (2009). The human perturbation of the carbon cycle.

Casula, M. (2013). *A modelling approach to estimate carbon dioxide exchange at regional scale.* PhD thesis. PhD dissertation, University of Sassari.

Christen, A., Coops, N., Crawford, B., Kellett, R., Liss, K., Olchovski, I., Tooke, T., Van Der Laan, M., and Voogt, J. (2011). Validation of modeled carbon-dioxide emissions from an urban neighborhood with direct eddy-covariance measurements. *Atmospheric Environment*, 45(33):6057–6069.

Christen, A., Coops, N. C., Kellett, R., Crawford, B., Heyman, E., Olchovski, I., Tooke, T. R., and van der Laan, M. T. (2010). A lidar-based urban metabolism approach to neighbourhood scale energy and carbon emissions modelling.

Churkina, G. (2008). Modeling the carbon cycle of urban systems. *Ecological Modelling*, 216(2):107–113.

Churkina, G., Brown, D. G., and Keoleian, G. (2010). Carbon stored in human settlements: the conterminous united states. *Global Change Biology*, 16(1):135–143.

Clapp, R. B. and Hornberger, G. M. (1978). Empirical equations for some soil hydraulic properties. *Water resources research*, 14(4):601–604.

Collatz, G. J., Ball, J. T., Grivet, C., and Berry, J. A. (1991). Physiological and environmental regulation of stomatal conductance, photosynthesis and transpiration: a model that includes a laminar boundary layer. *Agricultural and Forest Meteorology*, 54(2):107–136.

Contini, D., Donateo, A., Elefante, C., and Grasso, F. (2012). Analysis of particles and carbon dioxide concentrations and fluxes in an urban area: Correlation with traffic rate and local micrometeorology. *Atmospheric Environment*, 46:25–35.

Coutts, A. M., Beringer, J., and Tapper, N. J. (2007). Characteristics influencing the variability of urban CO_2 fluxes in Melbourne, Australia. *Atmospheric Environment*, 41(1):51–62.

Crawford, B. and Christen, A. (2014). Spatial source attribution of measured urban eddy covariance CO_2 fluxes. *Theoretical and Applied Climatology*, pages 1–23.

Crawford, B., Grimmond, C., and Christen, A. (2011). Five years of carbon dioxide fluxes measurements in a highly vegetated suburban area. *Atmospheric Environment*, 45(4):896–905.

Decker, E. H., Elliott, S., Smith, F. A., Blake, D. R., and Rowland, F. S. (2000). Energy and material flow through the urban ecosystem. *Annual Review of Energy and the Environment*, 25:685–740.

Falk, M., Pyles, R., Marras, S., Spano, D., Snyder, R., and Paw U, K. (2010). A regional study of urban fluxes from a coupled WRF-ACASA model. In *AGU Fall Meeting Abstracts*, volume 1.

Falk, M., Pyles, R. D., Marras, S., Spano, D., Paw U, K. T., and Snyder, R. L. (2012). Regional simulation of urban metabolism in Helsinki, Finland in 2008. submitted.

Falk, M., Pyles, R. D., Ustin, S. L., Paw U, K. T., Xu, L., Whiting, M. L., Sanden, B. L., and Brown, P. H. (2014). Evaluated Crop Evapotranspiration over a Region of Irrigated Orchards with the Improved ACASA-WRF Model. *Journal of Hydrometeorology*, 15(2):744–758.

Farquhar, G. and Von Caemmerer, S. (1982). Modelling of photosynthetic response to environmental conditions. In *Physiological plant ecology II*, pages 549–587. Springer.

Gioli, B., Toscano, P., Lugato, E., Matese, A., Miglietta, F., Zaldei, A., and Vaccari, F. (2012). Methane and carbon dioxide fluxes and source partitioning in urban areas: The case study of florence, italy. *Environmental pollution*, 164:125–131.

Grimmond, C. and Christen, A. (2012). Flux measurements in urban ecosystems. *Invited article in Flux-Letter–Newsetter of Fluxnet*, 5(1):1–7.

Grimmond, C., Salmond, J., Oke, T. R., Offerle, B., and Lemonsu, A. (2004). Flux and turbulence measurements at a densely built-up site in marseille:

Heat, mass (water and carbon dioxide), and momentum. *Journal of Geophysical Research: Atmospheres (1984–2012)*, 109(D24).

Harley, P., Thomas, R., Reynolds, J., and Strain, B. (1992). Modelling photosynthesis of cotton grown in elevated CO_2. *Plant, Cell & Environment*, 15(3):271–282.

Heiple, S. and Sailor, D. J. (2008). Using building energy simulation and geospatial modeling techniques to determine high resolution building sector energy consumption profiles. *Energy and Buildings*, 40(8):1426–1436.

Hiller, R. V., McFadden, J. P., and Kljun, N. (2011). Interpreting CO_2 fluxes over a suburban lawn: The influence of traffic emissions. *Boundary-layer meteorology*, 138(2):215–230.

Hoff van't, J. (1898). *Lectures on theoretical and physical chemistry. Part 1. Chemical dynamics.* Edward Arnold, London.

Hom, J., Grimmond, S., Golub, D., Offerle, B., Nowak, D., Heisler, G., Pouyat, R., and Zipperer, W. (2003). Studies on carbon flux and carbon dioxide concentrations in a forested region in suburban Baltimore. Baltimore Ecosystem Study Annual Meeting, Baltimore, MD, October 2002.

Imhoff, M. L., Bounoua, L., Ricketts, T., Loucks, C., Harriss, R., and Lawrence, W. T. (2004). Global patterns in human consumption of net primary production. *Nature*, 429(6994):870–873.

Järvi, L., Hannuniemi, H., Hussein, T., Junninen, H., Aalto, P. P., Hillamo, R., Mäkelä, T., Keronen, P., Siivola, E., Vesala, T., et al. (2009a). The urban measurement station SMEAR III: Continuous monitoring of air pollution and surface-atmosphere interactions in Helsinki, Finland. *Boreal environment research*, 14:86–109.

Järvi, L., Mammarella, I., Eugster, W., Ibrom, A., Siivola, E., Dellwik, E., Keronen, P., Burba, G., and Vesala, T. (2009b). Comparison of net CO_2 fluxes measured with open-and closed-path infrared gas analyzers in an urban complex environment. *Boreal Environment Research*, 14:499–514.

Järvi, L., Nordbo, A., Junninen, H., Riikonen, A., Moilanen, J., Nikinmaa, E., and Vesala, T. (2012). Seasonal and annual variation of carbon dioxide surface fluxes in helsinki, finland, in 2006–2010. *Atmospheric Chemistry and Physics*, 12(18):8475–8489.

Kennedy, C., Cuddihy, J., and Engel-Yan, J. (2007). The changing metabolism of cities. *Journal of industrial ecology*, 11(2):43–59.

Koerner, B. and Klopatek, J. (2002). Anthropogenic and natural CO_2 emission sources in an arid urban environment. *Environmental Pollution*, 116:S45–S51.

Lilleberg, I. and Hellman, T. (2011). The development of traffic in helsinki in 2010. *Helsinki City Planning Department*, 2011:2.

Lloyd, J. and Taylor, J. (1994). On the temperature dependence of soil respiration. *Functional ecology*, pages 315–323.

Marras, S., Casula, M., Pyles, R., Paw U, K., and Spano, D. (2011a). Evaluation of the impact of planning alternative strategies on urban metabolism with the ACASA model. In *AGU Fall Meeting Abstracts*, volume 1.

Marras, S., Pyles, R. D., Falk, M., Casula, M., Snyder, R. L., Paw U, K. T., and Spano, D. (2012). Urban fluxes estimation at local and regional scale by ACASA model. In *ICUC8 - 8th International Conference on Urban Climates, 6 - 10 August 2012. Dublin, Ireland*, volume 1.

Marras, S., Pyles, R. D., Sirca, C., Paw U, K. T., Snyder, R. L., Duce, P., and Spano, D. (2011b). Evaluation of the Advanced Canopy-Atmosphere-Soil Algorithm (ACASA) model performance over Mediterranean maquis ecosystem. *Agricultural and Forest Meteorology*, 151(6):730–745.

Matese, A., Gioli, B., Vaccari, F., Zaldei, A., and Miglietta, F. (2009). "carbon dioxide emissions of the city center of firenze, italy: measurement, evaluation, and source partitioning". *Journal of Applied Meteorology and Climatology*, 48(9):1940–1947.

Meyers, T. and Paw U, K. T. (1986). Testing of a higher-order closure model for modeling airflow within and above plant canopies. *Boundary-Layer Meteorology*, 37(3):297–311.

Meyers, T. P. (1985). *A simulation of the canopy microenvironment using higher order closure principles*. PhD thesis. PhD dissertation, Purdue University.

Meyers, T. P. and Paw U, K. T. (1987). Modelling the plant canopy micrometeorology with higher-order closure principles. *Agricultural and Forest Meteorology*, 41(1):143–163.

Milesi, C., Running, S. W., Elvidge, C. D., Dietz, J. B., Tuttle, B. T., and Nemani, R. R. (2005). Mapping and modeling the biogeochemical cycling of turf grasses in the united states. *Environmental Management*, 36(3):426–438.

Moriwaki, R. and Kanda, M. (2004). Seasonal and diurnal fluxes of radiation, heat, water vapor, and carbon dioxide over a suburban area. *Journal of Applied Meteorology*, 43(11):1700–1710.

Nemitz, E., Hargreaves, K. J., McDonald, A. G., Dorsey, J. R., and Fowler, D. (2002). Micrometeorological measurements of the urban heat budget and CO_2 emissions on a city scale. *Environmental Science & Technology*, 36(14):3139–3146.

Pataki, D., Alig, R., Fung, A., Golubiewski, N., Kennedy, C., McPherson, E., Nowak, D., Pouyat, R., and Romero Lankao, P. (2006). Urban ecosystems and the North American carbon cycle. *Global Change Biology*, 12(11):2092–2102.

Paw U, K. T. and Gao, W. (1988). Applications of solutions to non-linear energy budget equations. *Agricultural and Forest Meteorology*, 43(2):121–145.

Puliafito, E. (2006). Urban ecology: linking carbon emissions and air quality. First International Conference on Carbon Management at Urban and Regional Levels: Connecting Development Decisions to Global Issues, Global Carbon Project, Mexico City, September 4-8, 2006.

Pyles, R. D. (2000). *The development and testing of the UCD Advanced Canopy- Atmosphere-Soil Algorithm (ACASA) for use in climate prediction and field studies*. PhD thesis. PhD dissertation, Davis, University of California.

Pyles, R. D., Paw U, K. T., and Falk, M. (2004). Directional wind shear within an old-growth temperate rainforest: observations and model results. *Agricultural and forest meteorology*, 125(1):19–31.

Pyles, R. D., Weare, B. C., and Pawu, K. T. (2000). The UCD Advanced Canopy-Atmosphere-Soil Algorithm: Comparisons with observations from

different climate and vegetation regimes. *Quarterly Journal of the Royal Meteorological Society*, 126(569):2951–2980.

Pyles, R. D., Weare, B. C., U, K. T. P., and Gustafson, W. (2003). Coupling between the University of California, Davis, Advanced Canopy-Atmosphere-Soil Algorithm (ACASA) and MM5: Preliminary results for July 1998 for western North America. *Journal of Applied Meteorology*, 42(5):557–569.

Ramamurthy, P. and Pardyjak, E. R. (2011). Toward understanding the behavior of carbon dioxide and surface energy fluxes in the urbanized semi-arid salt lake valley, utah, usa. *Atmospheric environment*, 45(1):73–84.

Satterthwaite, D. (2008). Cities contribution to global warming: notes on the allocation of greenhouse gas emissions. *Environment and urbanization*, 20(2):539–549.

Soegaard, H. and Møller-Jensen, L. (2003). Towards a spatial CO_2 budget of a metropolitan region based on textural image classification and flux measurements. *Remote Sensing of Environment*, 87(2):283–294.

Spano, D., Marras, S., and Bellucco, V. (2014). Urban carbon budget modeling. In *Understanding Urban Metabolism: A Tool for Urban Planning*, pages 117–128. Routledge.

Staudt, K., Falge, E., Pyles, R. D., Paw, U., Foken, T., et al. (2010). Sensitivity and predictive uncertainty of the ACASA model at a spruce forest site. *Biogeosciences*, 7(11):3685–3705.

Staudt, K., Serafimovich, A., Siebicke, L., Pyles, R. D., and Falge, E. (2011). Vertical structure of evapotranspiration at a forest site (a case study). *Agricultural and forest meteorology*, 151(6):709–729.

Su, H.-B., Paw U, K. T., and Shaw, R. H. (1996). Development of a coupled leaf and canopy model for the simulation of plant-atmosphere interaction. *Journal of Applied Meteorology*, 35(5):733–748.

UN (2014). *World urbanization prospects: The 2014 revision, Highlights.* UN. United Nations. Department of Economic and Social Affairs. Population Division.

Velasco, E., Pressley, S., Allwine, E., Westberg, H., and Lamb, B. (2005). Measurements of CO_2 fluxes from the Mexico City urban landscape. *Atmospheric Environment*, 39(38):7433–7446.

Velasco, E. and Roth, M. (2010). Cities as net sources of CO_2: Review of atmospheric CO_2 exchange in urban environments measured by eddy covariance technique. *Geography Compass*, 4(9):1238–1259.

Velasco, E., Roth, M., Tan, S., Quak, M., Nabarro, S., and Norford, L. (2013). The role of vegetation in the CO_2 flux from a tropical urban neighbourhood. *Atmospheric Chemistry and Physics*, 13(20):10185–10202.

Vesala, T., Järvi, L., Launiainen, S., Sogachev, A., Rannik, Ü., Mammarella, I., Siivola, E., Keronen, P., Rinne, J., Riikonen, A., et al. (2008). Surface–atmosphere interactions over complex urban terrain in helsinki, finland. *Tellus B*, 60(2):188–199.

Vogt, R., Christen, A., Rotach, M. W., Roth, M., and Satyanarayana, A. (2003). Fluxes and profiles of CO_2 in the urban roughness sublayer. In *Fifth International Conference on Urban Climate. Lodz, Poland.*

Walsh, C. J., Oke, T., Grimmond, C., and Salmond, J. (2004). Fluxes of atmospheric carbon dioxide over a suburban area of Vancouver. In *Fifth Symposium on Urban Environments, Vancouver, BC, Canada.*

Wang, T., Tigerstedt, P., and Viherä-Aarnio, A. (1995). Photosynthesis and canopy characteristics in genetically defined families of silver birch (betula pendula). *Tree physiology*, 15(10):665–671.

Wolman, A. (1965). The metabolism of cities. *Scientific American*, 213(3):179–190.

Chapter 4

Estimations of the CO_2 flux over different ecosystems

4.1   Introduction

Carbon fluxes are the result of the net exchange between an ecosystem and the overlying atmosphere. In natural and managed ecosystems, it is due to the sum of biogenic components (ecosystem respiration and photosynthesis processes) (equation 2.1), and it is increased by human contributes in urban and suburban areas (equation 3.1).

Suburban areas, with a higher vegetation fraction than city centres, show a similar behaviour to natural ecosystems (Crawford et al., 2011). Vegetation behaves both as a source and a sink of CO_2, and in urban sites, the diurnal carbon uptake by plants and lawns can help in reducing CO_2 emitted by human activities. As vegetation cover decreases, CO_2 emissions increase because of the less plant photosynthesis uptake (Bergeron and Strachan, 2011; Velasco and Roth, 2010). This effect is particularly evident during the vegetation growing season as observed for example in Montreal (Bergeron

and Strachan, 2011) and Baltimore (Crawford et al., 2011).

In summer there is a negative correlation between daily CO_2 fluxes and vegetation cover fraction (λ_V) (Figure 4.1). In cities where $\lambda_V > 34\%$, vegetation is able to reduce emissions deriving from other CO_2 sources through photosynthesis uptake, but under this threshold the effect of lawns and trees is increasingly less effective (Bergeron and Strachan, 2011; Velasco and Roth, 2010). Moreover, when urban vegetation is scarce ($< 5\%$), soil and vegetation exchanges can be neglected (Matese et al., 2009; Moriwaki and Kanda, 2004; Velasco et al., 2009), whereas when the natural fraction is greater than 80%, cities can be considered sinks on an annual scale (Nordbo et al., 2012).

Another way to look at this relation is to observe carbon fluxes as function of urban density (Figure 4.2): the more the fraction of building is high, the more CO_2 fluxes are emitted, whereas the less the fraction of building is, the more the vegetation is likely to be important in the area in reducing carbon emissions.

In a recent study, Nordbo et al. (2012) has shown that the natural cover fraction (obtained as the difference between total land cover and urban fraction) is a robust proxy to estimate annual carbon exchange in urban sites. Natural (vegetation and bare soils) and urban (buildings and impervious) cover fraction can therefore address to an estimation of carbon emissions.

Based on this evidence, an interesting perspective is to figure out how different urban and non-urban ecosystems are related based on land cover fractions. So, the general aim of this work was to try to answer this question: is it possible to generalize these concepts so that, depending on the percentage of different land cover fractions, an estimation of carbon exchanges of any ecosystem can be inferred?

A first attempt towards this goal is the development of an integrated
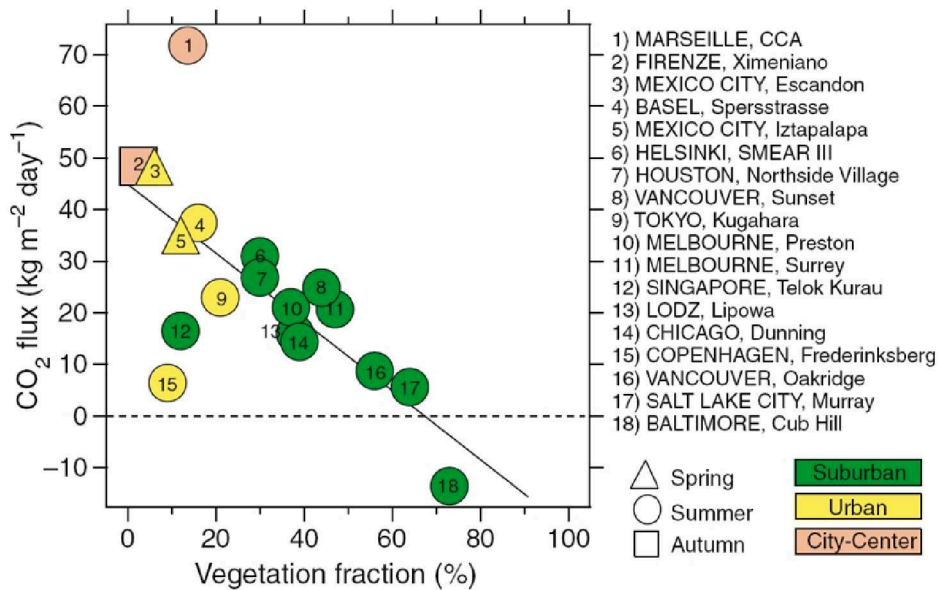
Figure 4.1: Urban CO_2 flux as function of different vegetation cover fraction (from Velasco and Roth, 2010).
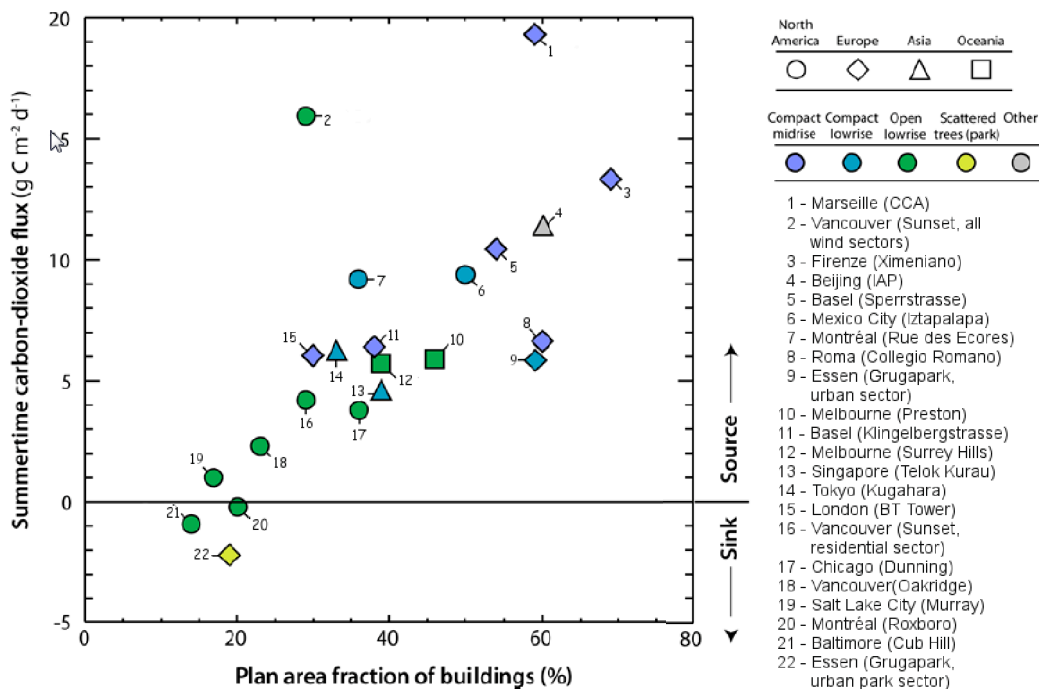

Figure 4.2: Urban CO_2 flux as function of different building cover fraction (modified from Grimmond and Christen, 2012).

model which simulates the mean daily trend of the vertical CO_2 flux based on empirical relations.

Recently, an application of a totally empirical modelling approach was showed over a suburban site by Crawford and Christen (2014). Each component of the vertical CO_2 flux in urban areas, namely photosynthesis uptake (P_V), ecosystem respiration (R_{eco}), human respiration (R_A), buildings emissions (E_B), and vehicular traffic emissions (E_V) (equation 3.1) was modelled as follows:

- P_V by using the non-rectangular hyperbola (equation 2.5),

- R_{eco} through the Lloyd and Taylor (1994) relation (equation 2.7),

- R_A from information of building cover,

- E_B by using the equation 3.3,

- E_V through an empirical linear relation based on impervious cover fraction.

In this case the empirical model was developed considering one suburban site. So, it is site-specific.

The aim of this work is to develop an integrated model based on empirical equations, usually used to simulate CO_2 fluxes of a single ecosystems, in order to apply it over different ecosystems (natural, agricultural, urban, and suburban), and figure out relations among them. The advantage of such a model is that, the empirical relations developed for specific sites, with distinctive characteristics, are generalized, so it can be used to aid estimations in a broad range of ecosystems.

A brief description of the modelling approach is reported in paragraph 4.2.2. The first module of the model, which simulates the biogenic contribu-

tion from soil and vegetation respiration and photosynthesis, was developed based on the empirical relations reported in Chapter 2. Here, a first validation is proposed both over a natural ecosystem, maily composed by Mediterranean Maquis vegetation, and over a suburban site (Helsinki). The anthropogenic module is actually under development but the pursued modelling approach is however reported.

4.2 Materials and Methods

4.2.1 Sites description and analysis

A total of six sites with different vegetation types and λ_V was considered for the model development: the natural Mediterranean Maquis site (Capo Caccia, Italy) and the two agricultural (Serdiana and Montalcino, Italy) ecosystems, fully described in Chapter 2, and three more sites, such as two suburban areas (Swindon, UK, and Baltomre, MD,USA), and a forest (Morgan Monroe State Forest, IN, USA) (Table 4.1).

Original datasets (non gap-filled) were used for the Mediterranean sites whereas data derived from literature were used for the forest and the suburban sites. A complete description of the three Mediterranean sites can be found in Chapter 2.

Swindon (51.58° N, 1.80° W) is a British town of 4700 inhabitants km^{-2}, located at about 120 km west of London (Ward et al., 2013). Eddy Covariance (EC) measurements were collected, above a 12.5 m high pneumatic mast, from May 2011 to April 2012 in a residential area (3 km north from the city center) (Ward et al., 2013). Within a radius of 500 m, slightly less than half of total land cover is vegetation ($\lambda_V = 0.44$), most of which (80%) is grass of parks and gardens ($\lambda_V = 0.36$), and the rest (20%) are deciduous

Veronica Bellucco, *Empirical estimations of CO_2 flux components over different ecosystems*, Tesi di Dottorato in "Scienze e Biotecnologie dei Sistemi Agrari e Forestali e delle Produzioni Alimentari", Indirizzo "Agrometeorologia ed Ecofisiologia dei Sistemi Agrari e Forestali", Università degli Studi di Sassari.

Table 4.1: *Description of the selected sites having different vegetation cover fractions* (λ_V)

Site	Area	Latitude	Period	% veg	λ_V
Morgan Monroe **State Forest** **(MMSF), IN, USA** (Schmid et al., 2000)	Deciduous forest	39.32° N 86.42° W	May–September (1998)	0 (grass) 100 (tree)	1
Baltimore, MD, USA (Crawford et al., 2011)	Suburban	39.41° N 76.52° W	Summer (2002–2006)	13.8 (grass) 53.6 (tree)	0.70
Swindon, UK (Ward et al., 2013)	Suburban	51.58° N 1.80° W	Summer (2011)	36 (grass) 9 (tree)	0.40
Serdiana, Italy (Marras et al., 2012)	Vineyard	39.36° N 9.12° E	Jun–Jul–Aug (2009–2011)	∼50 (grapevine)	∼0.50
Montalcino, Italy (Marras, 2008)	Vineyard	43.08° N 11.80° E	Jun–Jul–Aug (2005–2006)	∼50 (grapevine)	∼0.50
Capocaccia, Italy (Marras et al., 2011)	Mediterranean Maquis	40.61° N 8.15° E	Year (2005–2010)	∼70 (shrubs)	∼0.70

trees and shrubs ($\lambda_V = 0.09$) that have a mean height of 6 m. For more details see Ward et al. (2013).

In Baltimore, Maryland (USA), CO_2 fluxes were monitored for five years (2002 – 2006) in the suburban area of Cub Hill (39.41° N, 76.52° W) from an EC tower of 41.2 m height. The area is characterized by about 1500 inhabitants km^{-2} and a very high percentage of vegetation (67.4%), mostly deciduous trees of 11.4 m height on average (80% of total vegetation, $\lambda_V = 0.54$), and grass from parks and lawns (20% of total vegetation, $\lambda_V = 0.14$) (Crawford et al., 2011).

The Morgan-Monroe State Forest (39.32° N, 86.42° W) is a managed mixed broadleaf deciduous forest located in the south central Indiana (USA) presenting a total vegetation cover of 100% and a mean canopy height of 25–27 m. Annual EC data (March 1998 – February 1999) were sampled by a 46 m height tower (Schmid et al., 2000).

These measurements were sampled at 10 Hz or 20 Hz, post processed by the authors using common accepted procedures and checked for quality control.

EC measurements of these six sites were analyzed in order to look for general relations among different ecosystems and to develop the biogenic module.

The same methodology described in Chapter 2 was followed. Therefore, the vegetation growing season (usually summer for deciduous ecosystems) was selected, except for the evergreen Mediterranean maquis site of Capo Caccia.

Light response curves were analyzed for the six sites, fitting experimental data by using the non rectangular hyperbola (equation 2.6). The photosynthetically active radiation (PAR) as main predictor for photosynthesis and respiration processes.

The main steps of the methodology are briefly reported below:

- selection of daytime data ($R_g > 5$ W m^{-2}),

- calculation of median values of CO_2 flux measurements in bins of 50 μmol m^{-2} s^{-1} of PAR,

- fit of the light-response curve with LOESS (Locally Estimated Scatterplot Smoothing) regression (Cleveland et al., 1992),

- fit of the light-response curve using the non-rectangular hyperbola (NRH) and estimation of its α, β, γ, and θ coefficients through the non-linear least square regression.

Results of the fits of the light response curves for Swindon, Baltimore and the Morgan-Monroe State Forest are shown in Figure 4.3 and Table 4.2. For more details on Mediterranean sites, see Chapter 2.
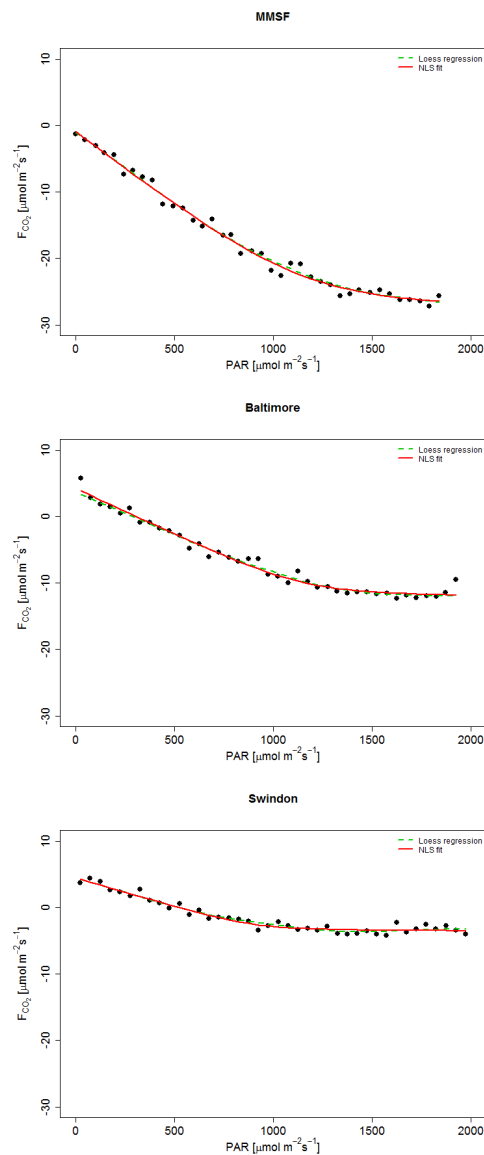
Figure 4.3: *Photosynthetic light response curves during the growing season in the Morgan-Monroe State Forest (MMSF) and the suburban areas of Baltimore and Swindon. Trends of daytime ($R_g > 5$ W m^{-2}) multi-year CO_2 fluxes as function of PAR. Data are sorted in bins of 50 μmol m^{-2} s^{-1} and fitted using the LOESS regression and a non-rectangular hyperbolae (equation 2.6) by nonlinear least squares. From top to bottom: MMSF (R^2 =0.96), Baltimore (R^2 =0.98) and Swindon (R^2 =0.99).*

Table 4.2: *Coefficients of the non-rectangular hyperbolae (equation 2.6) estimated by non-linear least squares. In brackets approximated standard errors of the estimates are showed for the new sites of Morgan-Monroe State Forest, Baltimore and Swindon. Results for Serdiana, Montalcino and Capo Caccia (both for total data and data splitted for soil water content (SWC)) are reported from Chapter 2 to summarize results. All the parameters estimates were significant with P < 0.0001.*

Site	λ_V	SWC [% vol]	α [μmol CO_2 μmol photons^{-1}]	β [μmol CO_2 m^{-2} s^{-1}]	γ [μmol CO_2 m^{-2} s^{-1}]	θ dimensionless
MMSF	1	/	0.022 (0.001)	27.588 (1.584)	-0.932 (0.426)	0.951 (0.028)
Baltimore	0.7	/	0.013 (0.001)	16.568 (0.938)	4.211 (0.412)	0.977 (0.019)
Swindon	0.4	/	0.009 (0.001)	8.106 (0.484)	4.473 (0.312)	0.98 (0.021)
Serdiana	0.5	/	0.018	8.207	1.597	0.881
Serdiana	0.5	22–23	0.016	6.192	0.932	0.881
Serdiana	0.5	> 23	0.019	8.804	1.657	0.881
Montalcino	0.5	/	0.013	9.469	1.917	0.862
Capo Caccia	0.7	/	0.013	6.814	1.74	0.972
Capo Caccia	0.7	15–18	0.005	2.648	1.861	0.91
Capo Caccia	0.7	18–20	0.008	5.918	1.809	0.91
Capo Caccia	0.7	20–38	0.012	10.394	0.929	0.91
Capo Caccia	0.7	>38	0.015	13.055	0.838	0.91

Differences in carbon uptake and emissions are particularly evident among the three sites: unsurprisingly, the forest site shows the highest uptake and the least CO_2 emissions, whereas the city of Swindon is responsible of higher carbon emissions and a lower vegetation uptake (Figure 4.3).

In agreement with Boote and Loomis (1991)(Boote and Loomis, 1991), α parameter has a little variability (between 0.01 μmol CO_2 μmol photons^{-1} and 0.02 μmol CO_2 μmol photons^{-1}) and, as expected, the gross photosynthetic assimilation (β) increases with the increase of vegetation varying from about 8 to more than 27 μmol CO_2 m^{-2} s^{-1}. The intercept (γ) provides an estimate of the ecosystem respiration (R_{eco}), which decreases as the vegetation cover fraction increases. During the day, R_{eco} is, in fact, mostly due to

the soil efflux than to canopy respiration. Finally, values range of the curvature parameter θ are between 0.86 and 0.98, in accordance with literature (Boote and Loomis, 1991; Gilmanov et al., 2003; Marshall and Biscoe, 1980; Ögren, 1993) (Table 4.2).

The preliminary analysis on the six selected sites allowed an investigation on relations among different ecosystems based on different vegetation cover fractions. This led to the development of the biogenic module of the empirical model proposed hereinafter.

4.2.2   Simple model

The model is constituted by two modules that take separately into account both biogenic and anthropogenic contributions to the total CO_2 flux (F_{CO_2}). As a remind, F_{CO_2} is the sum of different terms:

$$F_{CO_2} = E_T + E_B + R_A + (R_S + R_V - P_V) \qquad (4.1)$$

A description of each module is reported below.

Biogenic module

Biogenic components of the carbon flux are estimated as function of solar radiation (R_g) and vegetation cover fraction (λ_V). Figure 4.4 reports the schematic representation of the module and the related equation (NRH). It allows the estimation of the biogenic carbon flux across a range of vegetation cover fractions.

In the model, R_g is used to estimate the photosynthetically active radiation (PAR) considering that to photosynthesize leaves absorb radiation with wavelengths inside the visible spectrum range (0.4 μm $< \lambda <$ 0.7 μm). A median wavelength value of 0.55 μm was therefore used in the conversion of
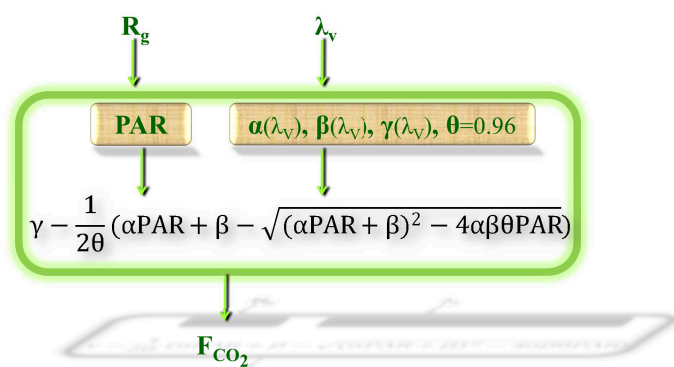
Figure 4.4: *Structure of the simple model. Solar radiation (R_g) and vegetation cover fraction (λ_V) are needed as input to estimate photosynthetically active radiation (PAR) and the four coefficients of the non-rectangular hyperbola (NRH) equation. The simulated carbon fluxes are calculated based on the NRH equations.*

R_g (W m^{-2}) into PAR (μmol m^{-2} s^{-1}). Furthermore, PAR was considered to be on average 0.46 of R_g (Tsubo and Walker, 2005).

The dependence between vegetation cover fraction and the light response curves fit with the NRH was first analyzed for the six sites. The four estimated coefficients of the NRH (Table 4.2), were plotted as function of vegetation cover fraction (Figure 4.5). The dependence of the NRH coefficients on λ_V led to the identification of linear relations among coefficients calculated from data not split for soil water content (SWC) (Figure 4.5).

These relations allows to estimate α, β, and γ coefficients as function of λ_V (Figure 4.5). θ was fixed to the median value (0.96) because a non clear relation was highlighted among sites.

In this way, by combining both PAR and NRH coefficients estimation, the mean trend of CO_2 fluxes (Figure 4.4) can be reproduced, as schematically represented in Figure 4.4.
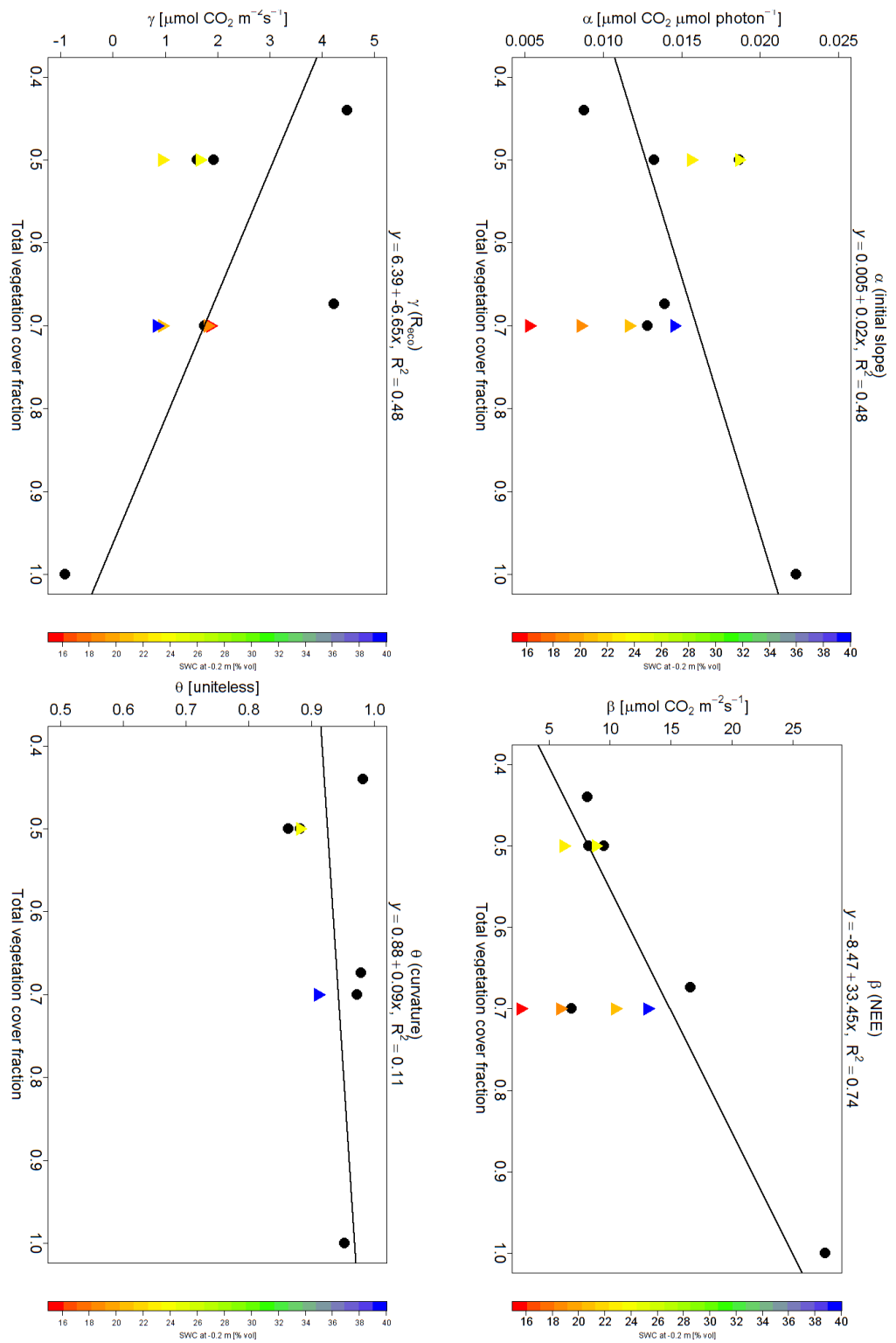
Figure 4.5: *Estimated coefficients of the non-rectangular hyperbola (equation 2.6) as function of vegetation cover fraction. Regression lines are calculated with data not sorted for soil water content.*

Anthropogenic module

Anthropogenic sources are characterized by a high variability level due to the different terms involved and to the complexity of the system. Therefore the emission sources are difficult to model and they are affected by local characteristics (morphology, population density, city sprawl, energy sources, meteorology, ect.) and by the intrinsic dynamics of the system.

In Chapter 3 are reviewed different ways (from more complex to simplified methods) to estimate emissions from traffic, buildings and humans. The attempt here is to estimate these terms by using few input data, which are commonly available and easy to collect.

The module is still under development, but the proposed approach is reported here. The estimation of different emission sources will be based on:

- information of fuel CO_2 emission and consumption for heating, building cover fraction, and building heating power for volume, to estimate E_B,

- information about building cover fraction, from which the population density can be inferred, and human respiration rate to estimate R_A,

- information on impervious cover fraction, to find linear regressions with traffic, to estimate E_V.

4.3 Results and discussion

So far, the simple model can simulate the biogenic components of the carbon balance over different ecosystems. Two sites, with different morphological characteristics, vegetation cover fractions, and climatic conditions, were chosen for this purpose: the suburban area of Helsinki ($\lambda_V = 0.52$, section 3.3.2) and the Capo Caccia unmanaged ecosystem of Mediterranean Maquis

($\lambda_V = 0.7$, section 2.2.3). Besides vegetation cover, these sites also differ for environmental conditions. In particular, the soil water content (SWC) greatly affects ecophysiological processes in Mediterranean ecosystems (Figure 2.15) especially during the dry summer season. The influence of SWC on Mediterranean sites is also evident in Figure 4.5. When λ_V=0.7 (Capo Caccia site), the β coefficient, which represents the range between the ecosystem respiration and the maximum uptake, changes depending on water stress conditions: during drought periods, β values range from 2.6 μmol m^2 s^{-1} (15% vol< SWC < 18% vol) to 10.4 μmol m^2 s^{-1} (20% vol < SWC < 38% vol), whereas a value of 13.1 μmol m^2 s^{-1} is reached at higher soil moisture (i.e. SWC > 38% vol), similarly to other non-Mediterranean sites. (Figure 4.5, Table 4.2). Therefore, data for the winter period (January, February, and March 2011), when the ecosystem is in well watered conditions and vegetation is at its maximum ecophysiological activity, were used to validate the model at the Capo Caccia site. During that period, SWC ranged from 40.4% vol (March) to 43.5% vol (January).

Two months of the summer season (June – July 2010) were chosen instead for the validation of this model over the urban site of Helsinki, as it is the period in which vegetation is at its maximum and vehicular traffic rates are reduced (Figure 3.10).

To validate the model over both sites, the CO_2 flux was sorted and averaged by time. Results of the simple model simulation are shown in Figures 4.6 - 4.7 and statistical indices are reported in Table 4.3.

Results for the urban site of Helsinki, shown in Figure 4.6, have highlighted high R^2 values, both on single months (June, $R^2 = 81\%$, and July, $R^2 = 88\%$) and on summed periods (June + July, $R^2 = 0.87\%$) (Table 4.3). This underlines the model capability to reproduce the diurnal mean trend of

CO_2 fluxes. The model is, as expected, able to catch the diurnal vegetation uptake, particularly evident in central hours, where the model simulation crosses experimental values (Figure 4.6). During the growing season, the vegetation in Helsinki is one of the most important contributor to the total vertical CO_2 flux, being on average a sink, with observed values ranging from a mean maximum of 6.02 μmol m^2 s^{-1} in June and 7.07 μmol m^2 s^{-1} in July, to a mean minimum of -10.42 μmol m^2 s^{-1} in June and -5.11 μmol m^2 s^{-1} in July. The range of variability is, on average, about 5.6 μmol m^2 s^{-1}. The Root Mean Squared Error (RMSE) varied from 2.61 μmol m^2 s^{-1} (June) to 3.11 μmol m^2 s^{-1} (July) and the Mean Absolute Error (MAE) was also lower in June than in July ranging from 2.28 μmol m^2 s^{-1} to 2.84 μmol m^2 s^{-1}. Moreover, the Mean Bias Error (MBE) showed a lower underestimation during June (-1.49 μmol m^2 s^{-1}) than in July (-2.84 μmol m^2 s^{-1}). At night, in the early morning, and in the evening, differences between modelled and experimental data are observed, and measurements have highlighted the presence of other sources, such as traffic emissions and human and animal respiration. However, the model simulation almost always falls within the range of variability of observed values, and both diurnal and nocturnal trend is reproduced, reaching Index Of Agreement (IAO) values of 0.88 in June and in the summed months (Table 4.3).

Simulations for the Capo Caccia site, shown Figure 4.7, have highlighted that the model is able to reproduce the mean daily trend of CO_2 fluxes, and it also matches almost perfectly with observations mainly representing the photosynthetic activity during the day and the respiration processes at night. This is confirmed by the high values of the IOA which range between 0.98 and 0.99. In this natural ecosystem, the regression between modelled and observed data explained from 93% to 96% of binned half-hourly variance,
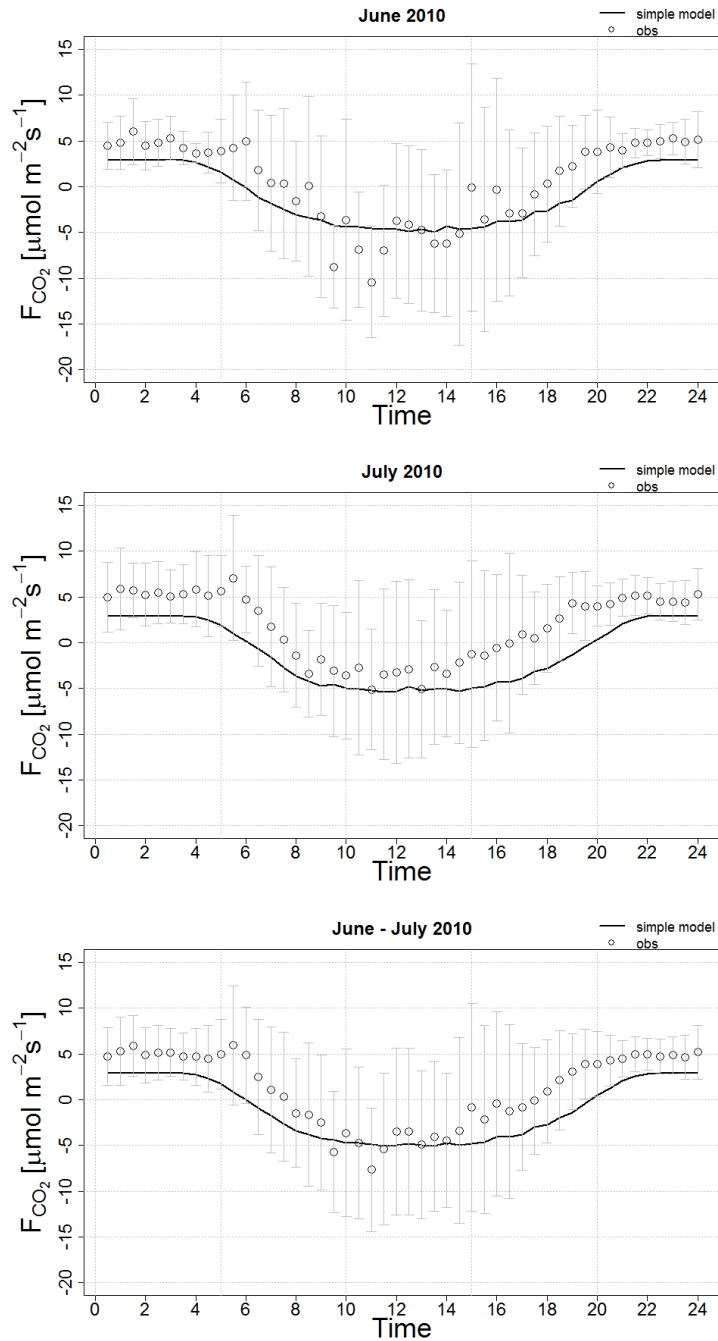
and up to 98% when considering the cumulated three winter months (Table 4.3). The RMSE varied from 0.82 μmol m^2 s^{-1} to 1.34 μmol m^2 s^{-1}, and MAE from 0.63 μmol m^2 s^{-1} to 0.98 μmol m^2 s^{-1}.

In all the considered periods, regression between simulated and measured CO_2 fluxes were statistically significant 0.001 probability.

Table 4.3: *Statistics of the simple model simulations for the sites of Helsinki (suburban) and Capo Caccia (unmanaged Mediterranean Maquis). Indices indicate the R-squared (R^2), the Root Mean Squared Error (RMSE), the Mean Absolute Error (MAE), the Mean Bias Error (MBE), and the Index Of Agreement (IOA). For the Mediterranena Maquis site of Capo Caccia an indication of the Soil Water Content (SWC) is also given into brackets. Significant values at 99% probability level.*

Helsinki

Period	R^2	RMSE	MAE	MBE	IOA
June	0.81	2.61	2.28	-1.49	0.88
July	0.88	3.11	2.84	-2.84	0.84
June + July	0.87	2.66	2.4	-2.21	0.88

Capo Caccia

Period	R^2	RMSE	MAE	MBE	IOA
January	0.93	0.99	0.72	0.09	0.98
February	0.96	1.25	0.97	-0.70	0.98
March	0.94	1.34	0.98	-0.48	0.98
Jan + Feb + Mar	0.98	0.82	0.63	-0.46	0.99

The statistical analysis underlines a better performance of the model in the natural Mediterranean site than in the suburban area of Helsinki, where underestimations are indicated by negative values of MBE. However, this is explained considering that the biogenic module does not take into account

Veronica Bellucco, *Empirical estimations of CO_2 flux components over different ecosystems*, Tesi di Dottorato in "Scienze e Biotecnologie dei Sistemi Agrari e Forestali e delle Produzioni Alimentari", Indirizzo "Agrometeorologia ed Ecofisiologia dei Sistemi Agrari e Forestali", Università degli Studi di Sassari.

Figure 4.6: *Comparison between mean binned half-hourly observations (dots) and simulation of CO_2 flux (solid line) in Helsinki during two monts of the vegetation growing season. Vertical bars indicate standard deviations of the binned values.*
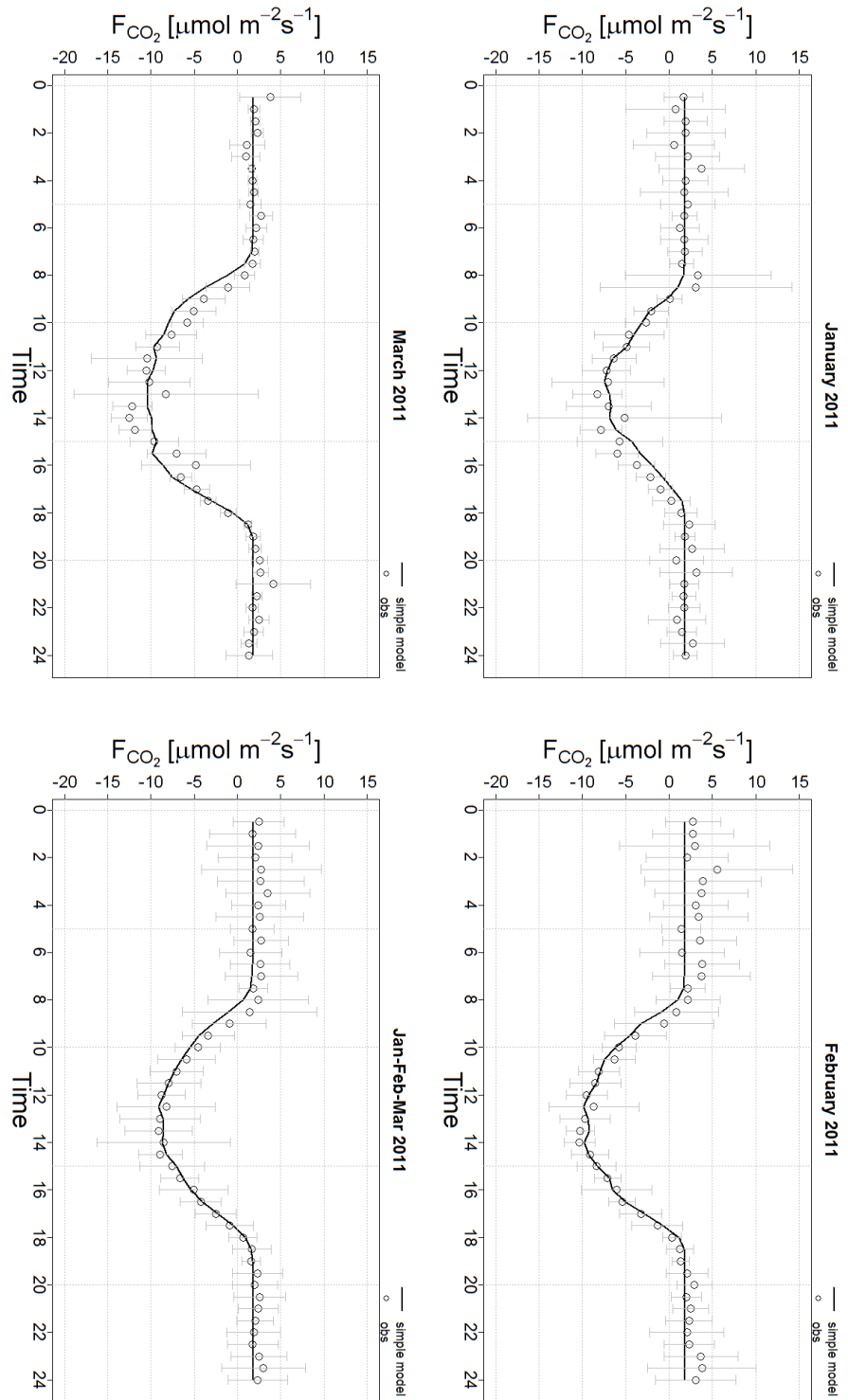
Figure 4.7: *Comparison between mean binned half-hourly observations (dots) and simulation of CO_2 flux measurements in the Mediterranean maquis site during the three most watered months of 2011. Standard deviations of the binned values are also indicated with vertical bars.*

any anthropogenic component of the urban carbon balance.

In conclusion, the good agreement of the model with both human modified and unmanaged ecosystems confirms the evidence that CO_2 fluxes depends on the amount of vegetation cover. Moreover, it opens a new perspective in the study of relations among different ecosystems and in understanding the role of vegetation in urban areas.

4.4 Conclusion

In this work, an extensive analysis of available literature was conducted in order to study different modelling techniques to estimate carbon dioxide exchanges between the surface and the atmosphere both on urban and natural ecosystem. The non-rectangular hyperbola (equation 2.6) is the most used empirical equation for simulations of biogenic carbon fluxes (Aubinet et al., 2012; Crawford and Christen, 2014; Gilmanov et al., 2003; Stoy et al., 2006).

Evidences of the dependence of urban CO_2 fluxes on vegetation cover were shown by Velasco and Roth (2010) and Nordbo et al. (2012) and this study is the first step in the construction of a simple empirical model based on land cover fraction and able to simulate carbon fluxes over different ecosystems.

The model is thought to be constituted by two main integrated modules, differing for biogenic and anthropogenic contributions. Both modules are based on commonly measured variables and information about land cover fraction to obtain estimates of the CO_2 flux.

So far, the biogenic module was developed from the analysis of the light response curves of six sites. Using solar radiation (R_g) to infer PAR values, and the vegetation cover fraction (λ_V) to calculate, through linear regression equations (Figure 4.5), variables coefficients of the Non-Rectangular Hyper-

Veronica Bellucco, *Empirical estimations of CO₂ flux components over different ecosystems*, Tesi di Dottorato in "Scienze e Biotecnologie dei Sistemi Agrari e Forestali e delle Produzioni Alimentari", Indirizzo "Agrometeorologia ed Ecofisiologia dei Sistemi Agrari e Forestali", Università degli Studi di Sassari.

bola, estimations of the CO_2 flux were calculated.

This simple model reproduces ecosystem respiration and vegetation uptake both in urban and natural ecosystem during periods when maximum ecophysiological processes occur.

Preliminary results have shown good performances with regressions between modelled and observed data explaining up to 0.88% and 98% of total variance over the suburban site of Helsinki and over the natural Mediterranean Maquis ecosystem, respectively. Thus, the development of such a model is interesting in the general purpose of catching a general behaviour of ecosystems.

The simple model was presented on a poster session titled "CO_2 fluxes estimation for different vegetation cover fractions", of the 31st American Meteorological Society Conference on Agricultural and Forest Meteorology that was held in May, 2014 in Portland, Oregon, USA.

Further improvements are planned in order to estimate ecosystem respiration with the Lloyd and Taylor (1994) relation (equation 2.7), and add the anthropogenic module, with E_V, E_B, and R_A components, to this model. Information about building and impervious cover fraction will be used.

However, with the aim to increase robustness of this simple model, and include the second anthropogenic module into it, a great number of sites should be considered. This necessarily implies collaborations with other universities, where a sharing of original Eddy Covariance datasets of urban and suburban areas is to be hoped. According to this idea, at the moment annual data of highly vegetated cities have been requested for Minneapolis-Saint Paul, Berlin, and Basel cities.

References

Aubinet, M., Vesala, T., and Papale, D. (2012). *Eddy covariance: a practical guide to measurement and data analysis.* Springer.

Bergeron, O. and Strachan, I. B. (2011). CO_2 sources and sinks in urban and suburban areas of a northern mid-latitude city. *Atmospheric Environment*, 45(8):1564–1573.

Boote, K. J. and Loomis, R. S. (1991). The prediction of canopy assimilation. *Modeling Crop Photosynthesis–from Biochemistry to Canopy*, 19:109–137.

Crawford, B. and Christen, A. (2014). Spatial source attribution of measured urban eddy covariance CO_2 fluxes. *Theoretical and Applied Climatology*, pages 1–23.

Crawford, B., Grimmond, C., and Christen, A. (2011). Five years of carbon dioxide fluxes measurements in a highly vegetated suburban area. *Atmospheric Environment*, 45(4):896–905.

Gilmanov, T. G., Verma, S. B., Sims, P. L., Meyers, T. P., Bradford, J. A., Burba, G. G., and Suyker, A. E. (2003). Gross primary production and light response parameters of four Southern Plains ecosystems estimated using long-term CO_2-flux tower measurements. *Global Biogeochemical Cycles*, 17(2).

Grimmond, C. and Christen, A. (2012). Flux measurements in urban ecosystems. *Invited article in Flux-Letter–Newsetter of Fluxnet*, 5(1):1–7.

Lloyd, J. and Taylor, J. (1994). On the temperature dependence of soil respiration. *Functional ecology*, pages 315–323.

Marras, S. (2008). *Evaluation of the Advanced Canopy-Atmosphere-Soil Algorithm (ACASA) model performance using micrometeorological techniques.* PhD thesis, Agrometeorology and Ecophysiology of Agricultural and Forest Ecosystems, University of Sassari.

Marras, S., Pyles, R. D., Sirca, C., Paw U, K. T., Snyder, R. L., Duce, P., and Spano, D. (2011). Evaluation of the Advanced Canopy-Atmosphere-Soil Algorithm (ACASA) model performance over Mediterranean maquis ecosystem. *Agricultural and Forest Meteorology*, 151(6):730–745.

Marras, S., Sirca, C., Duce, P., Arca, A., Zara, P., Bacciu, V., and D, S. (2012). Carbon sequestration monitoring in a typical Mediterranean vineyard. 30th American Meteorological Society Conference on Agricultural and Forest Meteorology, Boston, May 26th-June 2nd.

Marshall, B. and Biscoe, P. V. (1980). A model for c3 leaves describing the dependence of net photosynthesis on irradiance. *Journal of Experimental Botany*, 31(1):29–39.

Matese, A., Gioli, B., Vaccari, F., Zaldei, A., and Miglietta, F. (2009). "carbon dioxide emissions of the city center of firenze, italy: measurement, evaluation, and source partitioning". *Journal of Applied Meteorology and Climatology*, 48(9):1940–1947.

Moriwaki, R. and Kanda, M. (2004). Seasonal and diurnal fluxes of radiation, heat, water vapor, and carbon dioxide over a suburban area. *Journal of Applied Meteorology*, 43(11):1700–1710.

Nordbo, A., Järvi, L., Haapanala, S., Wood, C. R., and Vesala, T. (2012). Fraction of natural area as main predictor of net co2 emissions from cities. *Geophysical Research Letters*, 39(20).

Ögren, E. (1993). Convexity of the photosynthetic light-response curve in relation to intensity and direction of light during growth. *Plant Physiology*, 101(3):1013–1019.

Schmid, H. P., Grimmond, C. S. B., Cropley, F., Offerle, B., and Su, H.-B. (2000). Measurements of CO_2 and energy fluxes over a mixed hardwood forest in the mid-western United States. *Agricultural and Forest Meteorology*, 103(4):357–374.

Stoy, P. C., Katul, G. G., Siqueira, M., Juang, J.-Y., Novick, K. A., Uebelherr, J. M., and Oren, R. (2006). An evaluation of models for partitioning eddy covariance-measured net ecosystem exchange into photosynthesis and respiration. *Agricultural and Forest Meteorology*, 141(1):2–18.

Tsubo, M. and Walker, S. (2005). Relationships between photosynthetically active radiation and clearness index at bloemfontein, south africa. *Theoretical and applied climatology*, 80(1):17–25.

Velasco, E., Pressley, S., Grivicke, R., Allwine, E., Coons, T., Foster, W., Jobson, B., Westberg, H., Ramos, R., Hernández, F., et al. (2009). Eddy covariance flux measurements of pollutant gases in urban mexico city. *Atmospheric Chemistry and Physics*, 9(19):7325–7342.

Velasco, E. and Roth, M. (2010). Cities as net sources of CO_2: Review of atmospheric CO_2 exchange in urban environments measured by eddy covariance technique. *Geography Compass*, 4(9):1238–1259.

Ward, H., Evans, J., and Grimmond, C. (2013). Multi-season eddy covariance observations of energy, water and carbon fluxes over a suburban area in Swindon, UK. *Atmospheric Chemistry and Physics*, 13(9):4645–4666.

# Appendix A

Basics on the Planetary Boundary Layer structure

A.1 Atmospheric vertical profile

The *troposphere* is the lowest layer of the atmosphere which contains 75% of its gaseous mass as well as almost all water vapour and aerosols. The Earth surface acts as a boundary at the bottom whereas the *tropopause*, a temperature inversion layer, bounds the top (Figure A.1). The troposphere is characterized by having a decreasing vertical temperature profile and a vertical extension of about $10 - 11$ km (Oke, 1987; Stull, 1988). Within it, atmospheric phenomena range from local ($10^2 - 5 \cdot 10^4$ m) to micro ($10^{-2} - 10^3$ m) scales and occur in a time lapse of less than one hour (Oke, 1987). Processes occurring at smaller scales (<1 km and <1 day) are the principal object of micrometeorology (Foken and Nappo, 2008).

In a general dynamic description of fluids, it is common to identify one or more zones strongly affected by the proximity to the boundary. Similarly, approaching to the terrestrial surface, atmospheric motions are directly mo-

dified by the nearby surface and several distinguishable boundary layers can be detected (Hartmann, 1994; McIlveen, 1992; Oke, 1987; Stull, 1988).

A first distinction is made between the lower *Planetary Boundary Layer* (PBL) and the *free atmosphere* beyond (Figure A.1).
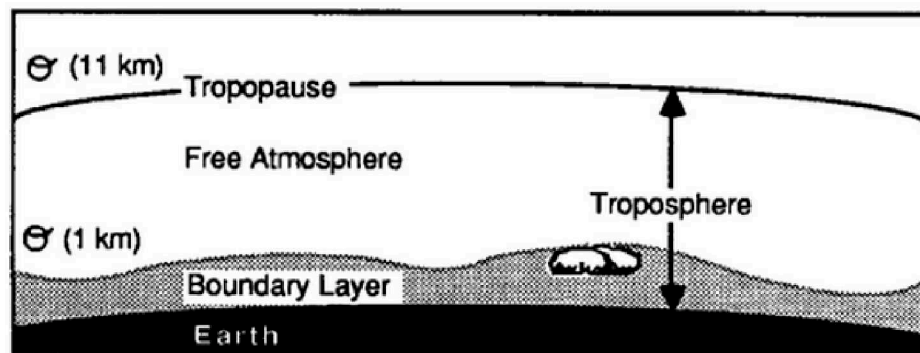
Figure A.1: *Vertical structure of the first 11 km of the atmosphere (from Stull, 1988)*

A.1.1   PBL structure and evolution

The free atmosphere does not directly experiences the effect of diurnal temperature surface variation except in case of strongly developed thermal convection conditions (Hartmann, 1994; Stull, 1988). Turbulence is occasional and negligible there, whereas within the PBL a well developed mixing is always present and dominates air motions.

The PBL experiences a strong friction against the terrestrial surface and its structure is variable in time and space responding very quickly to changes in surface characteristics, also depending on meteorological conditions. PBL non-constant height may change from a few meters ($\sim$ 30 m in conditions of strong stability) to a few kilometers ($\sim$ 3 km in conditions of developed turbulence). The depth is greater above irregular surfaces. However, its

Veronica Bellucco, *Empirical estimations of CO₂ flux components over different ecosystems*, Tesi di Dottorato in
"Scienze e Biotecnologie dei Sistemi Agrari e Forestali e delle Produzioni Alimentari", Indirizzo "Agrometeorologia ed
Ecofisiologia dei Sistemi Agrari e Forestali", Università degli Studi di Sassari.

typical vertical and horizontal extension is of about 1 km and 50 – 100 km, respectively, and alterations begin in a time scale of one hour and have a time period of about one day (Hartmann, 1994; Holton, 2004; Oke, 1987; Stull, 1988).

In the PBL, turbulent motions are generated mechanically by friction between the overlying air and the underlying surface, or by buoyancy effect of raising warmer and lighter air during the day. This updraught calls back the above heavier and colder air, thus generating atmospheric mixing. Vertical wind speed profile are generally logarithmic and in the upper part of the PBL (*Ekman layer*) wind direction changes anticlockwise (Northern hemisphere) up to 30° – 45° (Foken and Nappo, 2008).

Horizontal convective transport is called *advection*. Winds and turbulence can also be generated by horizontal pressure differences caused by horizontal temperature gradients from high towards lower pressure regions. The PBL tends to be thinner in high pressure than in low pressure regions. Here, vertical motions are directed downward (subsidence), whereas in low pressure regions the air is brought away from the surface to higher altitudes calling back air from the other high pressure regions and converging there.

The main characteristic that influences PBL height is the daytime heating of the surface with insolation. The typical daily cycle (Figure A.2) occurs in high pressure regions and fair weather conditions, typically over land in summer. By day, winds are stronger and the warmer air beneath is transported, by convection, upward in the cooler free atmosphere (Hartmann, 1994; Oke, 1987). Conversely, by night buoyancy is suppressed and the surface cools faster than the air above, so a thinner stable layer develops. More in detail, soon after sunrise the stable and stratified nocturnal boundary layer evolves with insolation into a very turbulent *mixed layer* in which turbulence is fed
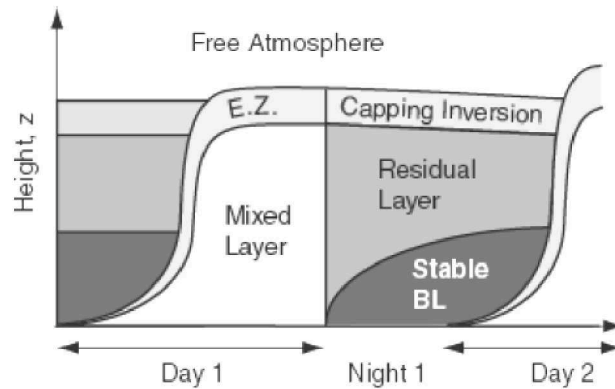
Figure A.2: *Evolution of the PBL vertical structure over land during fair weather summer days (modified from Wallace and Hobbs, 2006)*

both mechanically and thermally, by rising warm air heated by the ground beneath. The mixed layer grows by an entraining process until the top of the PBL (capping inversion) is reached. In this process, turbulent eddies inertially overshoot the capping inversion taking air from the free atmosphere and sinking it back into the mixed layer. This transition layer (*entrainment zone*), where atmospheric properties are well mixed and change rapidly, separates the mixed layer from the free atmosphere. Mixed layer maximum height is reached in the late afternoon but it decreases again about thirty minutes before sunset, when a stable layer starts to develop near the surface. As longwave radiation cools the surface, buoyancy ceases and the cold ground cools the overlying air. Thus a *stable boundary layer* grows in thickness and can trap pollutants up to the next day. Winds are weak near the surface and temperature shows an inversion vertical profile. At higher altitudes, a neutrally stratified *residual layer* is the rest of the diurnal mixed layer where turbulence is homogeneous (statistically the same in all directions). Again at sunrise, this two layers are caught up and destroyed by rising thermals (Foken and Nappo, 2008; Stull, 1988; Wallace and Hobbs, 2006).

Approaching to the terrestrial surface, new sublayers, with features more and more affected by the nearby boundary, can be defined: the turbulent surface layer, the roughness layer and the laminar boundary layer (Figure A.3). In these layers, fluxes indicate the rate of transfer of materials that transport mass, energy and momentum across a unit area.
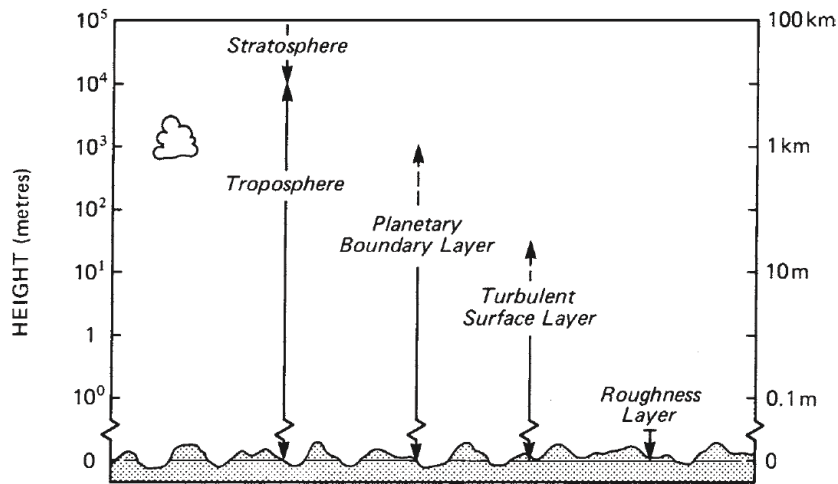
Figure A.3: *Layers within the troposphere (from Oke, 1987)*

The *turbulent surface layer* is the most turbulent part of the atmosphere where vertical momentum transfer is carried out by swirls of different dimensions called *eddies*. It is about 10% of the PBL and it can extend from few meters by night, in stability conditions, up to 50 m during daytime. It is horizontally homogeneous over period greater than 10 min (Holton, 2004; McIlveen, 1992; Oke, 1987; Stull, 1988). Under neutral conditions, when buoyancy is suppressed and turbulence is mechanically generated and driven by the intensity of the free atmosphere mean wind, there is a net transfer of kinetic energy from bigger to smaller eddies (*energy cascade*) but turbulent kinetic energy is not conserved because the smallest eddies disappear dissipating energy.

The *roughness layer* is from 1 to 3 times greater than the main dimen-

sions of the underlying objects whereas the *laminar boundary layer* is a few millimeters thick layer that adheres to any surface. Here motion is regular and predictable and its trajectories are opened, always parallel to the surface and mainly driven by molecular diffusion. The lower horizontal scale limit is $10^{-2} - 10^{-3} \, m$ (McIlveen, 1992; Oke, 1987).

It is within the turbulent surface layer, where the turbulent fluxes are constant, that eddy covariance method can be applied.

A.1.2   Canopy effects

The PBL structure and evolution described in the above section is typically observed in homogeneous underlying canopies, such as grasslands, forests deserts ect., which are characterized by having uniform surface coverage, roughness, and similar height among single elements. Cities greatly modify atmospheric vertical profile above them with respect to the surrounding rural areas. In analogy with vegetation, non-deformable buildings, considered as a whole, constitute the urban canopy and the distance between the roof level and the ground is called *urban canopy layer*. Within the street canyons, winds can accelerate and create "cavity" of circulation behind individual buildings where surface wind are directed contrariwise to the stronger wind beyond. At higher altitudes, mean wind flow slower over the whole city due to augmented surface roughness so that pollutant concentrations do not disperse far (Oke, 1987).

In fairweather conditions with cloudless sky and weak winds, the PBL is so modified by urban canopy as depicted in Figure A.4. At local scale, the surface layer mainly divides into two sublayers: the *inertial sublayer* (ISL), in which turbulence can be considered homogeneous and measurements of net exchange between the city and the atmosphere can be conducted, and
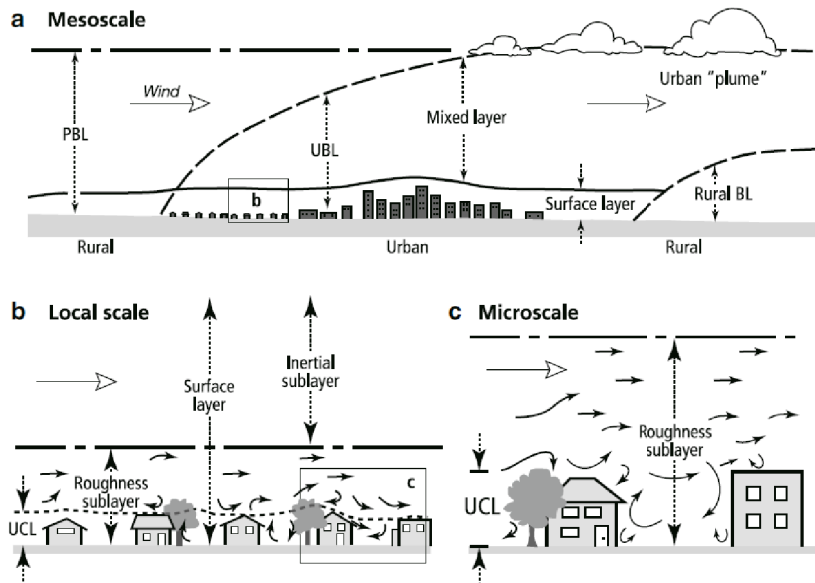
Figure A.4: *PBL modification over urban areas (picture from Aubinet et al., 2012 after Oke, 2006)*

the *roughness sublayer* (RSL), strongly influenced in space and time from the interaction of wind flow with microscale elements.

Considering the mesoscale urban region, mean wind flows, heat, and pollutant gas accumulated into the urban area are moved away from the city center and can be transported for several km into an *urban plume* extending over rural downwind areas. It has been observed that there convective clouds and precipitation can occur and the growing season can be 15 days longer than it would be without the urban warmth (Oke, 1987; Wallace and Hobbs, 2006).

A close circulation can form over cities in absence of wind. Convection can significantly enhance in the surface layer over an urban site and create a like sea-breeze counter circulation coming from the countryside to the city center with a weak return circulation toward the rural surrounding (Stull, 1988). Daily cycle is modified with mixing atmospheric conditions also during night

periods. For this reasons the mixed layer can be higher over urban areas.
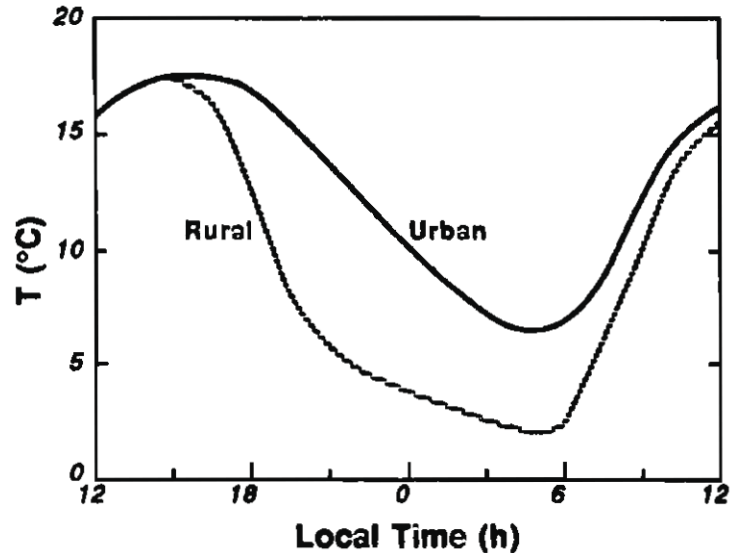
Figure A.5: *Rural and urban temperature cycle under fair weather condition and light winds (picture from Stull, 1988 after Oke, 1982)*

Urban sites significantly modify incoming and outcoming radiation, hydrologic and energy balance as well as carbon budget. Reflected and absorbed solar radiation, as well as incoming longwave radiation, increase both because of a reduced sky view factor due to the presence of tall buildings, and to pollutants, very good absorbers. In contrast, direct incoming shortwave radiation and outcoming longwave radiation decrease as a consequence of canyon geometry. Albedo is also reduced. Construction materials and concrete surfaces have greater thermal capacity so they convert and store incoming radiation into sensible heat (to be added to the other anthropogenic sources of heat and pollutants such as traffic and buildings). Less vegetation and less humidity cause less evapotranspiration whereas photosynthesis of urban vegetation is reduced, since pollutants filter shorter wavelengths.

In addition in an urban environment, anthropogenic sources of heat and pollutants are the main responsible of urban air warming. This phenomenon

is known as the *urban heat island* (UHI). The analogy with an island comes from the interpretation of surface weather maps which show isotherms closed and isolated over cities and opened ones over the cooler surroundings. Air temperature difference between the countryside and the city centre, where a temperature peak is usually observed, gives the *urban heat island intensity* (Oke, 1987). UHI occurs in very small towns as well as in the biggest ones, with rural-urban temperature gradients varying from about 2° C – 3° C, for about 1000 inhabitants, up to 8° C – 12° C for millions of inhabitants (Oke, 1987; Stull, 1988). UHI grows after sunset and reaches its maximum value $3 - 5$ hours later (Figure A.5). During the summer season, higher daytime and nighttime temperatures within the urban areas can cause general malaises and increased mortality. This is due to the heat stress on sensitive population during extreme heat events as well as to an increased energy and electricity demand, which in turn increases air pollutants and GHG emissions (U.S. Environmental Protection Agency, 2008).

A.2 Turbulence equations

Both over vegetated and urban ecosystems, turbulent motion changes both on spatial and temporal scale and its trajectories break up in eddies of different dimensions that overlap one another. They are responsible of the diffusion in the atmosphere of any energy, momentum, and trace gases not uniformly distributed. Turbulence is an intrinsic characteristic of the PBL and it is characterized by temporal and spatial irregularity, unsteadiness, hierarchy from larger to smaller eddies and three-dimensional structure. Because of its irregularity, it is not possible to follow each air particle so a statistical approach is necessary to study it and mean values, variance, covari-

ance, and its flux interpretation are used. Flux is the transfer of a quantity per unit area and time. In micrometeorology, the observed most common fluxes are mass, heat, humidity, momentum, and pollutants.

Wind intensity changes randomly and quickly around its mean value which in turn is not constant in time. In analogy with this description, variance is used to characterize the wind intensity.

According to Taylor (1938), there is a direct correspondence between spatial and temporal eddies dimensions. When turbulent eddies evolve in a time scale longer than the time used by a single eddy, turbulence can be observed and studied as if the swirls were stopped in a snapshot picture (*frozen turbulence*), so that timeseries of turbulence can be translated in spatial measurements (Stull, 1988).
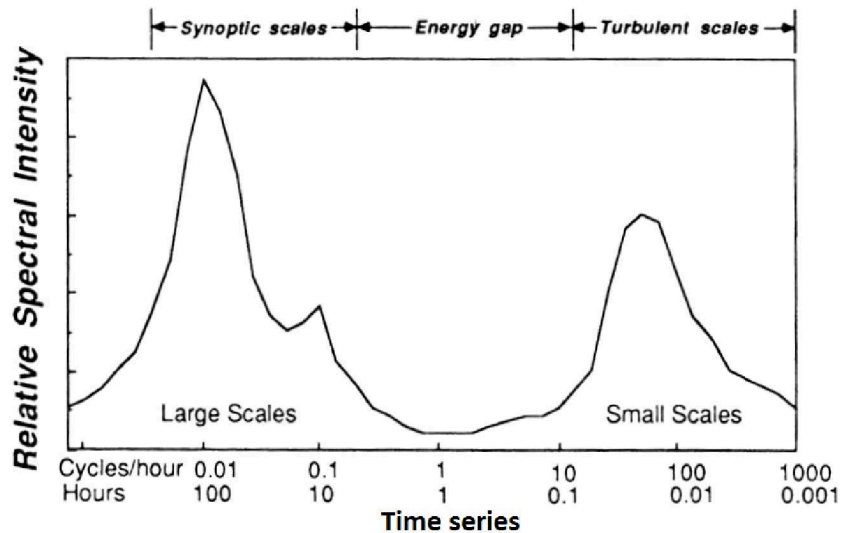
Figure A.6: *Wind speed spectrum near the surface (modified from Stull, 1988)*

Spectral analysis can tell us the composition of the turbulent signal showing how much each eddy contributes to it. Turbulence spectrum is a function of spectral energy distribution, the portion of energy associated to eddies dimensions (Figure A.6). The peaks of the spectrum give an indication of

which dimensions of eddies contribute to the turbulent kinetic energy. Large eddies have low frequencies and are more intense, whereas high frequencies are associated with smaller and weaker eddies.

The left hand side peak in Figure A.6 is associated to a mean wind with a period of about four days, whereas the right hand side peak is the one associated with turbulence: it is weaker and results from micro-scale eddies that vary in a time scale from 10 s up to 10 min. A weak peak is also centered around 24 hours showing daily variation of wind velocity. A spectral gap centered around temporal variation of about 1 hour (typical period of separation between turbulent and non turbulent motions) separates macro and micro-scale.

Looking at the turbulence spectrum, the spectral gap allows a mathematical translation of the separation between mean wind and fluctuations known as *Reynold's decomposition* (Stull, 1988):

$$x = \overline{x} + x' \tag{A.1}$$

where $\overline{x}$ is mean value of a generic variable and x' its instantaneous fluctuation with respect to the average. Reynold's decomposition is applicable to each meteorological variable (here generically indicated as x and y) and

follows simple rules of averaging (Stull, 1988):

$$\overline{a} = a$$

$$\overline{ax} = a\overline{x}$$

$$\overline{(\overline{x})} = \overline{x}$$

$$\overline{x'} = 0$$

$$\overline{x + y} = \overline{x} + \overline{y}$$

$$\overline{x'\overline{x'}} = \overline{x'\overline{y'}} = 0 \tag{A.2}$$

$$\overline{(\overline{x}y)} = \overline{x}\overline{y}$$

$$\overline{\frac{\partial x}{\partial t}} = \frac{\partial \overline{x}}{\partial t}$$

where a is a constant. It should be noted that:

$$\overline{x^2} = \overline{x}^2 + \overline{x'^2}$$

$$\overline{xy} = \overline{x}\,\overline{y} + \overline{x'y'} \tag{A.3}$$

Last terms in the right side of these equations ($\overline{x'^2}$ and $\overline{x'y'}$) represent the statistical variance (σ_x^2) and covariance (σ_{xy}) respectively. All the equations for turbulent fluxes are based on the covariance between fluctuations of vertical wind speed and a scalar quantity (indicating how these two variables vary together) which is interpreted as a kinematic vertical flux of that quantity:

- $\overline{w'c'}$ for a gas flux (F), where w is the vertical wind speed and c is gas concentration such as carbon dioxide,

- $\overline{w'T'}$ for sensible heat flux (H), related to temperature (T) changes,

- $\overline{w'e'}$ for latent heat flux (LE), related to water phase changes, where e is water vapour concentration

- $\overline{u'w'}$ for momentum flux (τ), where u is the horizontal wind speed in the x direction.

This method of splitting variables and its rules of averaging are used when describing atmospheric dynamic and thermodynamic so that the equation for the conservation of scalar quantities (such as pollutants), the equation of state (the Ideal Gas Law), the conservation equation for mass, moisture, heat and the three conservation equations for momentum (Navier-Stokes) are splitted and studied separately for the mean part and the perturbed part.

The conservation equation for scalar quantities, such as the concentration of carbon dioxide, states that (Stull, 1988):

$$\frac{dc}{dt} = K_c \nabla^2 c + S_c \tag{A.4}$$

where K_c is the molecular diffusion of the scalar quantity c and S_c is a *sink* or *source* term. Expanding the total derivative into local and advective contribute, equation (A.4) can be rewritten as:

$$\frac{\partial c}{\partial t} + \mathbf{u}\,\vec{\nabla}\,c = K_c\,\nabla^2 c + S_c \tag{A.5}$$

where the first and second term are the local temporal variation and the advective variation representing turbulent transport of c by the wind speed vector $\mathbf{u}$. Expanding variables into mean term and fluctuation and applying Reynold's average, equation (A.5) becomes:

$$\overline{\frac{\partial(\overline{c} + c')}{\partial t}} + \overline{(\overline{\mathbf{u}} + \mathbf{u'})\vec{\nabla}(\overline{c} + c')} = \overline{K_c\,\nabla^2(\overline{c} + c')} + \overline{(S_c + S'_c)} \tag{A.6}$$

and applying mathemathical properties of Reynold's average, with few pas-

sages the following equation is derived:

$$\underbrace{\frac{\partial \overline{c}}{\partial t}}_{\text{I}} + \underbrace{(\overline{u}\frac{\partial \overline{c}}{\partial x} + \overline{v}\frac{\partial \overline{c}}{\partial y} + \overline{w}\frac{\partial \overline{c}}{\partial z})}_{\text{II}} + \underbrace{(\frac{\partial \overline{u'c'}}{\partial x} + \frac{\partial \overline{v'c'}}{\partial y} + \frac{\partial \overline{w'c'}}{\partial z})}_{\text{III}} = \underbrace{K_c \nabla^2 \overline{c}}_{\text{IV}} + \underbrace{\overline{S_c}}_{\text{V}}$$

(A.7)

This equation can be simplified assuming that:

- in a turbulent flux molecular diffusion (K_c in term IV) is negligible

- mean horizontal concentration variation ($\partial \overline{c}/\partial x$ and $\partial \overline{c}/\partial y$ in term II) are negligible

- mean vertical wind speed ($\overline{w}$ in term II) is zero

- turbulence is horizontally homogeneous ($\partial \overline{u'c'}/\partial x$ and $\partial \overline{v'c'}/\partial y$ in term III are zero)

The simplified equation describing the turbulent evolution of the mean concentration of a scalar quantity is (Stull, 1988):

$$\frac{\partial \overline{c}}{\partial t} = \overline{S_c} - \frac{\partial \overline{w'c'}}{\partial z}$$

(A.8)

This is valid for an instant of a single air particle. It states that variations of mean concentration of a gas in an air particle is equal to the difference between a *source/sink* and the quantity transported vertically away by turbulence. If we imagine a finite volume enveloping an ecosystem it is necessary to vertically sum each contribution between the surface ($z = 0$) and the measure height (h_m):

$$\int_{z=0}^{h_m} \frac{\partial \overline{c}}{\partial t}dz = \int_{z=0}^{h_m} \overline{S_c}dz - \int_{z=0}^{h_m} \frac{\partial \overline{w'c'}}{\partial z}dz$$

(A.9)

The first term after the equal sign represents the net exchange between the ecosystem and the atmosphere and it is called *eddy covariance flux* which,

in the case of carbon dioxide is the *Net Ecosystem Exchange* (NEE):

$$F = \int_{z=0}^{h_m} \overline{S_c} dz$$

Equation (A.9) becomes thus:

$$F = \overline{w'c'} + \int_{z=0}^{h_m} \frac{\partial \overline{c}}{\partial t} dz = F^{EC} + F^{STO} \qquad \text{(A.10)}$$

NEE is the sum of the turbulent vertical flux and the storage between the surface and the measurement height. The storage term is often negligible so the eddy covariance flux can be simply expressed by

$$F^{EC} = \overline{w'c'} \qquad \text{(A.11)}$$

the covariance between the time series of vertical wind speed and measurements of gas concentration.

These equations and the theory discussed are the basis for eddy covariance method application.

A.2.1 Wind profile parameters and variables

Friction velocity, u_*, is an important variable related to wind gusts and the turbulent activity which dominates the surface layer. It quantifies turbulence originated mechanically by transferring kinetic energy from higher to lower layers. It is defined as

$$u_* = \sqrt{\frac{\tau}{\rho_a}} \qquad \text{(A.12)}$$

where ρ is the air density and τ is the Reynold's stress, a deforming force which exists only when a fluid is turbulent. Friction velocity can also be written as function of the vertical flux of horizontal momentum

$$u_* = \sqrt[4]{(\overline{u'w'})^2 + (\overline{v'w'})^2} \qquad \text{(A.13)}$$

which is simplified to

$$u_* = \sqrt{\overline{u'w'}} \qquad (A.14)$$

when the surface stress is aligned with the x direction. u_* typical value is about 0.3 m s^{-1} (Holton, 2004; McIlveen, 1992; Stull, 1988).

Within the surface layer, the vertical gradient of the mean wind speed $\overline{u}$ is characterized by increasing wind shear with decreasing height:

$$\frac{\partial \overline{u}}{\partial z} = \frac{u_*}{kz} \qquad (A.15)$$

with k being the *von Karman's constant* estimated to be ~ 0.4 in all neutral boundary layers. Assuming turbulent flux to be constant near the surface and considering that eddies dimensions are affected by the distance to the surface, kz can be thought as the mixing length.

The *logarithmic wind profile* can be derived integrating equation (A.15) with respect to the vertical axis:

$$\overline{u} = \frac{u_*}{k} ln \frac{z}{z_0} \qquad (A.16)$$

where z_0 is a constant called *roughness length*. It represents the height at which $\overline{u} = 0$ and it depends on the surface physical characteristics. It can vary from few millimeters over seas to few meters in urban environment and it depends on wind speed (Hartmann, 1994; Oke, 1987). Equation (A.16) states that in the surface layer the mean wind speed is determined by z_0 and u_*. It is valid for $z \gg z_0$, so it does not describe the mean wind velocity profile within the plant canopy or very close to a rough surface where wind follows a no general profile. Under tall canopies wind can have a relative maximum of speed. Above canopies the flow is logarithmic but the aerodynamic surface is located near the top of the canopy, at a height, d, called *zero plane displacement* (Figure A.7). Values of d depend on wind speed and
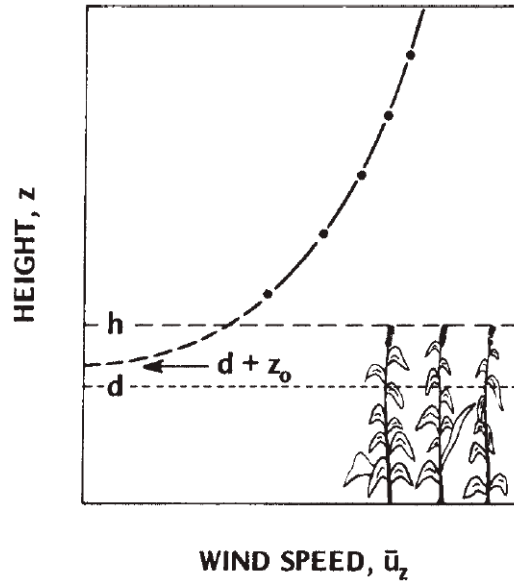
Figure A.7: *Logarithmic wind profile above a vegetated canopy and illustration of the zero plane displacement d (from Oke, 1987)*

range from $0.07 \, m$ over grasslands up to about $30 \, m$ over forests. Typically both d and z_0 are related to the canopy height h as follows: $d = \frac{2}{3}h$ and $z_0 = \frac{1}{10}h$. So, above canopies equation (A.16) varies and becomes:

$$\overline{u} = \frac{u_*}{k} \, ln \, \frac{z - d}{z_0} \qquad\qquad (A.17)$$

Another important parameter is the *stability parameter*, z/L, where L is the *Monin-Obukhov length*, which quantifies atmospheric turbulence generated by temperature vertical gradient. L is proportional to mechanical turbulence production and inversely proportional to buoyancy production ($L \propto -u^*/H$) so the stability parameter is used to indicate atmospheric conditions. Three cases can occur:

- $H > 0$ and $L < 0$ ($z/L < 0$) in unstable atmospheric conditions with raising warmer and less dense air,

- $H \approx 0$ and $L \approx \infty$ ($z/L \approx 0$) in neutral atmospheric stratification,

- $H < 0$ and $L > 0$ ($z/L > 0$) in stable atmospheric conditions (no convection occurring)

References

Aubinet, M., Vesala, T., and Papale, D. (2012). *Eddy covariance: a practical guide to measurement and data analysis*. Springer.

Foken, T. and Nappo, C. J. (2008). *Micrometeorology*. Springer.

Hartmann, D. L. (1994). *Global physical climatology*, volume 56. Academic press, San Diego.

Holton, J. R. (2004). *An introduction to dynamic meteorology*. Academic Press.

McIlveen, R. (1992). *Fundamentals of Weather and Climate*. Chapman Hall, London.

Oke, T. R. (1982). The energetic basis of the urban heat island. *Quarterly Journal of the Royal Meteorological Society*, 108(455):1–24.

Oke, T. R. (1987). *Boundary layer climates - 2nd ed.* Methuen, London.

Oke, T. R. (2006). Initial guidance to obtain representative meteorological observations at urban sites. Instrument and Observing Methods (IOM), report No.81, WMO/TD. No. 1250. World Meteorological Organization, Geneva.

Stull, R. B. (1988). *An Introduction to boundary layer meteorology*. Kluwer Academic Publisher, Dordrecht, Boston, London.

U.S. Environmental Protection Agency (2008). *Reducing Urban Heat Islands: Compendium of Strategies. Urban Heat Island Basics*. U.S. Environmental Protection Agency, Washington, DC.

Wallace, J. M. and Hobbs, P. V. (2006). *Atmospheric science: an introductory survey*, volume 92. Academic press.

Acknowledgments

This thesis is the result of a three-year research work at the Department of Science for Nature and Environmental Resources (DipNET), University of Sassari.

I really would like to thank my supervisor Prof. Donatella Spano for the support, which made me feel constantly appreciated and for giving me the opportunity to enhance my abilities also through important experiences abroad.

A special thanks to my tutor Dr. Serena Marras for being always present during my PhD. Thanks for the encouragements in facing up new experiences and for the constant support. For the friendship even outside of the department. Thanks for guiding me and constantly involving in the activities of the research group. Thank you for the determination, the passion for this work and the example you gave me. And thank you very much for the suggestions and the help in this intense period of final revision of this thesis.

Together with Prof. Donatella Spano and Dr. Serena Marras, I also thank the DipNET and the University of Sassari, for funding many important experiences during these three years. In particular, the two training courses about the Eddy Covariance technique: "5th Annual Summer Course in Flux Measurements and Advanced Modeling", that was held at the Mountain Research Station of the University of Colorado (Boulder, Colorado, USA)

and organized by Prof. Dave Moore, Prof. Paul Stoy, and Prof. Russ Monson, and "Corso su tecniche Eddy Covariance", that was held in Todi (Italy) and organized by ICOS - Italy, LI-COR Biosciences and Ecosearch srl.

A very intense and important period of this research work was carried out during the six-month internship in London, at King's College London. I sincerely thank Prof. Sue Grimmond, who supervisioned my work during my internship in London, welcoming and considering me as part of her team. For the passion, the enthusiasm and care that you dedicate to your work, and for the many useful corrections and suggestions.

I can not forget to thank Dr. Simone Mereu, for the advices, during this last year, when analysing data of the Mediterranean sites.

Thanks also to the University of Helsinki, and in particular to Leena Järvi, who provided traffic and Eddy Covariance measurements collected over the city of Helsinki.

I would also like to thank my PhD colleagues, in particular Viviana, Matteo, Sara, Andrea, Noemi, and Ilaria who shared with me many nice moments. I really would like to thank Lucía López Martínez, with whom I shared the office during the six-month period in London, for the sincere friendship, the many shared experiences and for having always supported me even after returning back to Italy.

I wish to express my profound gratitude to Gavino, who strongly supported me to apply for this PhD position. Thanks for the deep confidence, your true love, your closeness, your patience, and for all the sacrifices you did for us.

Finally, a really special thanks to my mother and my father, who always encouraged my steps especially during difficult periods. Thank you for having

always supported my studies, for the example you gave me. A big thanks also to my brother Emanuele and Tiziana for having always followed me. And thanks to people who are no longer here but that are always present in my heart.

Ringraziamenti

Questa tesi è il risultato del lavoro di ricerca durato tre anni presso il Dipartimento di Scienze della Natura e del Territorio dell'Università di Sassari.

Un primo ringraziamento va alla mia docente guida Prof.ssa Donatella Spano per aver creduto, fin dal primo momento di questa avventura, nelle mie potenzialità ed avermi dato la possibilità di valorizzarle, permettendomi di fare importanti esperienze all'estero. Grazie per l'incoraggiamento, per la stima e la fiducia che mi hanno fatto sentire costantemente supportata e apprezzata.

Un grazie speciale alla mia tutor Dr.ssa Serena Marras per essere sempre stata presente nelle fasi importanti di questo dottorato. Grazie per avermi "lanciato" in nuove esperienze e spronato nei momenti difficili. Per le esperienze condivise e l'amicizia costruita anche al di fuori del dipartimento. Grazie per avermi fatto da guida e avermi costantemente coinvolto nelle attività del gruppo di ricerca e incoraggiato a mettermi alla prova, a guardare oltre e puntare sempre in alto. Grazie per il tuo esempio, la tua grinta e la tua passione, e per avermi regalato la tua esperienza. E grazie infinite per i consigli e l'aiuto in questo intenso periodo di revisione finale della tesi.

Insieme alla Prof.ssa Donatella Spano e la Dr.ssa Serena Marras, si ringraziano anche il DipNET e la l'Università di Sassari, per aver finanziato e reso possibili tante esperienze importanti di questi tre anni. In particolare i due

corsi di formazione con i quali sono state approfondite le conoscenze sulla tecnica Eddy Covariance: "5th Annual Summer Course in Flux Measurements and Advanced Modeling" tenutosi presso la Mountain Research Station dell'Università del Colorado (Boulder, Colorado, USA) e organizzato da Prof. Dave Moore, Prof. Paul Stoy, and Prof. Russ Monson, e "Corso su tecniche Eddy Covariance", tenutosi a Todi (PG) e organizzato da ICOS - Italia, LI-COR Biosciences e Ecosearch srl. Un periodo di ricerca molto intenso e importante è stato svolto durante i sei mesi di tirocinio a Londra, presso il King's College London. Un grazie speciale alla Prof.ssa Sue Grimmond per aver guidato e supervisionato il mio progetto durante i sei mesi a Londra, e per avermi considerato parte del suo gruppo di ricerca. Per l'entusiasmo e l'impegno che testimonia nel suo lavoro. Grazie ancora i numerosi e utili consigli.

Non posso dimenticare di ringraziare il Dr. Simone Mereu, per i numerosi consigli, in questo ultimo anno, durante la fase di analisi dati dei siti Mediterranei.

Un ringraziamento anche all'Università di Helsinki, e in particolare a Leena Järvi per aver reso disponibili le misure di traffico e dati Eddy Covariance della città di Helsinki.

Desidero inoltre ringraziare le persone che mi sono state vicino in questi tre anni. I colleghi di dottorato in particolare a Viviana, Matteo, Sara, Andrea, Noemi e Ilaria per aver condiviso tanti momenti insieme. Un grazie particolare anche a Lucía López Martínez con la quale ho condiviso l'ufficio nei sei mesi di permanenza all'estero, per la sua sincera amicizia, le tante esperienze condivise e per essermi sempre stata vicina ed avermi sempre fatto sentire il suo supporto anche dopo il rientro a casa.

La mia più profonda gratitudine va a Gavino senza il quale probabilmente

non avrei neanche partecipato al concorso di selezione iniziale. Grazie per la tua profonda fiducia, il tuo sincero amore, la tua vicinanza, la tua pazienza, il tuo grande sostegno e tutti i sacrifici e le avventure per cercare di accorciare le distanze. Perchè sai farmi uscire dal mio guscio e farmi vedere le cose con occhi nuovi.

Infine, uno speciale ringraziamento a mia madre e mio padre, che hanno sempre sostenuto e incoraggiato ogni mio passo anche quando la strada sembrava particolarmente in salita. Grazie per aver sempre creduto nella mia formazione e avermi sostenuto negli studi trasmettendomi il valore dell'istruzione. Un grazie grandissimo a mio fratello Emanuele e a Tiziana per aver sempre fatto il tifo per me. Infine grazie anche alle persone che non ci sono più ma che sono sempre presenti nel mio cuore e che hanno contibuito ad essere la persona che sono oggi.